Kinetic Study of Denitrification and Hydrogen Production from NH_3/H_2O over Ni-loaded Catalysts

Ni 担持触媒を用いた NH_3/H_2O からの脱窒・水素製造の速度論的研究

Ryosuke Atsumi

熱海　良輔

Department of Chemical and Environmental Engineering,
Graduated School of Engineering, Gunma University

Supervisor: Assoc. Prof. Reiji Noda

Kinetic Study of Denitrification and Hydrogen Production from Dry/Wet-NH_3 over Ni-loaded Catalysts

Ni 担持触媒を用いた Dry/Wet-NH_3 からの脱窒･水素製造の速度論的研究

【要約】

水素キャリアとしての利用が期待できるアンモニアを、安価・高効率に水素へ変換するためには、Ni 触媒の開発が不可欠である。アンモニア分解を目的とした Ni 触媒の開発は、流通式固定層反応器を用いて幅広く行われてきたが、触媒層内での物質・熱移動の解析はほとんど行われてこなかった。本論文では、Ni/SiO_2 触媒を用いてラボスケール固定層の速度論解析、温度分布解析を行い、アンモニア分解に伴う温度分布と反応速度の関係を観察した。また細孔内における物質移動が触媒活性に与える影響を評価した。

また、高い活性を持つアンモニア分解 Ni 触媒の、アンモニアによる水素エネルギーシステム以外での適用ついて議論した。現在、肥料としてアンモニアの形態で大量に固定化されたアンモニアが、環境における富栄養化を引き起こしているという問題がある。本論文では排水処理におけるアンモニア態窒素の処理に注目し、排水中のアンモニア態窒素を Ni 触媒により熱化学的に脱窒・水素製造を行うプロセスを提案した。

第 2 章では、まず、流通式固定層反応器における温度分布が触媒反応速度に与える影響を評価した。固定層反応器は一般に伝熱が悪く、アンモニア分解反応に伴って形成される局部的な層内温度低下によってアンモニア転化率が減少してしまう可能性がある。Ni/SiO_2 触媒の活性を、種々の層高、流速、反応温度で評価し、層内温度分布を推算した。層内温度分布の挙動から、Ni 触媒において局所的な温度低下がアンモニア転化率の低下を引き起こすことが分かった。また層内温度分布が無視できる実験条件を探索し、高流速・低層高において層内温度がほぼ一定になる条件を明らかにした。

第 3 章では、種々の多孔質 SiO_2 担体を用いて、触媒細孔における物質移動が活性に与える影響を評価した。細孔径が約 14nm の触媒では、それ以上の細孔を持つ触媒に比べて活性化エネルギーの低下が観察できた。この触媒における Knudsen 数（Kn^{-1}）を評価したところ、$Kn^{-1} < 0.1$ となる条件で活性化エネルギーが大きく減少する傾向が観察できた。これは物質移動抵抗により見かけの活性化エネルギーが低下したためであると考察した。

第 4 章では、第 2 章で明らかにした温度分布の影響が無視できる実験条件において、種々のセラミック担体における Ni 触媒への担体効果を評価した。この結果、Ni/Al_2O_3 触媒が高い担体効果を持つことを明らかにした。また、担体の高い比表面積と塩基性が Ni 触媒の活性を上昇させることを確認した。

第 5 章では、高い触媒性能を持つ Ni/Al_2O_3 を用いて、加湿アンモニアにおけるアンモニア転化率を評価した。水蒸気共存下では、純アンモニアの分解試験と比較して Ni/Al_2O_3 でのアンモニア転化率が低下することが分かった。また、共存水蒸気濃度と反応温度が与える影響を観察し、触媒失活メカニズムの解明を試みた。種々の実験条件および熱力学平衡計算の結果は、Ni 表面への OH 基の吸着と $NiAl_2O_4$ の生成が触媒失活の原因であることを示唆した。

第 6 章では、共存水蒸気下でのアンモニア完全分解を目的として、第 4 章で用いた種々の触媒における共存水蒸気下での担体効果を評価した。SiO_2 担体では触媒失活が最も小さく、実施したアンモニア供給条件では 923K 以上の反応温度でアンモニアを完全分解した。

Kinetic Study of Denitrification and Hydrogen Production from NH_3/H_2O over Ni-loaded Catalysts.

Table of Contents

Chapter 1 General Introduction

1.1. Development and research of metal-loaded catalysts for NH_3 decomposition

In the last century, ammonia (NH_3) decomposition reaction on the metal surface had been investigated to gain insights into NH_3 synthesis for the development of Haber-Bosch process which is a nowadays well-known mass-production techniques of NH_3 [1-6]. After 1990s when the process had been stably operated, motivation in researches for the NH_3 decomposition catalysts have been researched for the development of effective hydrogen storage and transportation processes via NH_3 energy-carrier [7]. Yin et. al. reviewed the catalytic activity of various metals (Ru, Ir, Ni, Rh, Pt, Pd, Fe) and catalyst support (SiO_2, Al_2O_3, MgO, Ce_2O, TiO_2, ZrO_2, activated carbons, carbon nanotubes [CNTs]) [8], and they found that Ru-loaded CNTs (designated as Ru/CNTs) has the highest activity for NH_3 decomposition reaction, which can be attributed to a high rate of electron transfer from CNTs to loaded-Ru particles.

On the other hand, Ni, which is one of "non-noble" metals which is the most effective of transition metals catalysts [8]. Some researchers investigated the support effects of various support materials and promoters on the activity of Ni [9,10]. Muroyama et. al. systematically evaluated the performance of Ni-loaded catalysts for NH_3 decomposition with views toward support material (Al_2O_3, SiO_2, La_2O_3, MgO, Ce_2O, TiO_2, ZrO_2) and Ni-loading amount (for 10-70 wt% of Ni) [11]. Their results figured out that Ni/Al_2O_3 and Ni/SiO_2 catalysts exhibited the highest NH_3 decomposition rate, and suggested that the high surface area of Al_2O_3 and SiO_2 facilitated the dispersion of Ni nanoparticles.

As mentioned above, Ni-loaded catalyst is a possible candidate of NH_3 decomposition catalysts in hydrogen storage and transportation system via NH_3. In this thesis, various applications of this cheap but active catalyst will be discussed: this thesis will propose two application of Ni-loaded catalysts for

(i). NH_3 decomposition for hydrogen production process in NH_3 energy system

(ii). Thermochemical denitrification of ammonia nitrogen (NH_4^+) in wastewater treatment.

In section 1.2, NH_3 energy system will be reviewed to specify the subjects on the application of Ni-loaded catalysts. Section 1.3 will be review increasing concern about eutrophication derived from ammonia-nitrogen in the global ecosystems and a progress in development of novel denitrification techniques of wastewater to propose a thermochemical denitrification via Ni catalysts.

1.2. Ni-loaded catalysts application to NH_3 chemical hydrogen-storage system

NH_3 decomposition catalysts had been widely investigated because liquid NH_3 is a possible candidate of hydrogen carrier [7,12-14]. As shown in Fig. 1.1, NH_3 has relatively high hydrogen-mass-density (17.7 wt%) which is comparable to hydrocarbons such as methanol (12.3 wt%), ethanol (13.0 wt%) and dimethyl-ether (13.1 wt%). In addition, contrary to pure hydrogen, NH_3 can be liquefied under mild conditions (e.g. 0.8 MPa, 298 K). To utilize NH_3 as a hydrogen fuel for fuel cells or internal combustion engines [15-17], it is necessary to develop effective catalysts for NH_3 decomposition reaction. Fig. 1.2 shows a NH_3 energy process targeted in this thesis.

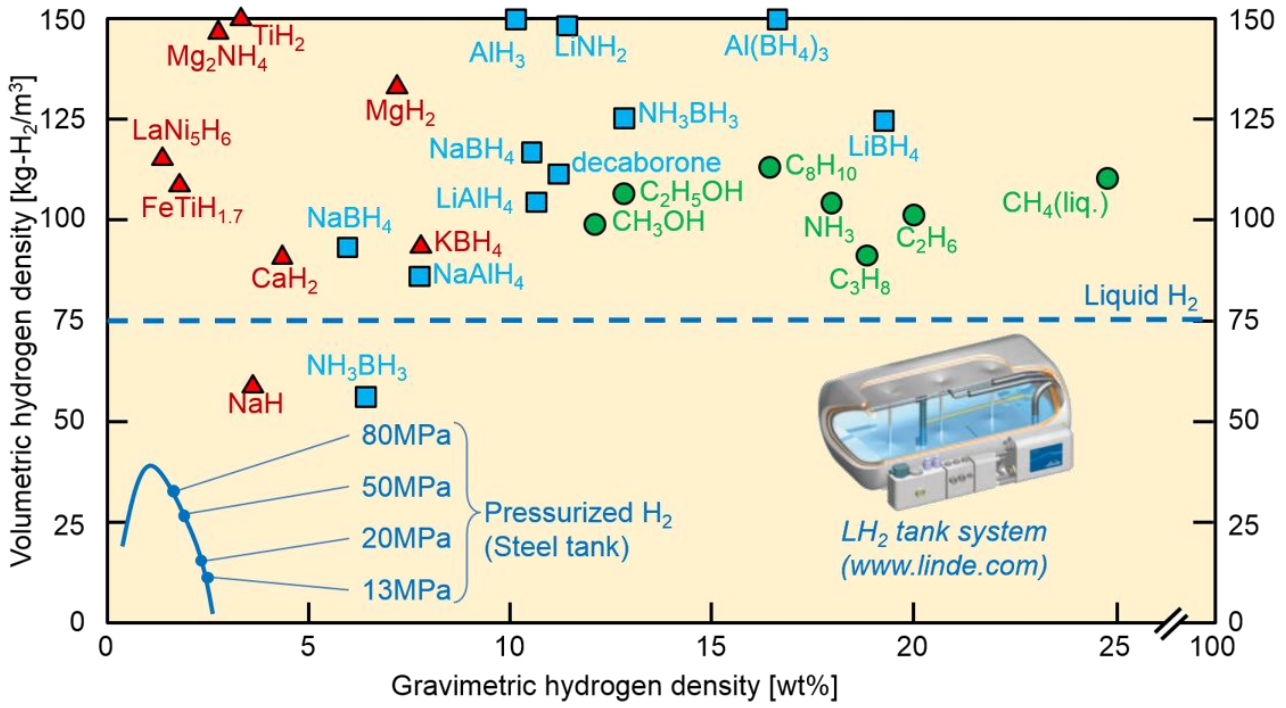

Fig. 1.1 Mass and volumetric density of hydrogen of various hydrogen storage materials.

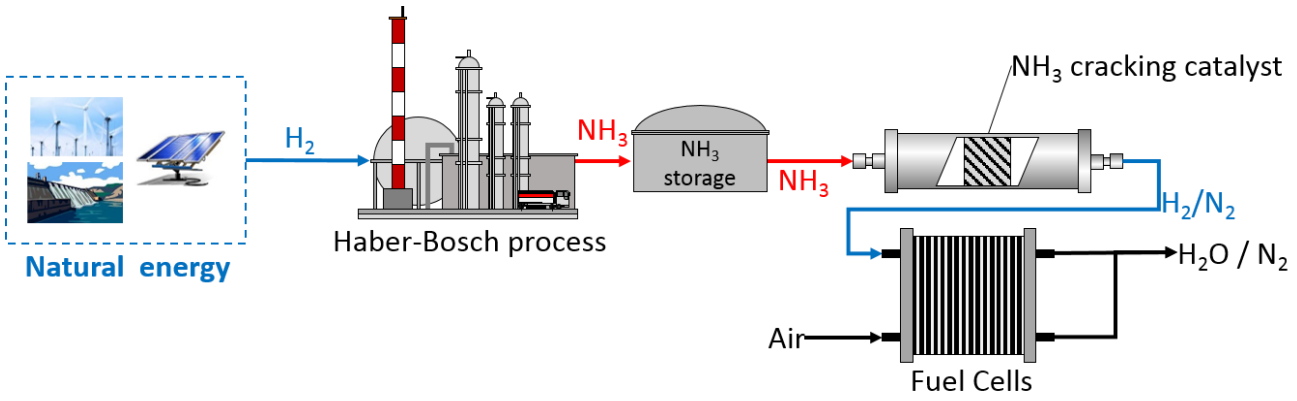

Fig. 1.2 Schematic illustration of fuel cells power generation system via NH_3 as a hydrogen storage and transportation media.

In this process, hydrogen, which is produced by natural energy sources such as sunlight, wind, geothermal and ocean wave, is converted to NH_3 as a hydrogen storage and transportation material via Haber-Bosch process. Synthesized NH_3 is transported to and stored in an application site in the form of liquid-NH_3. A fuel cells (FCs) system attached with a NH_3 decomposition reactor converts NH_3 to H_2 and N_2 and then generate electricity in the FCs using H_2.

As mentioned in the previous section, Ni-loaded catalysts have been widely investigated using a contentious-gas-flow fixed-bed reactor [8]. A fixed-bed reactor is characterized by lower heat conductivity, thus there is considering about cold-spot formation along with NH_3 decomposition which potentially decreases NH3 conversion in the catalyst bed. However few works have investigated influences of heat transfer in a bed on kinetics of NH_3 decomposition. Furthermore, mass transfer in the porous support of Ni-loaded catalysts for NH_3 decomposition have been hardly understood so far. Therefore, this thesis will

(i). observe influences of temperature distribution in Ni/SiO_2 bed on NH_3 decomposition in Chapter 2,

(ii). examine Ni/SiO_2 catalysts with different pore diameters to observe the correlation between the kinetics of the catalysts and pore diffusion in Chapter 3,

(iii). estimate support effects of various ceramic materials under conditions where influences of the temperature distribution can be ignored in Chapter 4.

1.3. Ni-loaded catalysts application to thermochemical denitrification of wastewater

In this section, nitrogen cycle in the present world will be reviewed to understand that anthropogenic nitrogen fixation which converts atmospheric nitrogen to NH_3 have caused eutrophication of the global ecosystems. The progress of wastewater treatment techniques to denitrify ammonia nitrogen also will be summarized, and propose a novel thermochemical denitrification using Ni-loaded catalysts.

1.3.1. Nitrogen cycle in the pre-industrial or present world

The nitrogen cycle is one of the most important material cycles of the Earth. Along with human understanding of nitrogen flow in ecosystems, the global nitrogen-cycle was broadly elucidated [18-20]. In the absence of human activities, in other words “in the pre-industrial world”, Delwiche [21] stated that transformation from atmospheric N (nitrogen molecule, N_2) to reactive nitrogen compounds (designated as N_r) and those returned back again were balanced. Fig.1.1 shows the schematic illustration of the pre-industrial nitrogen-cycle in the soil-atmosphere ecosystem [20]. This illustration is the adapted and simplified from Ref. [20]. As shown in Fig. 1.3, biotic nitrogen fixation (BNF) in soil as the primary source of N_r potentially provides 90-130 Tg-N yr^{-1}. N_2 production via biological denitrification process is on the same order (80-180 Tg-N yr^{-1}).

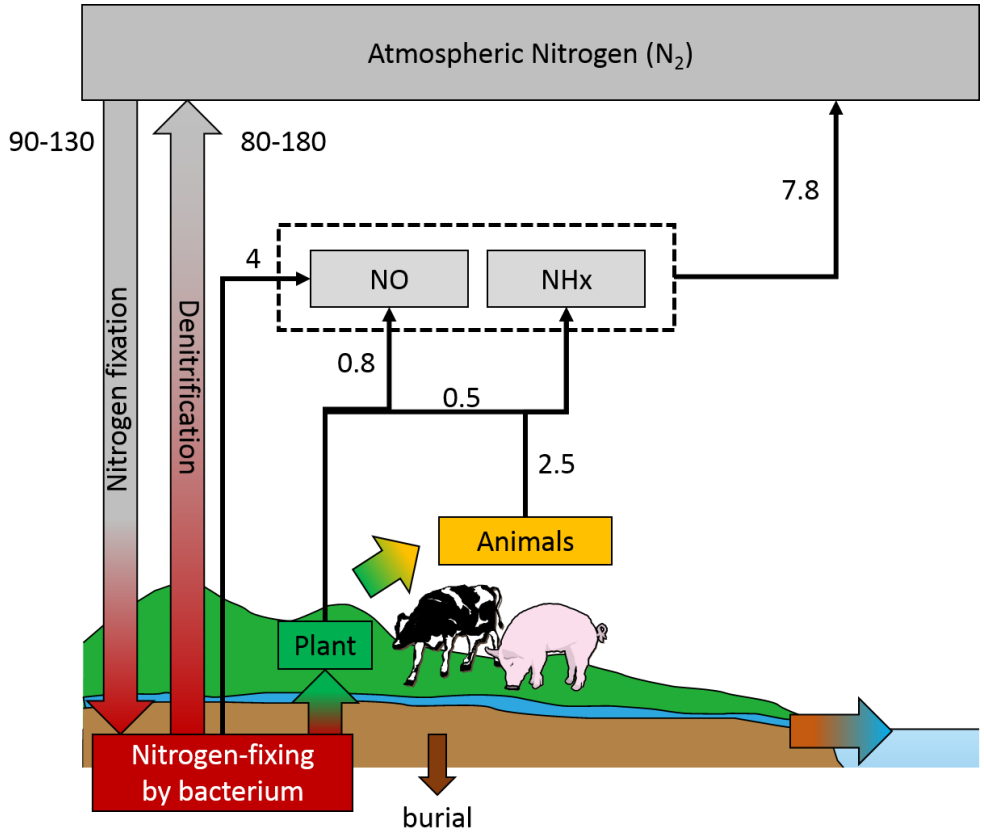

Fig. 1.3 Balance of Nitrogen fixation and denitrification (Tg-N yr^{-1}) between soil and atmosphere ecosystem in the pre-industrial world.

Thus it is considered that, in the absence of the human activities, the amount of BNF and that of biological denitrification were balanced [17,18].

On BNF in soil, atmospheric N_2 are fixed within the fixing organisms to be converted to organic N (N_{org}) [22]. N_{org} are up-taken by vegetation [20,23], or mineralized to form NH_3 or NH_4^+. NH_3 volatizes into atmosphere as gaseous NH_3, whereas a part of and NH_4^+ are uptake by vegetation converted into NO_3^-. These Nr compounds such as NH_3, NH_4^+ and NO_3^- are decomposed by denitrification organisms in soil. N_{org} in vegetation is up-taken by animals to form animal protein, and the N_{org} in the animal is excreted and returned to soil [22,23].

Because the supply of N_r is necessary for all life forms, an increase in nitrogen supply from the atmospheric N_2 into soil have been exploited in agricultural zone to increase the yield of crops for providing food along with world human-population explosion [24-26]. However, as shown in Fig. 1.3, the amount of fixing nitrogen is limited (90-130 Tg-N yr^{-1}). As summarized by Vaclav [27], the N_r applied in agricultural is derived from atmospheric N_2, however most agricultural N is industrially fixed by the Haber-Bosch process in

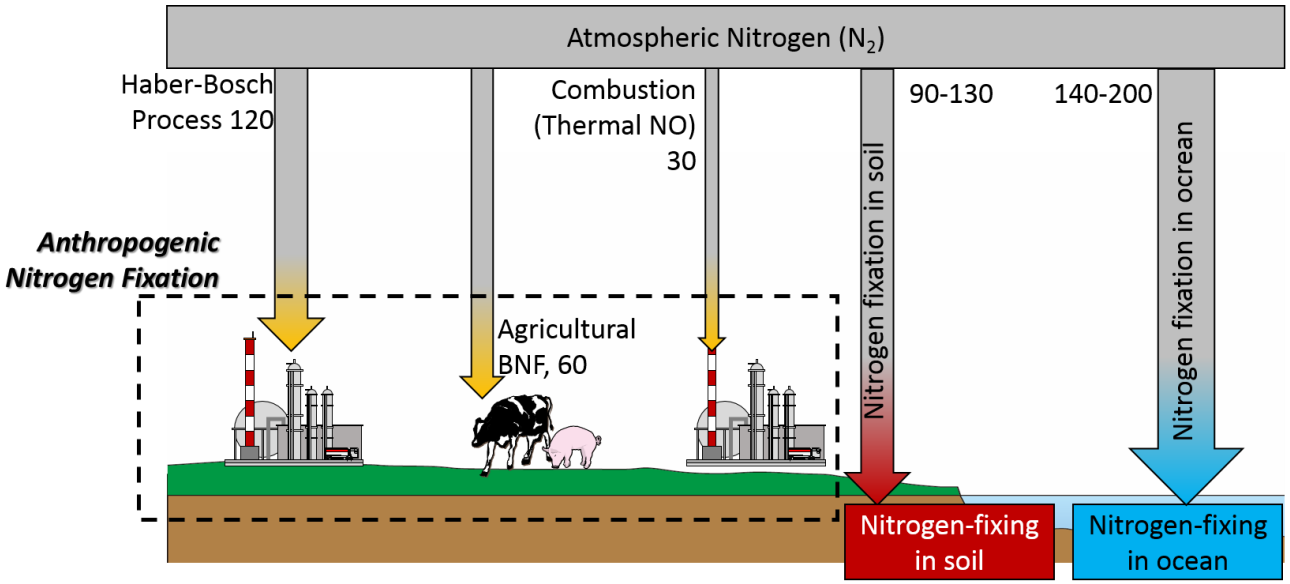

Fig. 1.4 Magnitude of the amount of biological and anthropogenic nitrogen fixation (Tg-N yr^{-1}) in the present world.

the form of NH_3 as a chemical fertilizer [27,28].

As described above, the magnitude of nitrogen fixation due to human activities have not been ignored. Fig. 1.4 shows the schematic illustration of the amount of biological and anthropogenic nitrogen fixation in the present world (this figured was illustrated by adapting and simplifying the data and figures from Refs. [18], [20] and [29]). As shown in this figure, 120 Tg-N of nitrogen have been fixed per year via Haber-Bosch process. Haber-Bosch process is one of the most important and fundamental chemical processes in the present world [27, 28-30]. In this process, ammonia gas is synthesized from hydrogen and nitrogen under high temperature and pressure [30]. N_2 in the air was used as a reactant, and hydrogen is generally produced via natural gas reforming. The magnitude of nitrogen fixation utilizing Haber-Bosch process have been larger than or comparable to that by nitrogen-fixing organism in soil (90 -130 Tg-N yr^{-1}). Overviewing the global nitrogen fixation, the total amount of anthropogenic nitrogen fixation such as Haber-Bosch process, agricultural BNF and combustion is 210 Tg yr^{-1}. This value is comparable to the magnitude of natural BNF in soil and marine (230-330).

One of the serious problems along with this drastic change of the nitrogen fixation in soil is an eutrophication of groundwater [31-34]. For instance, Hatano et. al. (2005) had been monitored the nitrogen concentration in the stream water and soil and discharge of wastes from agricultural fields and livestock in order to figure out the local nitrogen balance and the environmental impacts associated with nitrogen eutrophication [32]. Their investigation was conducted in a farm in Hokkaido University, geography of which is an alluvial fan

constructed by the Kepau River. They found that when the contribution of nitrogen fixation by 6.4 Mg-N yr^{-1} of chemical fertilizer and 12.6 Mg-N yr^{-1} of BNF, 12.7 Mg-N yr^{-1} was not used as surplus N for the farm. In other word, the amount of discharge in stream water and accumulation in soil is 12.7 Mg-N yr^{-1}.

Hatano et. al. had not figured out local nitrogen discharge from farm to the Kepau river, the global amount of discharge from agricultural zone and farm to river and groundwater was estimated 40-70 and 4 Tg yr^{-1}, respectively [20]. A part of nitrogen which discharged to water in stream was derived from animal wastes. To reduce the discharged to river and groundwater ecosystem, it is considered that suitable treatment of animal waste should be conducted with denitrifying the nitrogen compounds in animal waste such as N_{org} within the proteins and NH_4^+.

1.3.2. Energy recovery process from NH_4^+-containing wastewater

In the present wastewater treatment system biological process have carried out to denitrify nitrogen compounds within wastewater, biological processes generally has relatively large reactor and the reaction rates are too slow [35]. Thus the development of processes which can simply treat wastewater with small reactor have been desired [35-40]. Botte et. al. have investigated an electro-oxidation of NH_4^+ in an aqueous solution to recover hydrogen energy from wastewater [36-41]. They demonstrated the ammonia electrolysis at the ambient pressure and room temperature [36]. In the KOH/NH_3 aqueous solution, hydrogen can be produced as following equation in principle:

Anode $2NH_3(aq) + 6OH^- \rightarrow N_2(g) + 6H_2O + 6e^-$ $E^o = -0.77$ V versus SHE (Eq. 1-1)

Cathode $6H_2O + 6e^- \rightarrow 3H_2(g) + 6OH^-$ $E^o = -0.83$ V versus SHE (Eq. 1-2).

The total reaction in the cell is expressed as:

$2NH_3(aq) \rightarrow N_2(g) + 3H_2(g)$ (Eq. 1-3) ,

where $NH_3(aq)$ means the ammonia molecule solved in water. Using this cell, they obtained hydrogen gases with high purification [36].

This is one of possible techniques to produce hydrogen energy from NH_4^+-containing wastewater. However there are some significant problem to implement it for wastewater treatment. One is the problem that the electrolysis cell potentially uses the noble metals such as Pt, Ru, Ir [36] and Rh [36,37]. Another is that the electrode was tested only in KOH/NH_3 electrolysis solution without impurities: practical wastewater includes sulfur, halogen compounds and silicates (SiO_xH_y), and these can be ignored in catalyst deactivation. As Endo et. al. pointed out [42], even if these impurities are removed, there is also an intrinsic deactivation by intermediate products. The elementary reactions in Eq. 1-1 are expresser by following equations:

$NH_3\text{-}(s) + OH^- \Leftrightarrow NH_2\text{-}(s) + H_2O + e^-$ (Eq. 1-4)

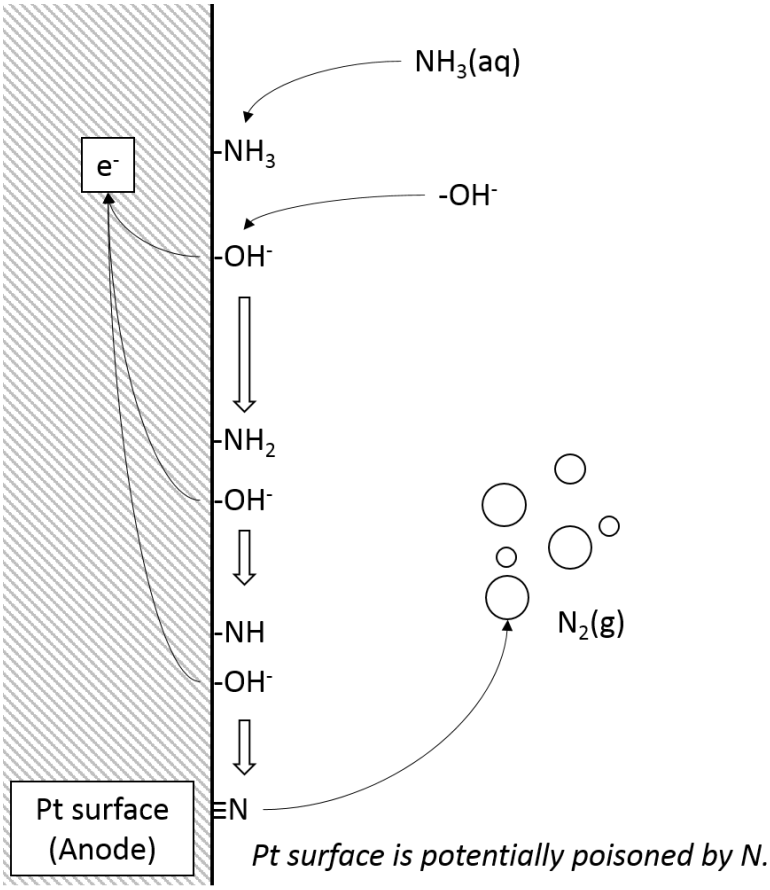

Fig. 1.5 Reaction path on anode electrode of ammonia electrolysis cell and deactivation mechanisms of Pt surface [36,42]

NH_2-(s) + OH^- ⇔ NH-(s) + H_2O + e^- (Eq. 1-5)

NH-(s) + OH^- ⇔ N-(s) + H_2O + e^- (Eq. 1-6)

N-(s) 0.5 ⇔ N_2-(s) (Eq. 1-7) .

where (s) is the active site of anode electrode (Pt). Adsorbed Nitrogen, N-(s) in Eq. 1-6 can be bonded with Pt active sites by triple linkage (N≡Pt) to occur poisoning of Pt surface as shown in Fig. 1.5. In Botte's study, the electrolysis cell showed the decrease of the hydrogen yield with time [36], and they have not overcome the deactivation at high current densities [36-39].

1.3.3. Development of thermochemical wastewater treatment for denitrification

As described in the previous section, ammonia electrolyte is potentially unstable device for denitrification because of the deactivation of absorbed nitrogen atom. Thus stable and efficient denitrification techniques which can co-produce hydrogen are desirable. This study proposes the process of the thermochemical ammonia decomposition for denitrification and hydrogen production as shown in Fig. 1.6. In the proposed process, NH_4^+-containing is sprayed onto Ni-loaded bed at high temperature, and vaporized NH_3

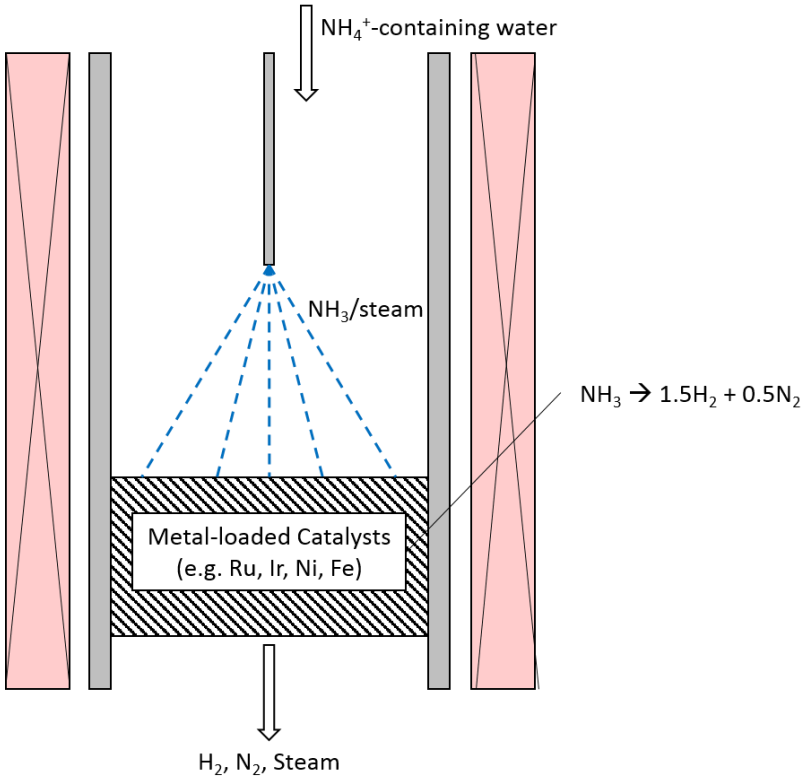

Fig. 1.6 Schematic illustration of NH_3/Steam decomposition for denitrification and hydrogen production over metal-loaded catalysts.

is decomposed over the Ni surface to generate nitrogen and hydrogen.

The thermochemical decomposition of NH_3 at the ambient pressure requires high temperatures above 773 K to decompose NH_3 almost perfectly (> 99.9 % of conversion) [43]. Thus it is considered that the latent heat loss along with vaporizing wastewater decreases the process efficiency, and heat source for reaction heat of NH_3 decomposition is required. To overcome these problems, this study proposes a thermochemical NH_3/H_2O decomposition process combined with methane fermentation system. Fig. 1.7 shows the schematic illustration of the process. Along with methane fermentation of biomass or organic compounds in wastewater, NH_4^+ concentration decrease and the methane production rate declines due to NH_4^+-poisoning for methane-fermenting organisms [44,45]. This inhabitation by ammonia for methane-fermenting is reported to occur above pH 7.4 in range of ca. 1,600 to 3,000 ppm-NH_3 in the fermenter [44]. In the proposed process, NH_4^+ in the digestive juices in the fermenter is removed by an adsorbent. For instance, magnesium phosphate ($MgHPO_4$) have been investigated as the adsorbent to remove NH_4^+ in the wastewater [46]. MgHPO4 can remove NH_4^+ in aqueous solution as following equation

$$MgHPO_4 + xH_2O + NH_4^+ \rightarrow MgNH_4PO_4 \cdot (xH_2O) + H^+ \text{ , } x = 1 \text{ or } 6 \qquad \text{(Eq. 1-8).}$$

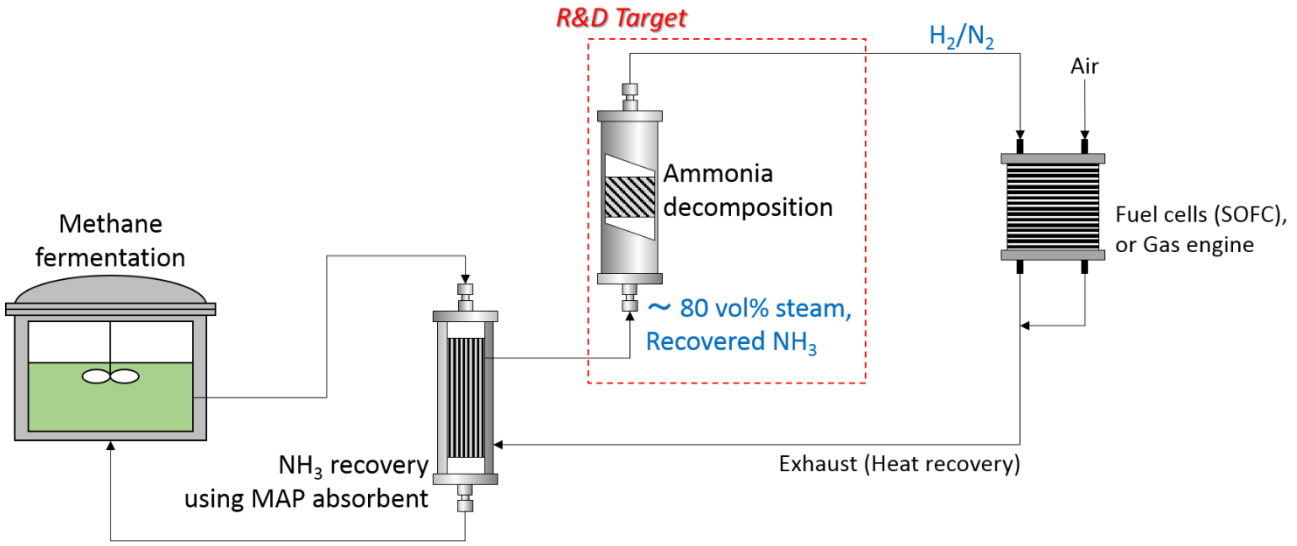

Fig. 1.7 Denitrification and hydrogen production process proposed in this study.

Thermochemical ammonia decomposition reactor and adsorption process using ammonium-magnesium-phosphate (MAP) are combined to methane fermentation system.

Espiel et. al. demonstrated NH_3 recovery from practical wastewater using $MgHPO_4$, and 90 percent of NH_4^+ was removed [46]. As Fumoto et. al. demonstrated [47], the ammonium-magnesium-phosphate (MAP, $MgNH_4PO_4$) can thermally decompose above 350 K to release gaseous NH_3. In the proposed system, NH_4^+ in the fermenter assumed to be separated using this adsorbent and exhaust heat from FCs or gas engines is used for desorption of NH_3 from MAP. Recovered NH_3 and steam is provided onto the Ni catalyst bed at high temperature. Hydrogen from the NH_3 decomposition reactor is used as a heat source of NH_3 decomposition reactor via combustion or a fuel for fuel cells. Most of reaction heat which is required by NH_3 decomposition reactor is provided by partial combustion of biogas obtained from the methane fermentation.

In Chapter 5 and 6, to discuss the feasibility the thermochemical denitrification using Ni-loaded catalysts as shown in Fig. 1.7, NH_3 decomposition over Ni-loaded catalysts in steam atmosphere was conducted. There have been few research to conducted catalytic decomposition of NH_3 co-existing steam. It is speculated that deactivation of Ni catalysts occurs due to e.g. Ni oxides formation and adsorption of hydroxyl group. Thus the catalytic activities of various Ni catalysts and deactivation behavior by steam were observed using fixed-bed reactor providing NH_3 and steam to explore the most effective catalyst for NH_3/H_2O decomposition. Moreover deactivated catalyst was analyzed by XRD to discuss the deactivation mechanisms of steam deactivation of Ni catalysts.

Reference

[1] S. F. Yin, B. Q. Xu, X. P. Zhou, C. T. Au. A mini-review on ammonia decomposition catalysts for on-site generation of hydrogen for fuel cell applications. *Applied Catalysis A : General*, 277, 1-9 (2004)

[2] J. J. Vajo, W. Tsai, W. H. Weinberg. Mechanistic details of the heterogeneous decomposition of ammonia on platinum. Journal of Physical Chemistry, 89, 3243-3251 (1985)

[3] K. Tamaru, A new general mechanism of ammonia synthesis and decomposition on transition metals. Accounts of chemical Research, 21, 88-94 (1988)

[4] A. Boisen, S. Dahl, J. K. Norskov, C. H, Christensen. Why the optimal ammonia synthesis catalysts is not the optimal ammonia decomposition catalyst. Journal of Catalysis, 230, 2, 309-312 (2005)

[5] W. Arabczyk, J. Zamlynny. Study of the ammonia decomposition over iron catalysts. Catalysis Letters, 60, 3, 167-171 (1999)

[6] G. Djega-Mariadasou, C. shin, G. Bugli. Tamaru's model for ammonia decomposition over titanium oxynitride. Journal of Molecular Catalysis A: chemical, 141, 263-267 (1999)

[7] D. Miura, T. Tezuka. A comparative study of ammonia energy systems as a future energy carrier, with particular reference to vehicle use in Japan. *Energy*, 68, 428-436 (2014)

[8] S. F. Yin, B. Q. Xu, X. P. Zhou, C. T. Au. A mini-review on ammonia decomposition catalysts for on-site generation of hydrogen for fuel cell applications. *Applied Catalysis A : General*, 277, 1-9 (2004)

[9] A. S. Chellappa, C. M. Fischer, W. J. Thomsom. Ammonia decomposition kinetics over Ni-Pt/Al_2O_3 for PEM fuel cell applications.

[10] J. Zhang, H. Xu, W. Li. Kinetic study of NH_3 decomposition over Ni nanoparticles: the role of La promoter, structure sensitivity and compensation effect. *Applied Catalysis A : General*, 296, 257-267 (2005)

[11] H. Muroyama, C. Saburi, T. Matsui, K. Eguchi. Ammonia decomposition over Ni/La_2O_3 catalyst for on-site generation of hydrogen. *Applied Catalysis A : General*, 443-444, 119-124 (2012)

[12] D. J. Durbin, C. Malardier-Jugroot. Review of hydrogen storage techniques for on-board vehicle applications. *International Journal of Hydrogen Energy*, 38, 14595-14617 (2013)

[13] R. Lan, J. T. S. Irvine, S. Tao. Ammonia and related chemicals as potential indirect hydrogen storage materials. *International Journal of Hydrogen Energy*, 37, 1482-1494 (2010)

[14] S. Satyapal, J. Petrovic, C. Read, G. Thomas, G. Ordaz. The U.S. department of energy's national hydrogen storage project: Process towards meeting hydrogen-powered vehicle requirements. *Catalysis Today*, 120, 246-256 (2007)

[15] M. A. E. Soberanis, A. M. Femandez. A review on the technical adaptions for internal combustion engines

to operate with gas/hydrogen mizture. *International Journal of Hydrogen Energy*, 35, 12134-12140 (2010)

[16] S. Verhelst. Recent progress in the use of hydrogen as a fuel for internal combustion engines. *International Journal of Hydrogen Energy*, 39, 1071-1085 (2014)

[17] Y. Wang, K.S. Chen, J. Mishler, S.C. Cho, X.C. Adroher. A review of polymer electrolyte membrane fuel cells: technology, applications, and needs on fundamental research, *International Journal of Hydrogen Energy*, 88, 1981-1007 (2011)

[18] D. Fowler et. al. The global nitrogen cycle in the twenty-fist century. *Philosophical Transactions of the Royal Society B*. 368 (2013)

[19] J. N. Galloway, A. M. Leach, A. Bleeker, J. W. Erisman. A chronology of human understanding of the nitrogen cycle. *Philosophical Transactions of the Royal Society B*. 368 (2013)

[20] J. N. Galloway, W. H. Schlesinger, H. Levy II, A. Michaels, J. L. Schnoor. Nitrogen fixation: Anthropogenic enhancement-environmental response.

[21] C. C. Delwiche. The Nitrogen Cycle. *Scientific American*. 233, 137-146 (1970)

[22] C. J. Stevens et. al. The impact of nitrogen deposition on acid grassland in the Atlantic region of Europe. Environmental Pollution. 159, 2243-2250 (2011)

[23] A. M. Leach, J. N. Galloway, A. Bleeker, J. W. Erisman, R. Kohn, J. Kitzes. A nitrogen footprint model to help consumers understand their role in nitrogen losses to the environment. Environmental Development, 1, 40-66 (2012)

[24] M. Manzanares, J. L. Tenorio, L. Ayerbe. Sowing time, cultivation plant population and application of N fertilizer on Kenad in Spain's central plateau. *Biomass and Bioenergy*, 12, 263-271 (1997)

[25] C. M. Mutero, P. N. Ng'ang'a, P. Wekoyela, J. Githure, F. Konradsen. Ammonium sulphate fertilizer increase larval populations of Anopheles arabienisis and culicine mosquitoes in rice fields. *Acta Tropic*, 89, 187-192 (2004)

[26] H. Chu, T. Fujii, S. Morimoto, X. Lin, K. Yagi. Population size and specific nitrification potential of soil ammonia-oxidizing bacteria under long-term fertilizer management. *Soil Biology and Biochemistry*, 40, 1960-1963 (2008)

[27] V. Smil. Enriching the Earth: Fritz Haber, Carl Bosch, and the transformation of World Food Production, Cambridge, *MIT Press* (2001)

[28] J. W. Erisman, M. A. Sutton, J, Galloway, Z. Kilmont, W. Winiwarter. How a century if ammonia synthesis changed the world. *National Geoscience*, 1, 636-639 (2008)

[29] D. F. Herridge, M. B. Peoples, R. M. Boddey, Global inputs of biological nitrogen fixation in agricultural

sysytems. *Plant Soil*, 311, 1-18 (2008)

[30] H. Liu. Ammonia synthesis catalyst 100 years: Practice, enlightenment and challenge. *Chemical Journal of Catalysis*. 35, 1619-1640 (2014)

[31] P. M. Vitousek, J. D. Aber, R. W. Howarth, G. E. Linkens, P. A. Matson, D. W. Schindler, W. H. Schesinger, D. G. Tilman. Human alternation of the global nitrogen cycle: sources and consequences. *Journal of Applied Ecology*, 7, 737-750 (1997)

[32] R. Hatano, T. Nagumo, H. Hata. K. Kuramochi. Impact of nitrogen cycling on stream water quality in a basin associated with forest, glassland, and animal husbandry, Hokkaido Japan. *Ecological Engineering*. 24, 50-9-515 (2005)

[33] U. Mander. Y. Hayakawa, V. kuusemets. Purification processes, ecological functions, planning and design of riparian buffer zones in agricultural watersheds, *Ecological Engineering*, 24, 421-432 (2005).

[34] M. A. Zonderland-Thomassen, M. Liffering, S. F. Ledgard. Water footprint of the beef cattle and sheep produced in New Zealand: water scarcity and eutrophication impacts. *Journal of Cleaner Production*, 73, 253-262 (2014)

[35] S. M. Oakley et. al., nitrogen control through decentralized wastewater treatment: Process performance and alternative management strategies, 36, 1520-1531 (2010)

[36] F. Vite, M. Cooper, G. G. Botte. On the use of ammonia electrolysis for hydrogen production, *Journal of Power Sources*, 142, 18-26 (2005)

[37] M. Cooper, G. G. Botte. Hydrogen production from the electro-oxidation of ammonia catalyzed by platinum and rhodium raney nickel substrate. *Journal of Electrochemical society*. 153, A1894-A1901 (2006)

[38] E. P. Bonnin, E. J. Biddinger, G. G. Botte. Effect of catalyst on electrolysis of ammonia effluents, *Journal of Power Sources*, 182, 284-290 (2008)

[39] B. K. Boggs, G. G. Botte. On-bord hydrogen storage and production: An application of ammonia electrolysis. *Journal of Power Sources*, 192, 573-581 (2008)

[40] B. K. Boggs, G. G. Botte. Optimization of Pt-Ir on carbon fiber paper for the electro-oxidation of ammonia in alkarine media, *Electrochemica Acta*, 55, 5287-5293 (2010)

[41] D. A. Daramola, G. G. Botte. Theoretical study of ammonia oxidation on platinum clusters – Adsorption of ammonia and water fragments. *Computational and Theoretical Chemistry*, 989, 1-17 (2012)

[42] K. Endo, K. Nakamura, Y. Katayama, T. Miura. Pt-Me binary alloys as an ammonia oxidation anode. *Electrochemica Acta*. 49, 2503-2509 (2004)

[43] S. F. Yin, B. Q. Xu, X. P. Zhou, C. T. Au. A mini-review on ammonia decomposition catalysts for on-site generation of hydrogen for fuel cell applications. *Applied Catalysis A : General*, 277, 1-9 (2004)

[44] H. B. Nielsen, I. Angelidaki. Strategies for optimizing recovery of the biogas process following ammonia inhibiation, Biosource Technology, 99, 7995-8001 (2008)

[45] F. Abouelenien, W. Fujiwara, Y. Namba, M. Kosseva, N. Nishio, Y. Nakashimada. Improved methane fermentation of chicken manure via ammonia removal by biogas recycle. Biosource Technology, 101, 6388-6373 (2010)

[46] J. M. Chimenos et. al., Removal of ammonium and phosphates from wastewater resulting from the process of cochineal extraction using MgO-containing by-products, Water Research, 37, 1601-1607 (2003)

[47] E. Fumoto, T. Tago, T. Masuda. Recovery of Ammonia and Ketones from Biomass wastes. Environmental technologies, 22, 1263-1272 (2001)

Chapter 2 Kinetics of Ni/SiO_2 Catalyst for Ammonia Decomposition

2.1. Introduction

Ni-loaded catalysts for NH_3 decomposition has been widely and systematically investigated, because Ni is one of the non-noble metals [1-6]. For instance, Muroyama et. al. evaluated the performance of various Ni-loaded catalysts for NH_3 decomposition to compare support effects within the ceramic materials (Al_2O_3, SiO_2, La_2O_3, MgO, Ce_2O, TiO_2, ZrO_2) using a contentious-gas-flow fixed bed reactor [5]. Their results indicates that Ni/Al_2O_3 and Ni/SiO_2 catalysts has the highest catalytic activity for NH_3 decomposition, because of high surface area of those support. In addition, those catalysts were tested in the temperature ranged from 623 to 923 K at specific NH_3 flow rate, $F' = 100$ ml min^{-1} g^{-1}, and it is found that Ni/Al_2O_3 and Ni/SiO_2 can decompose NH_3 perfectly at 923 K.

Usually only 0.1 g of catalyst particles was used with catalysts tests for NH_3 decomposition to eliminate influences of non-uniform temperature distribution in a fixed-bed [1]. However, even if a small amount of Ni was packed in the reactor, serious cold-spot formation can occur under low gas velocities because NH_3 decomposition rate on Ni surface is so fast at high temperatures. Although reaction heat along with NH_3 decomposition reaction

$$NH_3 \rightarrow 1.5\ H_2 + 0.5\ N_2 \quad , \Delta H^o = 45.90\ kJ\ mol^{-1} \qquad \text{(Eq. 2-1)},$$

was relatively low, Ni catalysts decompose NH_3 under high space velocity [6]. Furthermore, a fixed bed reactor is potentially characterized by a low heat conductivity [8, 9]. There have been few research which discussed the correlation between catalytic activities and temperature distribution along with NH_3 decomposition. Hence it is considered that influences of temperature distribution on catalytic activities should be investigated to correctly evaluate the catalytic activities of Ni-loaded catalysts.

In this chapter, based on the calculation of temperature distribution, the kinetics of Ni/SiO_2 was evaluated using design equation of a plug-flow-reactor (PFR). Temperature distribution in the Ni/SiO_2 catalyst fixed-bed was also analyzed under various temperature, gas velocity and bed height to explore and discuss the experimental conditions which the influence of temperature distribution can be ignored. For simplicity, temperature in radial direction was assumed to be constant and axial temperature distribution in the bed was calculated based on an enthalpy balance and steady-state heat transfer.

2.2. Experimental

2.2.1. Ni/SiO_2 catalyst synthesis

Ni/SiO_2 catalysts were prepared by a wet impregnation method with a nominal Ni loading of 10 wt% [1, 6]. A porous silica particles CARiACT Q-30 (the particle size is ranged from 75 to 150 μm, mean diameter is 112.5 μm, 100 m^2 g^{-1} of surface area, Fuji Silysia, Ltd.) was used as support materials. Nickel(II) nitrate hexahydrate ($Ni(NO_3)_2$•$6H_2O$, Wako Pure Chemical Industries, Ltd.) was used as a precursor. The nominal Ni precursor and 10 g of SiO_2 were dissolved in 100 ml of ion-exchanged water. The slurry was stirred for 24 h and dried using a rotary evaporator at 383 K. The supported Ni catalyst was calcined at 973 K for 1 h under flowing argon (Ar) and was then reduced at 973 K for 2 h under flowing H_2.

2.2.2. Characterization of Ni/SiO_2

Prepared Ni/SiO_2 was characterized using an X-ray fluorescence instrument (XRF, EDX-7000, SHIMADZU Co. Ltd.) and an X-ray diffractometer (XRD, Rint-2000, Rigaku Co. Ltd.) to evaluate Ni-loading amount and the crystallite size of loaded-Ni nanoparticles (D_{Ni}). XRD was operated at 30 kV / 20 mA with a scanning rate of 0.1^o min^{-1}.

The results from XRF indicated that loading amount of Ni was 9.2 wt%. D_{Ni} was calculated using the Scherrer equation and the result from XRD. The catalyst was analyzed at Crystallite sizes were evaluated using the Scherrer equation

$$D_{Ni} = \frac{K\lambda}{B\cos\theta} \qquad \text{(Eq. 2-2)}$$

where

D_{Ni} [nm] is a crystallite size of Ni nanoparticle,

λ [nm] is the wave length of the CuKα, 0.1574 nm,

K [-] is the Scherrer constant, 0.9,

B [-] is a half width of the peak derived from Ni,

θ [rad] is a diffraction angle.

Scherrer constant, K is equal to 0.9 for each calculation because B is determined as the broadening width at the half of the peak height. The results of Scherrer equation indicated D_{Ni} = 30.9 nm.

2.2.3. Catalyst tests

The catalytic activity of Ni/SiO_2 was estimated using a contentious-gas-flow reactor [6] at the ambient pressure (0 MPaG). Figure 2.1 shows the schematic illustration of the experimental setup. The reactor consisted of a stainless steel tube (SUS316, inner diameter = 8 mm) with three internal K-type sheathed-thermocouples

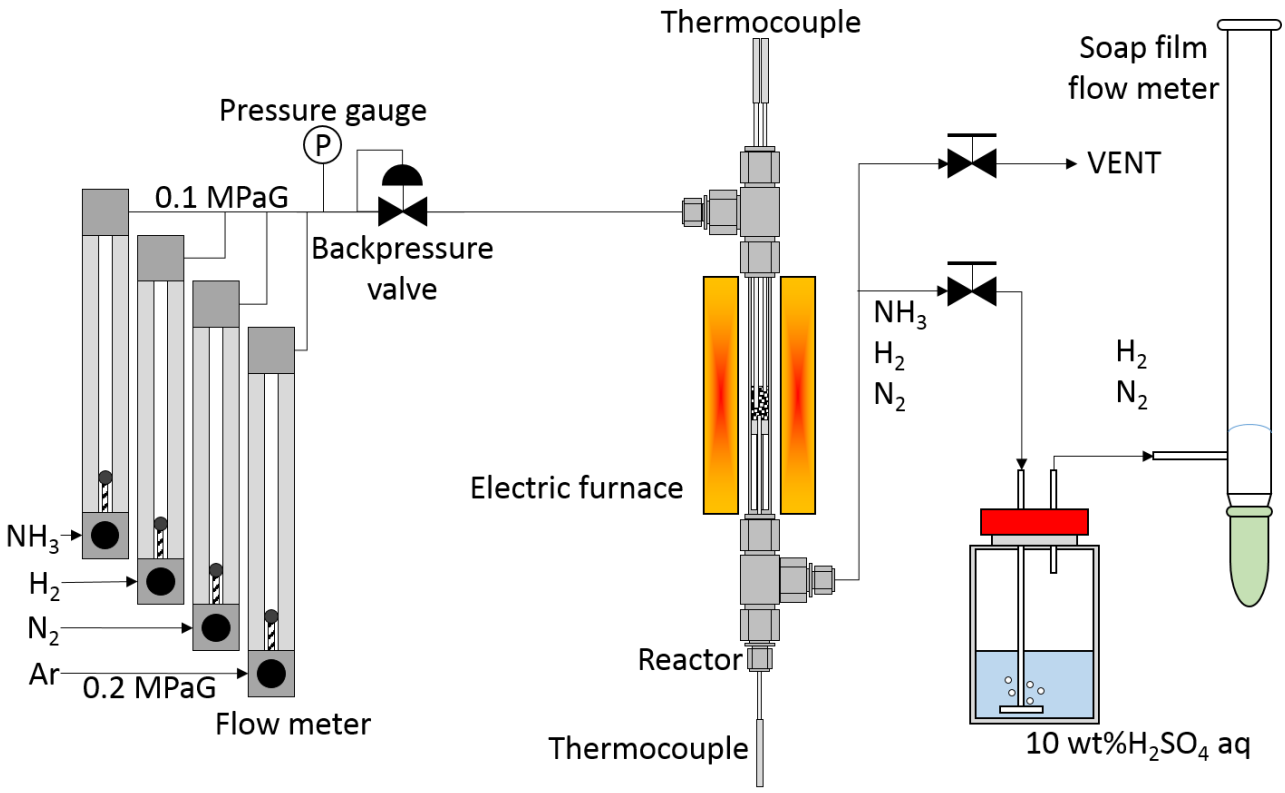

Fig. 2.1 Schematic illustration of experimental setup.

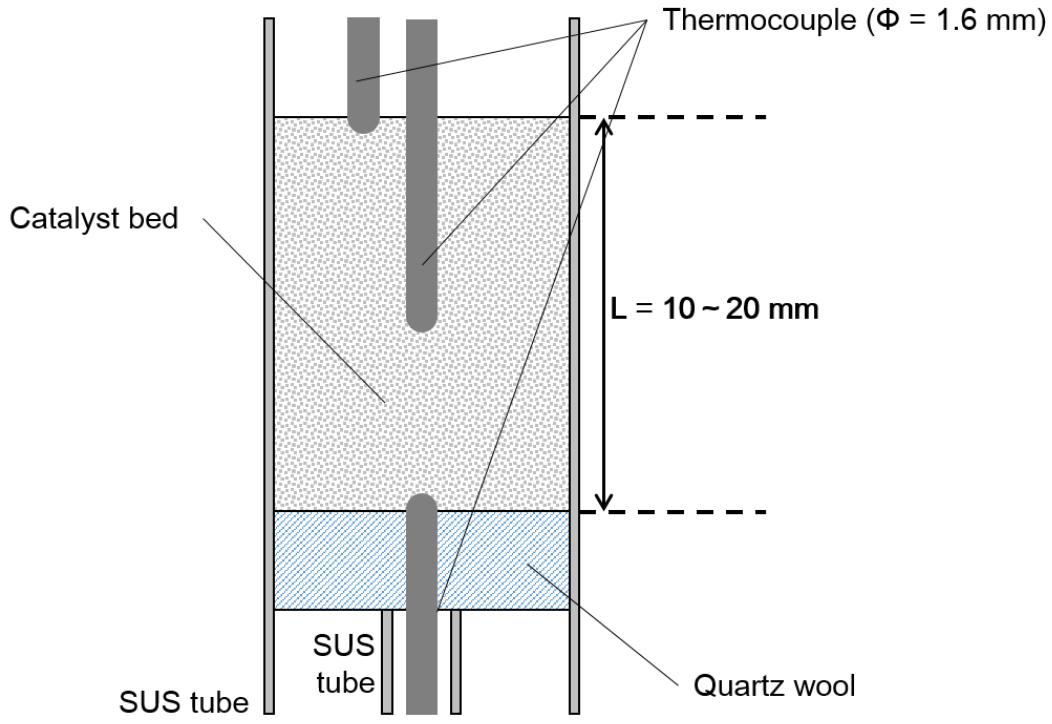

Fig. 2.2 Schematic illustration of Ni/SiO_2 bed monitored its temperatures by K-type thermocouples.

(outer diameter = 1.6 mm, CHINO Co, Ltd.) as shown in Fig. 2.1. These thermocouples monitored the top, middle and bottom of Ni/SiO_2 bed.

The catalysts bed was supported on a bed of quartz glass wool in the middle of the reactor. Catalyst particle was packed in the reactor, and the packed amount of Ni/SiO_2 was varied from 0 to 0.5 g in catalyst tests: bed height is up to 20 mm. The catalysts bed was heated using an electric furnace monitoring the temperature of the middle in the bed. Prior to the NH_3 decomposition test, the packed catalysts was reduced with pure H_2 gas at a flow rate of 100 ml min^{-1} for 1 h at 973 K. Following reduction, the catalyst bed was flushed with Ar gas, and reaction temperature was adjusted to 773, 823, 873, 923 or 973 K. A reactant gas, NH_3 (99.999 % purity, Tomoe Shokai. Co., Ltd.) was provided into the reactor, the flow rate of which was controlled by a float meter. Unreacted NH_3 and product gases (H_2 and N_2) from the reactor was treated by 10 wt% H_2SO_4 solution in an impinger to remove unreacted NH_3 gas, and then the flow rate of H_2 and N_2 mixture was measured be a soap film meter to estimate a conversion of NH_3. NH_3 decomposes as following equation:

$$NH_3 \rightarrow 1.5H_2 + 0.5N_2 \qquad \text{(Eq. 2-3).}$$

NH_3 conversion, X_{NH3} [-] was calculated by

$$X_{NH3} = 0.5F_{H2,N2} / F_{NH3} \qquad \text{(Eq. 2-4)}$$

where F_{NH3} and $F_{H2,N2}$ [ml min^{-1}] are flow rate of NH_3 and H_2/N_2 mixture respectively.

2.3. Results and discussion

2.3.1. Kinetic study of Ni/SiO_2 based on design equation of plug-flow-reactor

Figure 2.3 shows the NH_3 conversion over 0.1 g of Ni/SiO_2 bed (bed height, L = 0.4 mm) against GHSV at 873-973 K. GHSV was varied from 40,000 to 180,000 h^{-1}, in the specific NH_3 flow rate (per catalyst weight) of 1,300-6,000 ml min^{-1} g^{-1}. NH_3 conversions increased as temperature increased because higher temperatures can enhance the NH_3 decomposition reaction which is an endothermic reaction (see Eq. 2.1). Decreasing residence time, τ also increased NH_3 conversions at the whole temperatures examined. Below 923 K Ni/SiO_2 could not decompose NH_3 perfectly at 40,000 h^{-1}, however the results shows it can decompose NH_3 perfectly at 973 K and 40,000 h^{-1}.

To evaluate the kinetic constant, k and the activation energy, E_a of the tested Ni/SiO_2, a kinetic study was carried out based on the design equation of plug-flow-reactor (PFR) [7, 9]:

$$\tau = \int_{C_{NH3,0}}^{C_{NH3}} \frac{dC_{NH3}}{-r_{NH3}} \qquad \text{(Eq. 2-5)}$$

where τ is the residence time of gases [s], C_{NH3} is the concentration of NH_3 [mol m^{-3}], $C_{NH3,0}$ is the initial

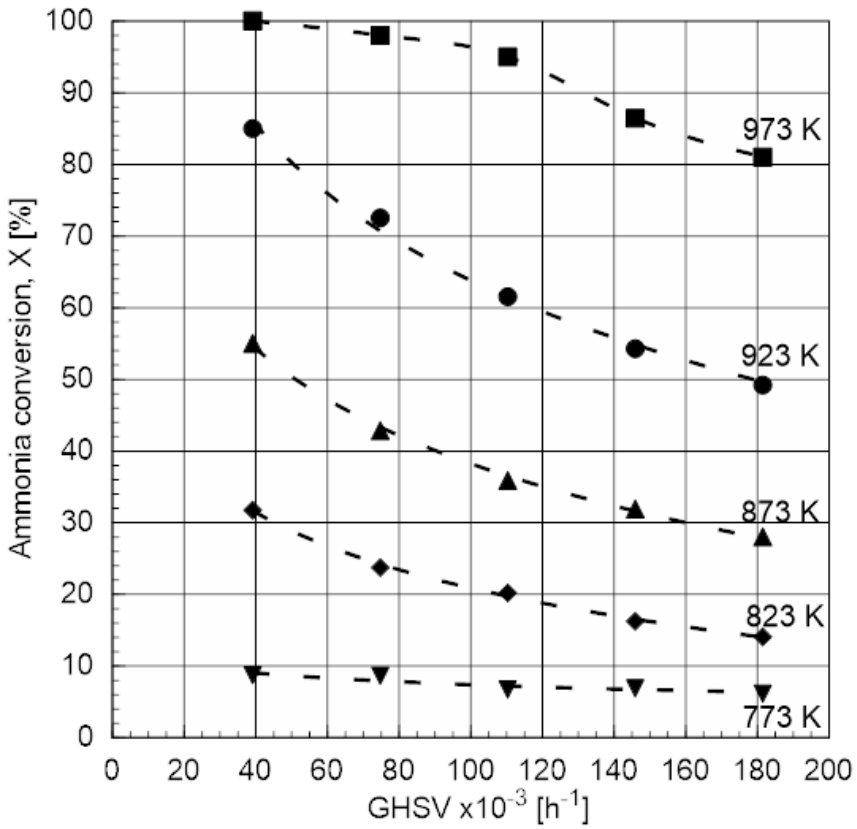

Fig. 2.3 NH_3 conversion over Ni/SiO_2 against GHSV at 873-973 K in a fixed-bed reactor.

GHSV is ranged from 40,000 to 180,000 h^{-1} and bed height is 4 mm.

concentration of inlet gas [mol m^{-3}] and $-r_{NH3}$ is the decomposition rate of NH_3 per unit volume [mol s^{-1} m^{-3}]. NH_3 decomposes according to Eq. 2-1, therefore a total gas volume is increases as NH_3 decomposes in a constant-pressure system. Here the fractional change in gas volume, V [m^3] of the system, ε_{NH3} is defined as:

$$\varepsilon_{NH3} = \frac{V_{X=1}-V_{x=0}}{V_{x=0}} = \frac{(1.5+0.5)-1}{1} = 1 \qquad \text{(Eq. 2-6)}$$

Using ε_{NH3} and X, C_{NH3} can be expressed as

$$C_{NH3} = \frac{\varepsilon_{NH3}-X}{\varepsilon_{NH3}+X} C_{NH3,0} = \frac{(1-X)}{(1+X)} C_{NH3,0} \qquad \text{(Eq. 2-7).}$$

Assuming a first-order reaction, the following equation can be obtained from Eq. 2-5 and 2-7

$$-r_{NH3} = \frac{k(1-X)}{(1+X)} C_{NH3,0} \qquad \text{(Eq. 2-8).}$$

where k [s^{-1}] is the kinetic constant of NH_3 decomposition reaction. Eq. 2-8 is inserted into Eq. 2-5 to obtain Eq. 2-9:

$$k\tau = 2\ln \frac{1+X}{1-X} - X \qquad \text{(Eq. 2-9)}$$

Fig. 2.4 shows plots of $k\tau = 2\ln \frac{1+X}{1-X} - X$ vs. τ for Ni/SiO_2 catalyst at 873-973 K. As shown in Fig. 2.4, linearity was obtained for theses plots. This linearity ensures that a first-order reaction is an applicable assumption (see Eq. 2-8). Values of slopes for 873–973 K obtained from Fig. 2.4 indicate kinetic constants, k. Using kinetic constants obtained from Fig. 2.4, temperature dependency of k can be shown as Fig. 2.5: this diagram is known as an Arrhenius plot. The activation energy, E_a and frequency factor, k_0 can be calculated from the slope and the intercept of vertical axis in this diagram respectively. From Fig. 2.4 E_a = 133 kJ mol^{-1} and k_0 = 21.4 s^{-1} were obtained.

2.3.2. Influences of temperature distribution in Ni/SiO_2 bed on kinetics

2.3.2.1. Gap between apparent and true kinetic constants at lower GHSV

Kinetic parameters, k and E_a of Ni/SiO_2 catalysts were analyzed from the Arrhenius plot shown in Fig. 2.5. However, as shown in Fig. 2.6, there are gaps between the "apparent" kinetic constant calculated from the Arrhenius plot and kinetic constants calculated from each residence time and NH_3 conversion. This result shows that kinetic constants increases with increasing of GHSV below 80,000 h^{-1}, whereas kinetic constants above 80,000 h^{-1} indicates almost same value. Generally heat conductivity in a fixed bed reactor

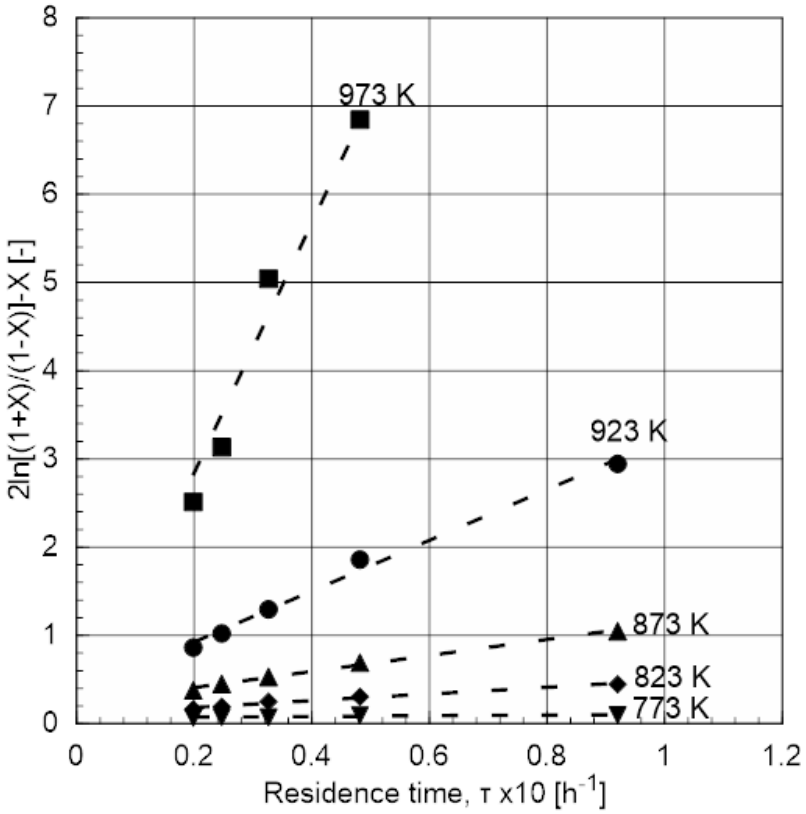

Fig. 2.4 $k\tau = 2\ln \frac{1+X}{1-X} - X$ against τ for Ni/SiO_2 fixed bed at 873-973 K.

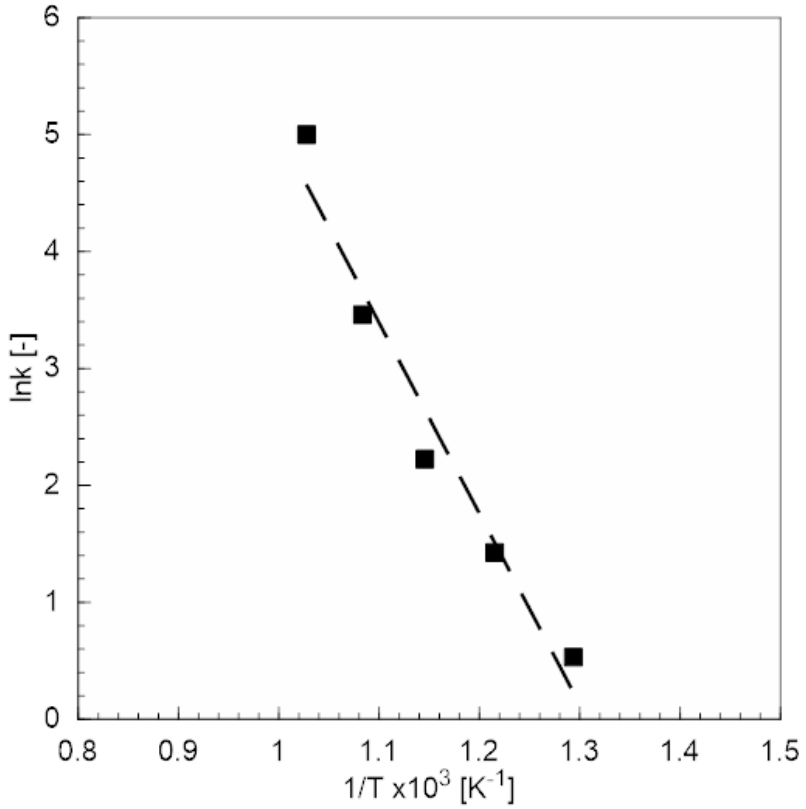

Figure 2.5 Arrhenius plot of Ni/SiO_2 catalyst for NH_3 decomposition.

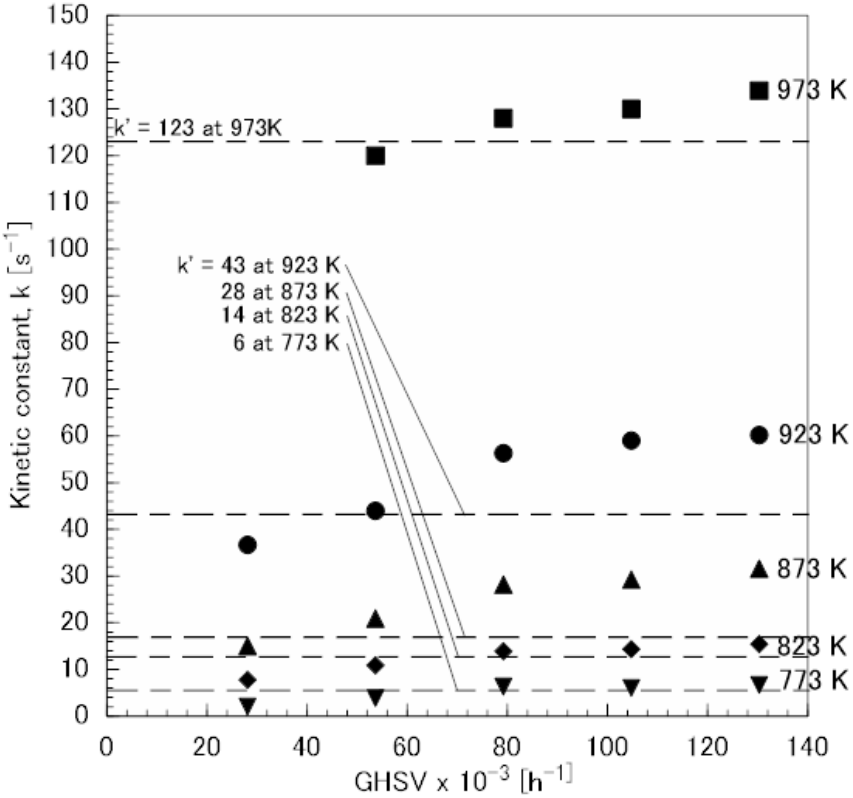

Fig. 2.6 Kinetic constants for each GHSV and apparent kinetic constants calculated from the Arrhenius plot (see Fig .2.5) against GHSV at 773-973 K.

is relatively low: this means that temperature distribution formed in a fixed-bed can cause a gap between apparent and true kinetic constants like observed in Fig. 2.6 [9]. However higher gas velocity can enhance the heat transfer in the bed [8, 9]. Thus it is considered that observed kinetic constants below 80,000 h^{-1} of GHSV was lower than true kinetic constants because of lower gas velocity: a formation of cold-spot in the bed along with NH_3 decomposition can decrease the reaction rate. On the other hand, it is considered that the observed kinetic constants at higher gas velocity (> 80,000 h^{-1}) is almost equal to true kinetic constants. Kinetic constants for 80,000 h^{-1} indicated E_a = 149 kJ mol^{-1} and k_0 = 23.2 s^{-1} were obtained.

2.3.2.2. Enthalpy balance and steady-state heat transfer in plug-flow-reactor

To estimate the influence of cold-spot formation in the fixed bed reactor, temperature distribution in the bed was analyzed. At the bed height, L = 4 mm (0.1 g of Ni/SiO_2 packed), although the temperature in the middle of the bed was monitored, it is difficult to measure temperatures for several bed height because the catalyst layer is very thin. Therefore, by monitoring temperatures of top, middle and bottom in fixed beds for L = 10, 16 and 20, the temperature distribution for L = 4 mm was speculated. The temperatures of these three place were measured using K-type thermocouple as shown in Fig. 2.2. Temperature distribution in the fixed-bed was estimated based on an enthalpy balance and a steady-state heat transfer in the axial direction (see Fig. 2.7) [7-10]; temperature distribution in the radial direction was assumed to be constant in each condition.

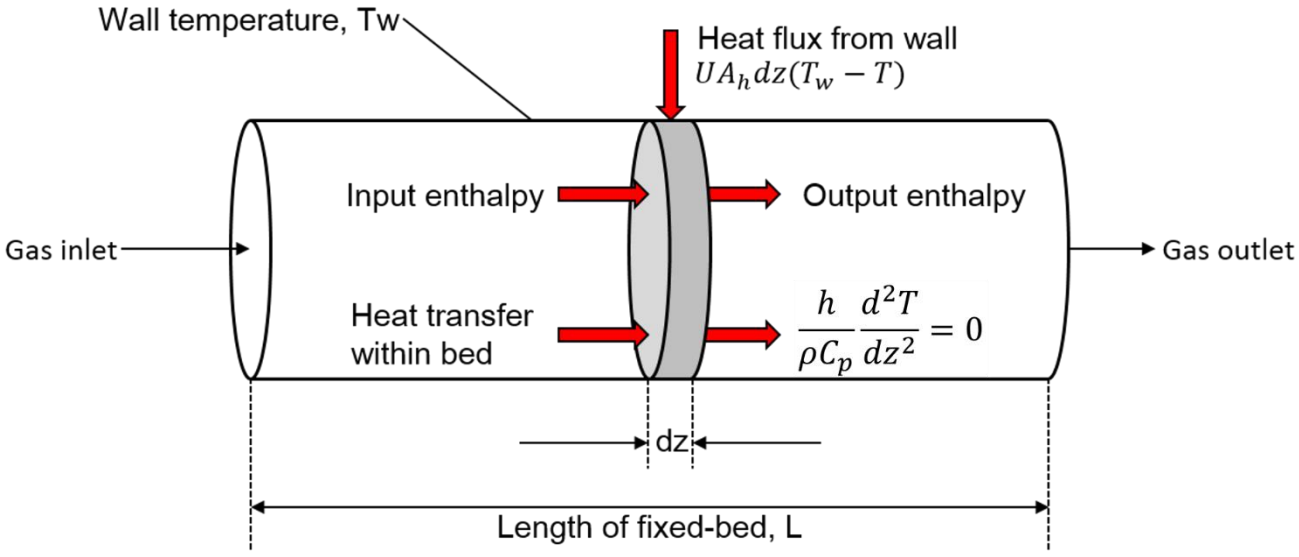

Fig. 2.7 Model of the enthalpy balance and heat steady state heat transfer in axial direction.

For simplicity, temperature distribution in the radial direction was assumed to be uniform in this system.

As shown in Fig. 2.7 take a thin place of the PFR: considering enthalpy balance and heat transfer between bed and wall, heat balance at steady state gives

(Heat transfer with wall) + (Input Enthalpy) = (Output enthalpy) (Eq. 2-10)

in symbols

$$UA_h dz(T_w - T) + \sum F_i H_i = \sum F_i H_i + \frac{d\sum F_i H_i}{dz} dz \quad \text{(Eq. 2-11-a)}$$

$$UA_h dz(T_w - T) = d\sum F_i H_i \quad \text{(Eq. 2-11-b)}$$

where

U [W m^{-2} K^{-1}] is the overall heat transfer coefficient,

A_h [m^2 m^{-1}] is the heat-transfer area per unit length of the reactor,

z [m] is the length in the axial length,

F [mol s^{-1}] is the molar flow rate of a reactant species, i (i = NH_3)

H [J mol_{-1}] is the enthalpy of a reactant species, i.

Developing equation Eq. 2-11-b, following equation can be obtained:

$$UA_h(T_w - T) = F_i \sum dH_i/dz + H_i \sum dF_i/dz \quad \text{(Eq. 2-12-a)}$$

$$UA_h(T_w - T) = F_i \sum (dH_i/dT)(dT/dz) + H_i \sum dF_i/dz \quad \text{(Eq. 2-12-b)}$$

$$UA_h(T_w - T) = \sum F_i C_{pi}(dT/dz) + H_i \sum dF_i/dz \quad \text{(Eq. 2-12-b)}$$

where

C_{pi} [J mol^{-1} K^{-1}] is the molar heat capacity at constant temperature of a reactant species.

In this system, second term in the right hand side of Eq. 2-12-b expresses the reaction heat along with NH_3 decomposition. Therefore

$$H_i \sum dF_i/dz = S(-r_{NH3})\Delta H_{NH3} \quad \text{(Eq. 2-13).}$$

where

S [m^2] is the crass-section area in the reactor,

r_{NH3} [mol s^{-1} m^{-3}] is the reaction rate of the NH_3 per unit volume.

Inserting Eq. 2-13 into Eq. 2-14-b, the following equation can be obtained

$$UA_h(T_w - T) = F_{NH3} C_{p,NH3}(dT/dz) + S(-r_{NH3})\Delta H_{NH3} \quad \text{(Eq. 2-14)}$$

In this equation, reaction rate, r can be expressed using ammonia conversion, X as

$$F_{NH3} dX_{NH3}/dz = -r_{NH3} \quad \text{(Eq. 2-15).}$$

Eq. 2-14 and 2-15 are the design equation of the isothermal PFR, therefore temperature distribution can be obtained by solving these equations.

Note that it is easy to evaluate the temperature distribution if the Eq. 2.14 was expressed by independent variable X_{NH3}, not z [9]. From the experimental results as shown in Fig. 2.3, the change of residence time, τ against ΔX_{NH3} can be obtained. Thus Eq. 2.14 and 2.15 should be rewritten as

$$dT/dX_{NH3} = \Delta T_{ad} + \{UA_h(T_w - T)/C_{p,NH3}\}/(-r_{NH3}S) \quad \text{(Eq. 2-16)}$$

$$dz/dX_{NH3} = F_{NH3}/(-r_{NH3}S) \quad \text{(Eq. 2-17)}$$

where

ΔT_{ad} [K] is the adiabatic temperature change, which is defined as $\Delta T_{ad} = -\Delta H_{NH3}/C_{p,NH3}$.

As shown in Fig. 2.7, heat transfer equation in the axial direction at steady state can be expressed in symbols as

$$\frac{h}{\rho\, C_{p,bed}} \frac{d^2T}{dz^2} = 0 \quad \text{(Eq. 2-18)}$$

where

h [J s^{-1} m^{-1} K^{-1}] is the heat-transfer coefficient of the bed,

$C_{p,bed}$ [J kg^{-1} K^{-1}] is the heat capacity of the bed,

ρ [kg m^{-3}] is the bulk density of the bed.

Discretizing d^2T/dz^2 as

$$\frac{d^2T}{dz_{NH3}^2} \approx \frac{T_{z+\Delta z} + T_{z-\Delta z} - 2T}{\Delta z^2} \quad \text{(Eq. 2-19)} \quad ,$$

numerical calculation was carried out to evaluate temperature distribution [7].

2.3.2.3. Temperature distribution in the fixed bed reactor for L = 10, 16 and 20 mm

Using Eq. 2-16, 2-17 and 2-19, temperature distribution was estimated. As shown in Fig. 2.2, the temperatures at the top, middle and bottom (T_{inlet}, T_r and T_{outlet}) of the bed were measured. Therefore, using U and T_w as fitting parameters, suitable values were given to U and T_w as calculated T_{inlet}, T_r and T_{outlet} were equal to measured values.

Fig. 2.8 shows the NH_3 conversion change against specific NH_3 flow rate for L = 20 mm. Fig. 2.9 shows a calculated temperature distribution and a change of conversion against bed height for the experimental conditions, L = 20 mm, GHSV = 80,000 h^{-1} and T_r = 923 K. This figure shows that temperatures in the bed domestically declined to ca. 820 K, and temperatures gradually increased to ca. 965 K. Note that a cold-spot was formed in the bed at L = 2 mm, and it is considered that this cold-spot formation caused the decreasing the apparent kinetic constants. Conversion change against bed height was affected by the temperature distribution. Note that kinetic constants for > 80,000h^{-1} was used to calculate NH_3 conversion. Below 2 mm of bed height the slope of the curve decreased, whereas at downstream of cold spot formation the slope increased due to

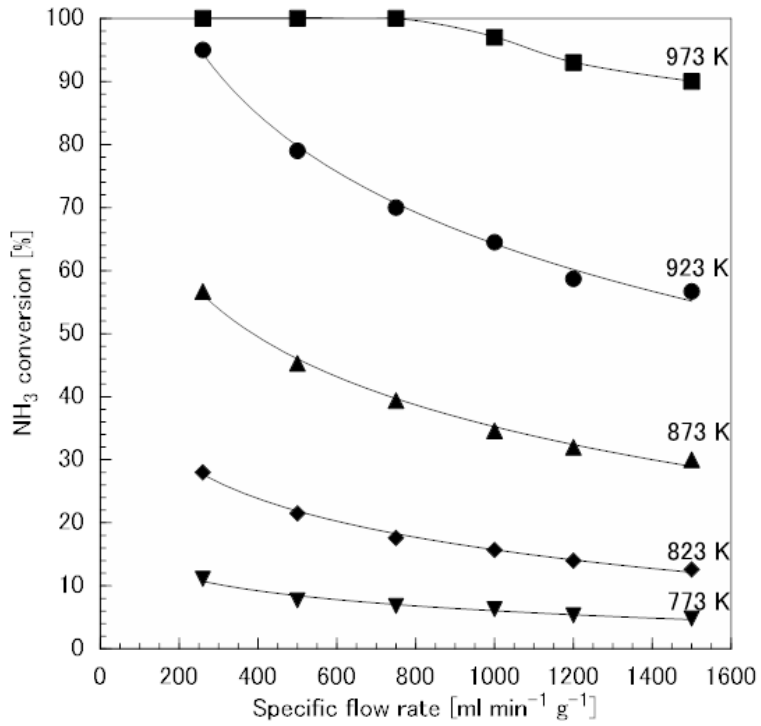

Fig. 2.8 NH_3 conversion against specific NH_3 flow rate (per catalyst weight) at 873-973 K.

Ni/SiO_2 Bed height was 20 mm.

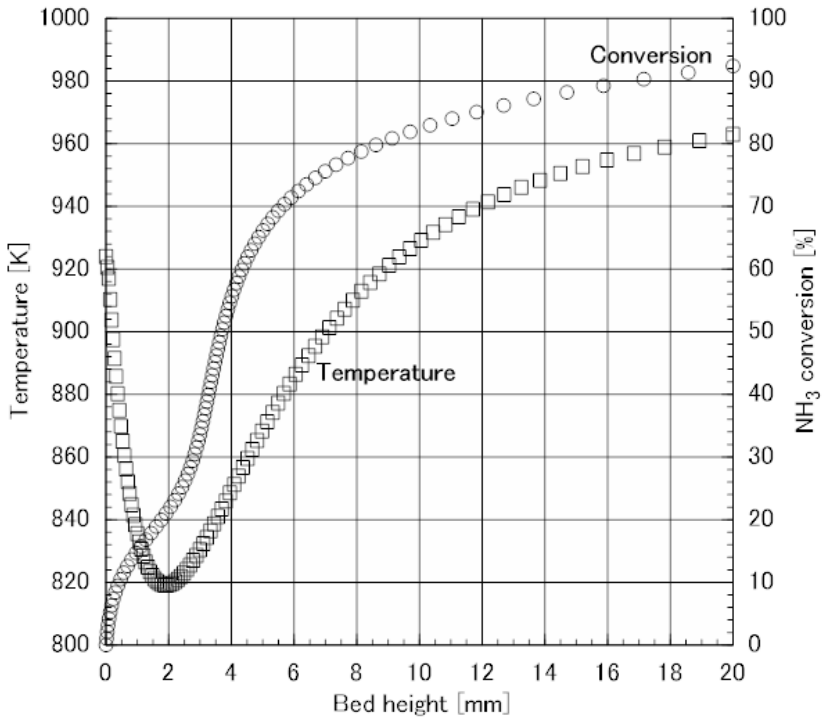

Fig. 2.9 Temperature and NH_3 conversion against bed height.

0.5 g of Ni/SiO_2 was packed (bed height, L = 20 mm),

and temperature of the middle in the bed was controlled as it maintained 923 K.

increase of the temperature. Calculated NH_3 conversion was equal to 93 %, whereas measured NH_3 conversion was 92 %. Thus it is concluded that calculation results shown in Fig. 2.9 is valid.

Temperature distribution for L = 20 mm and 873-973 k was shown in Fig. 2.10 (see the next page). As shown in this figure, temperature distribution was more uniform at higher gas velocity at whole temperatures examined. At 973 K, temperature declined from 973 K to ca. 800 K for 10 cm s^{-1} of gas velocity, whereas declined to 870 K for 25 cm s^{-1}. It is considered that higher gas velocity increased the overall heat transfer coefficient, U to uniform the temperature distribution. Fig. 2.11 shows U against gas velocity at 873-973 K. As shown in this figure U is monotonically increases as gas velocity increases at whole temperatures examined. Thus it is found that higher gas velocity is necessary to eliminate the gas between apparent and true kinetic constants.

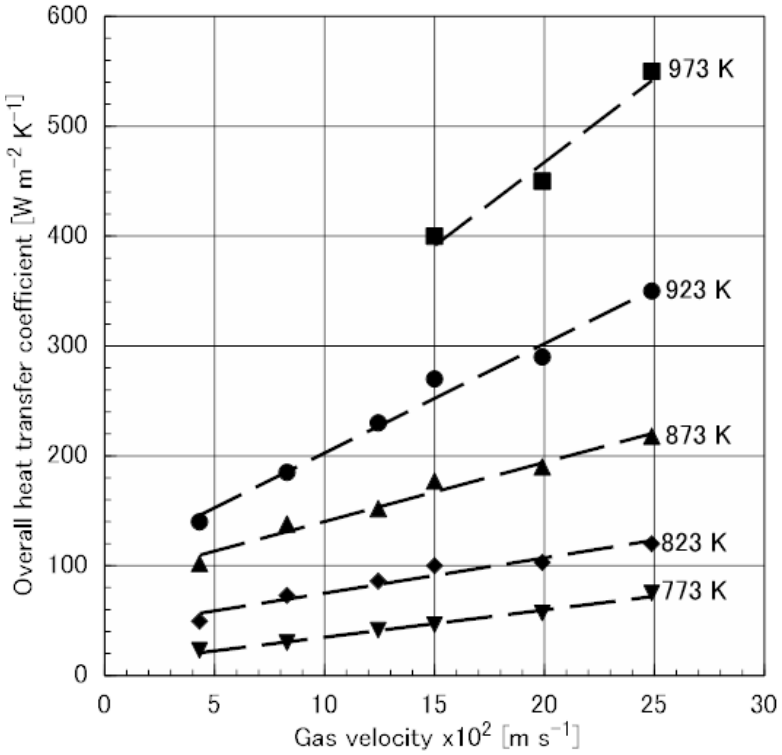

Fig. 2.11 Overall heat transfer coefficient vs. gas velocity at 873-973 K and L = 20.

At 923 K temperature for 25 cm s^{-1} of gas velocity decreased to ca. 900 K below L = 2 mmm, thus it is found that temperature distribution was more uniform at lower reaction temperature. This is because higher temperature can facilitate the NH_3 decomposition rate to increase NH_3 conversion, in other words more heat in the bed was consumed along with NH_3 decomposition. Below 823 K temperatures in the bed was almost constant and independent of gas velocity, because at lower temperature NH_3 conversions were very low as shown in Fig. 2.8.

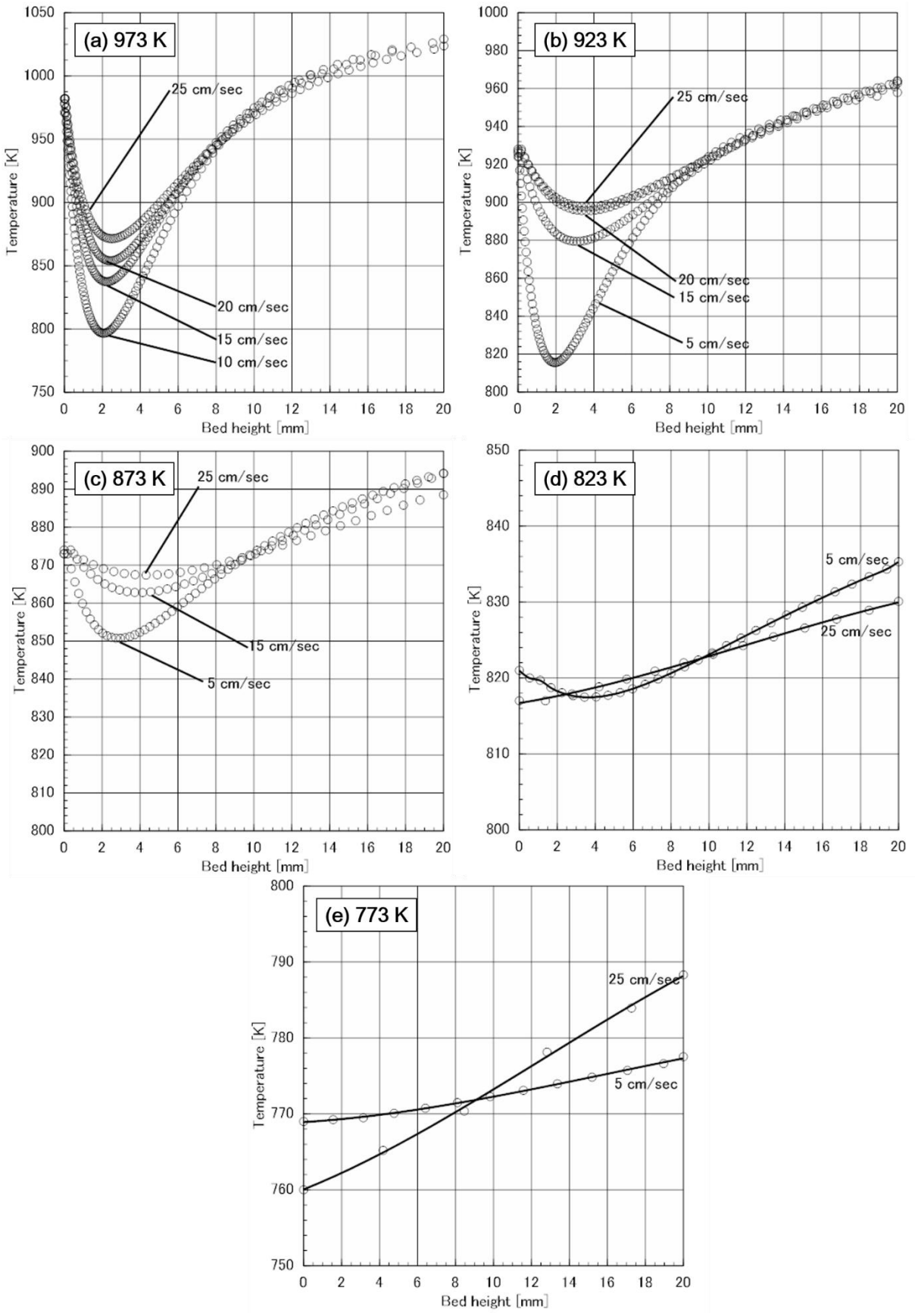

Fig. 2.10 Temperature distribution for L = 20 mm at 873-973 K.

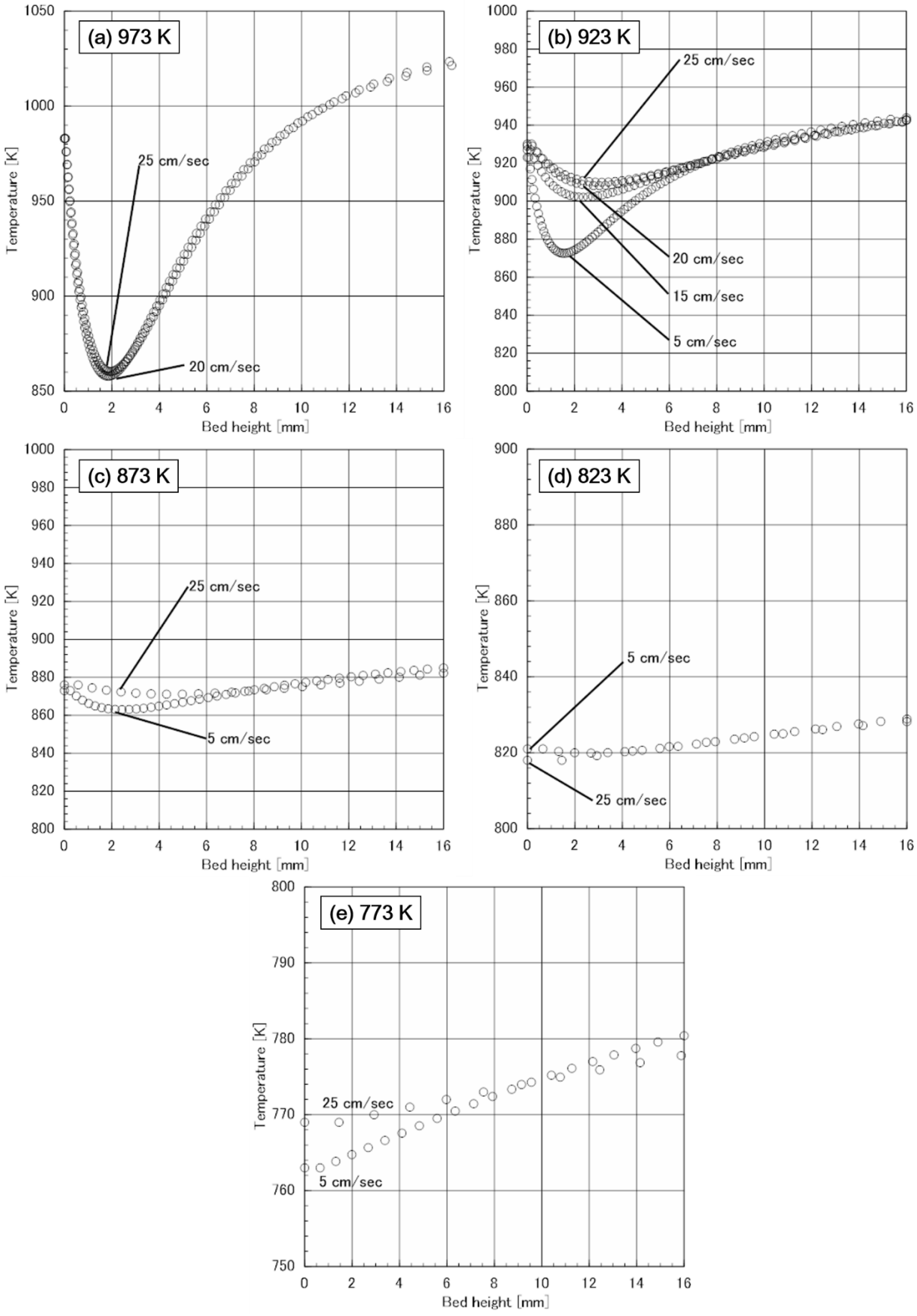

Fig. 2.12 Temperature distribution for L = 16 mm at 873-973 K.

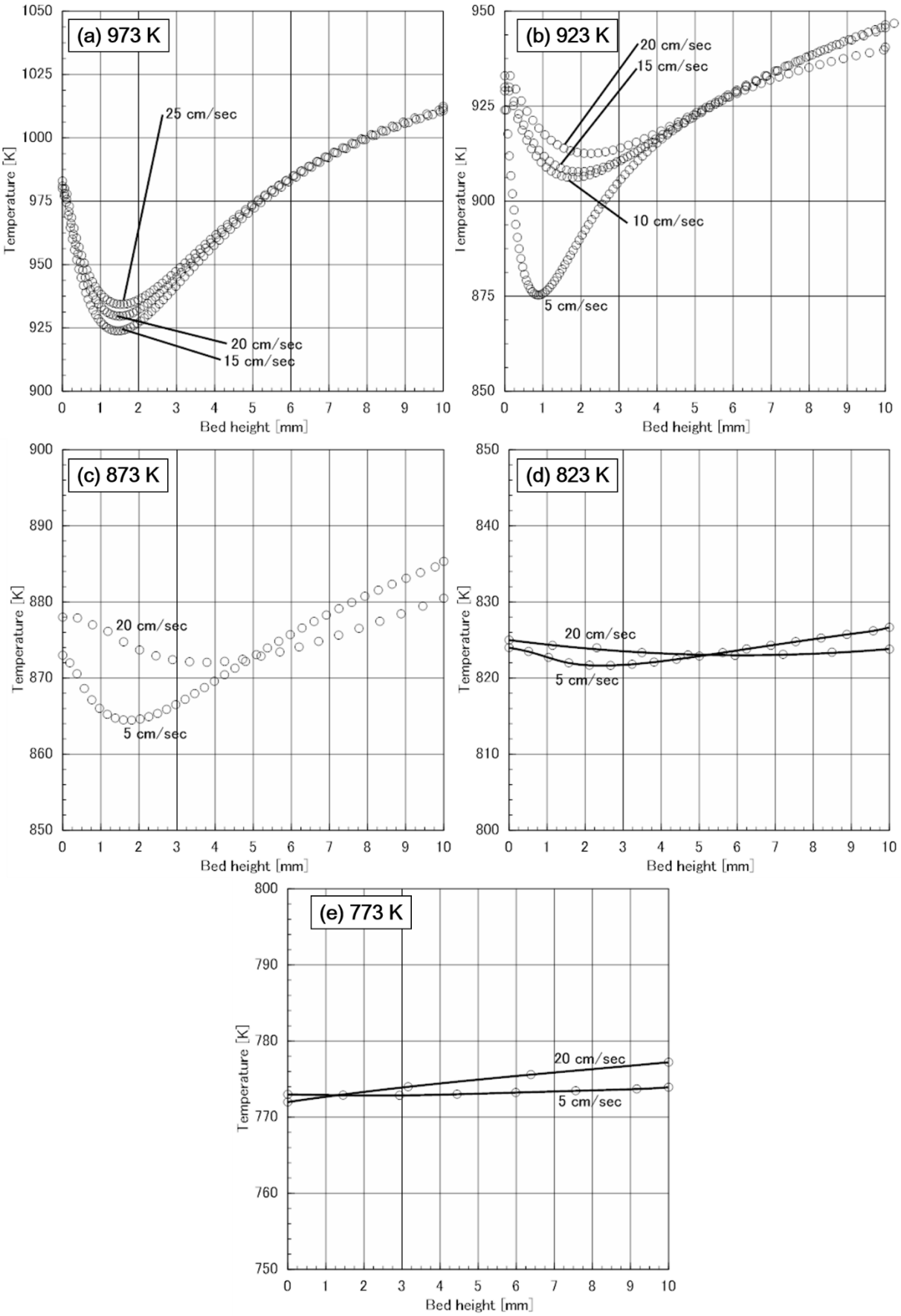

Fig. 2.13 Temperature distribution for L = 10 mm at 873-973 K.

Temperature distribution for L = 16 and 10 mm was also calculated (see Fig. 2.12 and 2.13). Note that temperature distribution where NH_3 conversion is 100 % can't be calculated (see Eq. 2-9). These figures show that lower bed height can make the temperature distribution uniform at whole temperatures examined. For instance, Fig. 2.14 shows the temperature distribution for L = 10, 16 and 20 mm at T_r = 923 K. minimal values of the three curves in this figure are 914, 907 and 897 K for L = 10, 16 and 20 mm respectively. It is considered that, in the lower bed height, heat transfer in the axial direction was dominant and makes the temperatures in the bed uniform. Thus it is speculated that the temperature distribution of the Ni/SiO_2 bed for L = 4 mm should be more uniform than those above 10 mm of bed height.

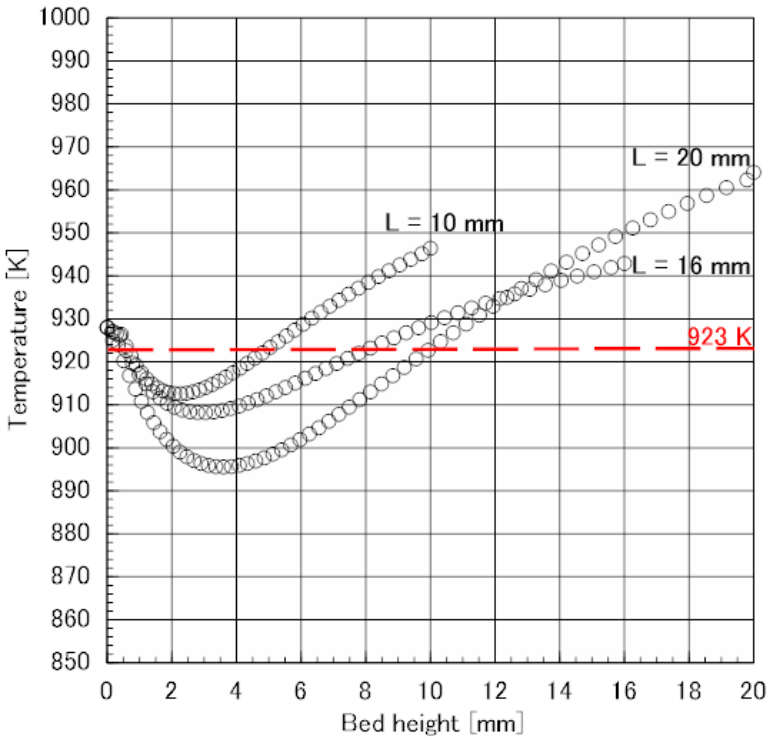

Fig. 2.14 Temperature distribution at T_r = 923 K for L = 10, 16 and 20 mm. NH_3 gas velocity is 20 cm s^{-1} in each case.

2.3.2.4. Estimation of temperature distribution in the fixed bed reactor for L = 4 mm

Using the results obtained from Fig. 2.10, 2.12 and 2.13, a temperature distribution for L = 4 mm was tried to estimate. As shown Fig. 2.10 to 2.14, inlet temperatures was equal to the temperatures in the middle of the beds, T_r or up to 5 K higher than T_r. Therefore the inlet temperature for L = 4 mm was assumed to be equal to T_r + 5 K. Wall temperatures, T_w was estimated by T_w for L = 10-20 mm. Fig. 2.15 shows the T_w against gas velocity for L = 10, 16 and 20 mm at T_r = 923 K.

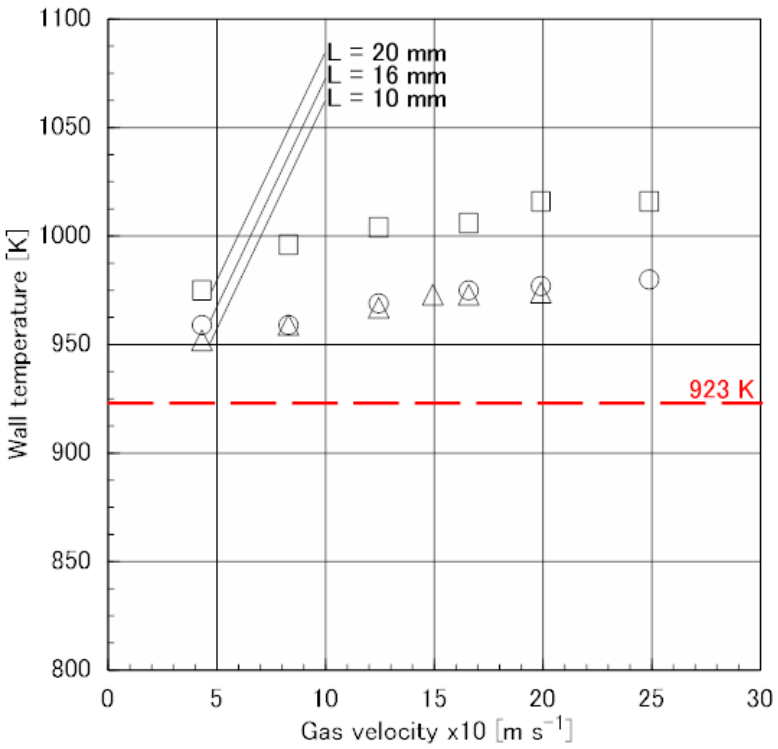

Fig. 2.15 Wall temperature, T_w against gas velocity for L = 10, 16 and 20 mm at T_r = 923 K.

As shown in this figure, the T_w for L = 20 was higher than that for L = 16, whereas those for L = 10 and 16 is almost same. Though not shown, similar tendency was observed at whole temperature examined, thus it is assumed that T_w for L = 4 mm was same to that for L = 10 mm.

Temperature distribution for L = 4 mm was estimated in the T_r ranged from 773 to 973 K as shown in Fig. 2.16. At T_r = 973 K, temperature distribution was more uniform at higher gas velocity. Above 20 cm s^{-1} temperature distribution was almost uniform: variation in temperatures are less than ±5 K and at 15 cm s^{-1} the minimal temperature is 10 K lower than T_r. As shown in Fig. 2.6, kinetic constants at T_r = 973 K decreased below 80,000 h^{-1} (15 cm s^{-1} of gas velocity). Thus, gas velocity should be more than 15 cm s^{-1} to eliminate cold-spot formation as the variation of temperature was less than ±10 K to evaluate a true kinetic constant of a catalyst. Below T_r = 923 K, more than 15 cm s^{-1} of gas velocity can make uniform the temperature distribution as variations of temperature were less than ±5 K. Therefore it is considered that conditions of less than ±5 K temperature distribution is necessary to evaluate a true kinetic constant below 923 K.

Muroyama et. al. examined 10 wt% Ni/SiO_2 catalysts using a fixed-bed reactor, however they conducted catalysts test at specific NH_3 flow rate, F´ = 100 ml min^{-1} g^{-1} [5]. If the inner diameter of the reactor which they used had been same to those in this study, the gas velocity was only 0.3 cm s^{-1}. For instance their Ni/SiO_2 decomposed 85 % of NH_3 at 873 K, and this means the kinetic constant in this condition should be

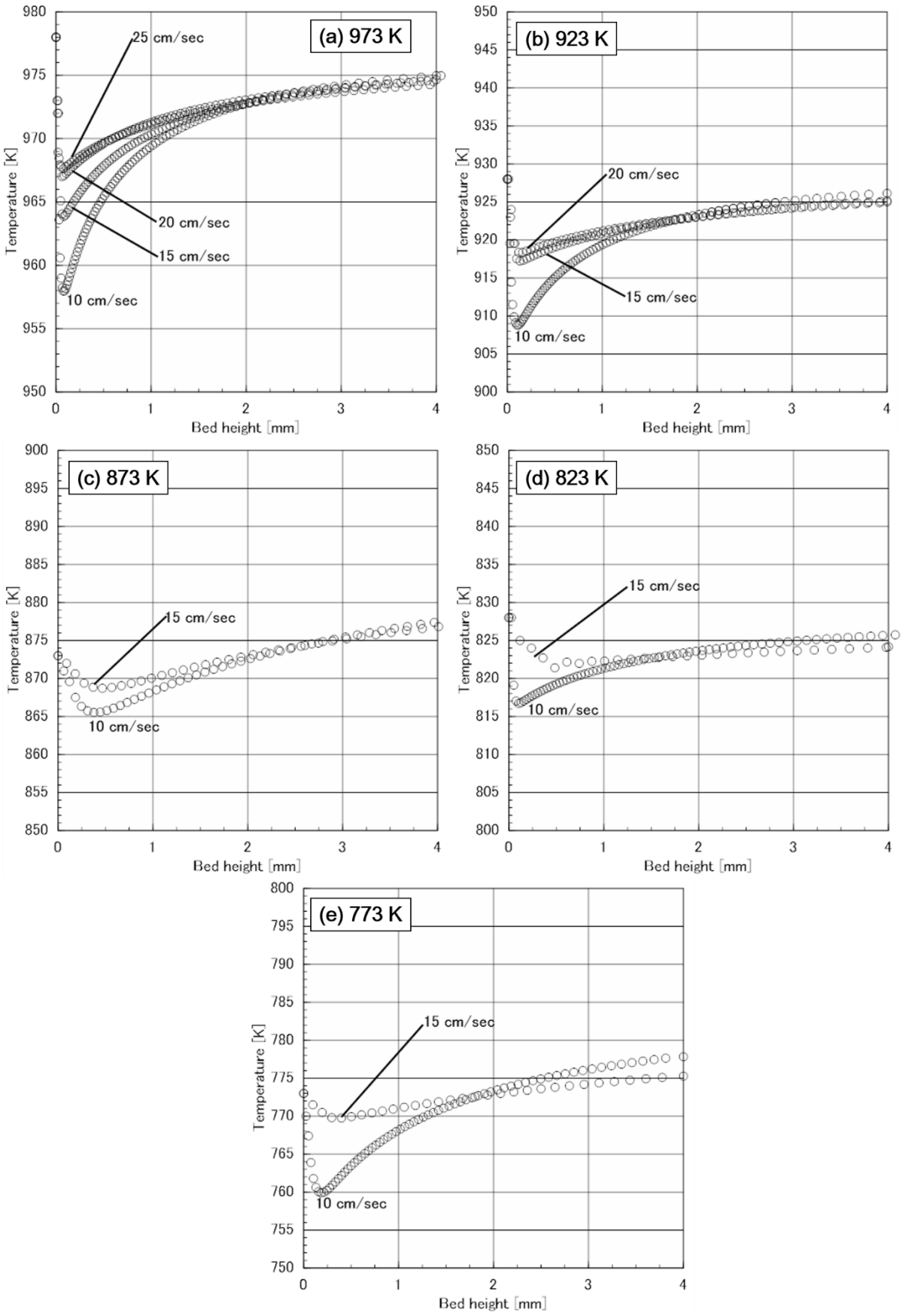

Fig. 2.16 Estimated temperature distribution for L = 4 mm at 873-973 K.

equal to 2.3 s^{-1}, whereas k for more than 15 cm s^{-1} of gas velocity was 28 s^{-1} in this study. This results indicated that their data was affected by cold-spot formation. Thus it is important to estimate various Ni catalysts under the experimental conditions where influences of temperature distribution were eliminated.

2.4. Summary

In this chapter, kinetics of Ni/SiO_2 was studied as 0.1 g of the catalyst was packed in the fixed-bed reactor based on a design equation of a plug-flow reactor. Apparent kinetic constants were evaluated in the gas velocities ranged from 5 to 25 cm s^{-1} (in the GHSV ranged from 40,000 to 180,000 h^{-1}), however there were gas between apparent kinetic constants and kinetic constant, k for >80,000 h^{-1} (> 15 cm s^{-1} of gas velocity) Although k for >80,000 h^{-1} for each gas velocity was almost constant, those for < 15 cm s^{-1} decreased as gas velocity decreased. It is considered that low gas velocities indicated the formation of cold-spot in the bed to decreases the decomposition rate. Form experimental results, k for GHSV ranged from 5 to 25 cm s^{-1} indicated E_a = 133 kJ mol^{-1} and k_0 = 21.4 s^{-1}, whereas k for > 15 cm s^{-1} indicated E_a = 149 kJ mol^{-1} and k_0 = 23.2 s^{-1}. Thus more than 15 cm s^{-1} of gas velocity is necessary to evaluate true value of k.

To observe the influences of the cold-spot formation on the catalytic activities, temperature distribution of Ni/SiO_2 bed was estimated. The temperature distribution was estimated solving an enthalpy balance and a heat transfer in the axial direction in the bed. Estimated temperature distribution indicated that higher gas velocity make distribution in the bed more uniform in the whole temperature examined. At more than 15 cm s^{-1} of the gas velocity, the variation of the temperature distribution for T_r = 973 K was less than ±10 K, and those below 923 K was less than ±5 K: in these conditions the influences can be eliminated to evaluate certain kinetic constants.

Reference

[1] S. F. Yin, B. Q. Xu, X. P. Zhou, C. T. Au. A mini-review on ammonia decomposition catalysts for on-site generation of hydrogen for fuel cell applications. *Applied Catalysis A : General*, 277, 1-9 (2004)

[2] A. S. Chellappa, C. M. Fischer, W. J. Thomsom. Ammonia decomposition kinetics over Ni-Pt/Al_2O_3 for PEM fuel cell applications.

[3] T. V. Choudhary, C Sivadinarayana, D. W. Goodman. Catalytic ammonia decomposition: COx-free hydrogen production for fuel cell applications. *Catalyst letter*, 72, 197-201 (2001)

[4] J. Zhang, H. Xu, W. Li. Kinetic study of NH_3 decomposition over Ni nanoparticles: the role of La promoter, structure sensitivity and compensation effect. *Applied Catalysis A : General*, 296, 257-267 (2005)

[5] H. Muroyama, C. Saburi, T. Matsui, K. Eguchi. Ammonia decomposition over Ni/La_2O_3 catalyst for on-site generation of hydrogen. *Applied Catalysis A : General*, 443-444, 119-124 (2012)

[6] R. Atsumi, R. Noda, H. Takagi, L. Vecchione, A. Di Carlo, Z. Del Prete, K. Kuramoto. Ammonia decomposition activity over Ni/SiO_2 catalysts with different pore diameter. *International Journal of Hydrogen Energy*, 39, 13954-13961 (2014)

[7] O. Leavenspiel. Chemical Reaction Engineering (3rd edition). P101. *John Wiley and Sons, Inc.*, New York (1998)

[8] R. B. Bird, W. E. Stewart, E. N. Lightfoot. Transport Phenomena (Second Edition). P301. *John Wiley and Sons, Inc.*, New York (2002)

[9] 橋本健治, 反応工学 改訂版, 培風館 (1993)

[10] 久保田宏, 関沢恒男, 反応工学概論 第 2 版, 日刊工業新聞社 (1986)

Chapter 3 Influences of Pore Diameter on Kinetics of Ni/SiO_2 Catalysts for Ammonia Decomposition

3.1. Introduction

In Chapter 2, kinetic study was conducted based on a design equation of a plug-flow-reactor. Furthermore, the influences of a cold-spot formation on kinetics of Ni/SiO_2 fixed-beds for NH_3 decomposition were discussed to evaluate true kinetic constants of the catalysts. Experimental results indicated that higher gas velocities 15 cm s^{-1} or faster can eliminate the influences of temperature distribution and make it uniform as the variation of temperature distribution is ±5 or ±10 K at $\leq$ 923 K or 973 K, respectively.

As discussed in previous chapter, heat transfer in catalyst beds is dominant in the kinetics of catalysts. On the other hand, mass transfer in catalyst's pores potentially affects the apparent kinetic constants and activated energies [1-3]. However few research have not investigated the correlation between pore structure and kinetics of NH_3 decomposition. In this chapter, to clarify influences of pore diffusion in catalysts on catalytic activities, the NH_3 conversions was evaluated in a fixed-bed for various GHSV conditions using Ni/SiO_2 with different pore diameters.

3.2. Experimental

3.2.1. Catalyst test

10 wt% Ni/SiO_2 catalysts were prepared by a wet impregnation method (see Chapter 2). The porous silica particles CARiACT Q-3, Q-15, Q-30, and Q-50 (the particle size is ranged from 75 to 150 μm, mean diameter is 112.5 μm, Fuji Silysia, Ltd.) were selected as support materials; these particles possessed mean pore diameters ranging from 3.7 to 19.9 nm, which is nearly equal to the mean free path of an NH_3 molecule. Pore diameters smaller than mean free path would have decreased the apparent activation energy for NH_3 decomposition [1-3].

Ni/SiO_2 catalysts with different mean pore diameter were tested in the fixe-bed reactor as shown in Fig. 2.1 (see Chapter 2). 0.1 g of the catalyst was packed in the stainless tube, and NH_3 in the GHSV ranged from 10,000 to 180,000 h^{-1} was provided into the catalyst bed.

3.2.2. Characterization

The crystallite diameters of Ni nanoparticles, D_{Ni} were determined by an XRD (Rint-2000, Rigaku Ltd.) operated at 30 kV / 20 mA with a scanning rate of 0.1^{o} min^{-1}. Crystallite sizes were evaluated using the Scherrer equation. Amount of loaded-Ni for each Ni/SiO_2 was evaluated by an XRF. The specific surface area of catalysts was measured by the Brunauer-Emmett-Teller (BET) method with N_2 adsorption at 77 K. Pore structure was determined by means of a mercury intrusion technique (Autopore IV 9520, Micrometrics Ltd.). The characteristics of the Ni/SiO_2 catalysts are presented in Table 3.1.

Table 3.1 Characteristics of Ni/SiO_2 catalysts.

D_{Ni} [nm]	M_{Ni} [wt%]	S_{BET} [m^2 g^{-1}]	d' [nm]	V_{pore} [ml g^{-1}]
13.8	9.9	410	7.7	0.51
26.7	9.3	160	16.6	2.34
30.9	9.2	100	26.7	2.26
24.9	9.3	60	34.8	2.45

D_{Ni}: crystallite size of Ni nanoparticles, M_{Ni}: amount of loaded-Ni S_{BET}: specific BET surface area, d': mean pore diameter, V_{pore}: pore volume of catalyst.

3.3. Results and discussion

3.3.1 The influences of pore diameter on catalytic activities of Ni/SiO_2

To observe the kinetics in pore, NH_3 decomposition tests via Ni/SiO_2 catalysts with different pore diameter were carried out. As shown in Table 3.1, mean pore diameters were varied from 7.7 to 34.8 nm. The extent of NH_3 conversion is plotted against GHSV in Fig. 3.1. Although silica-supported catalysts with different pore diameters exhibited difference activities, there was only poor correlation between pore diameter and catalytic activity. At reaction temperature of 773, 823 and 873 K, the activity for the smallest mean diameter, $\bar{d}$ = 7.7 nm, was the highest (see Fig. 2.11 a-c). To clarify the relationships between crystallite size of Ni nanoparticles (D_{Ni}) and catalytic activity, D_{Ni} was evaluated by means of XRD (see Table 3.1). Fig. 3.1 and Table 3.1 indicate that the catalytic activity increased as decreased D_{Ni} for temperatures lower than 873 K. Smaller pores provided a higher surface area to increase the dispersion of Ni. It was concluded that this was the reason why the highest catalytic activity was observed for Ni supported on the smallest silica particles. These results illustrate that dispersion of loaded metal enhances catalytic activity. However, at 923 and 973 K, the catalytic activity for D_{Ni} = 13.8 nm and $\bar{d}$ = 7.7 nm was found to be slightly lower; Ni/SiO_2 for D_{Ni} = 30.9 nm and $\bar{d}$ = 26.7 nm was the most active at these temperatures. It was speculated that the pore diffusion

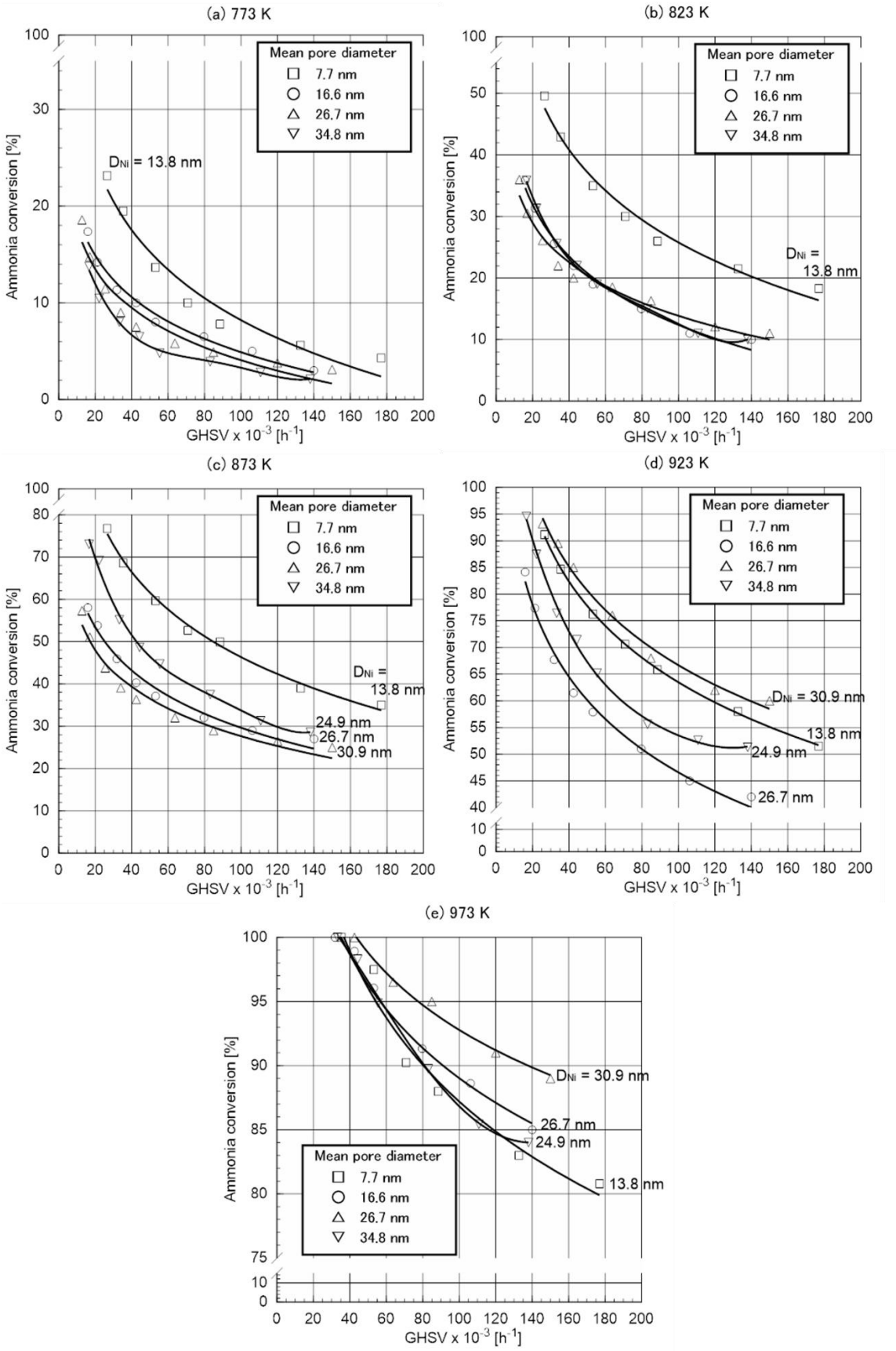

Fig. 3.1 NH_3 conversion against GHSV over Ni/SiO_2 catalysts with different pore diameter from 773 to 973 K.

resistance decreased NH_3 conversion for $\bar{d}$ = 7.7 nm at 923 and 973 K.

Almost complete decomposition of NH_3 was achieved at 973 K and GHSV of 36,000, 32,000, 42,000, and 3,300 for $\bar{d}$ = 7.7, 16.6, 26.7 and 34.8 nm, respectively; therefore, it was conducted that the Ni/SiO_2 catalyst with $\bar{d}$ = 26.7 nm was the most active from the view point of efficient hydrogen production. Kinetic study for each Ni/SiO_2 catalyst was carried out to make clear the correlation between NH_3 decomposition rates and pore diffusion process. As mention in Chapter 2, kinetic constants were evaluated using Eq. 2-9. Note that the data of conversions for > 80,000 h^{-1} were used for evaluation of k to eliminate the influences of a cold-spot formation. Fig. 3.2 shows the Arrhenius plot for Ni/SiO_2 catalysts from 773 to 973 K. The activation energy and frequency factor for each catalyst are summarized in Table 3.2 and Fig. 3.3. It is found that the activation energy and frequency factor for $\bar{d}$ = 7.7 nm are lower than those for other Ni/SiO_2 catalysts, which all had similar activation energies and frequency factors. It is concluded that the high diffusion resistance of the small pores must have decreased the apparent activation energy and the NH_3 conversion of Ni/SiO_2 for $\bar{d}$ = 7.7 at 973 K. From Fig. 3.1 (d) and (e), it is shown that Ni/SiO_2 for these properties exhibited lower activity than others due to increasing of the diffusion resistance.

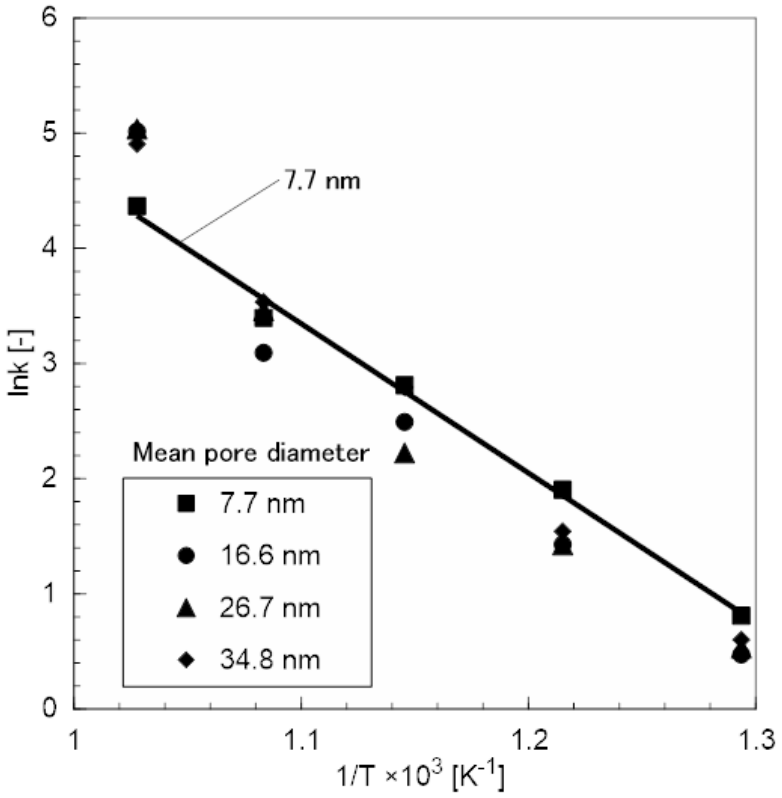

Fig. 3.2 Arrhenius plot of Ni/SiO_2 catalysts with different mean pore diameters from 773 to 973 K.

The data of conversions for > 80,000 h^{-1} of GHSV was used to calculate kinetic constants.

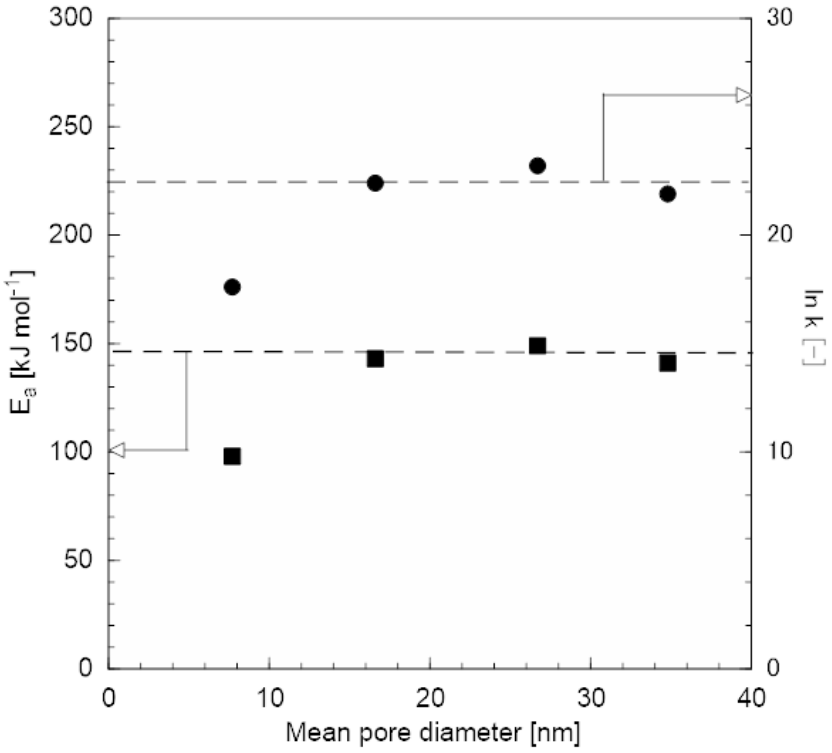

Fig. 3.3 Activation energy and frequency factor plotted against pore diameter of Ni/SiO$_2$ catalysts.

Table 3.2 Activation energy and frequency factor on Ni/SiO$_2$ catalysts.

$\bar{d}$ [nm]	Activation energy [kJ mol^{-1}]	Frequency factor [s^{-1}]
7.7	98	17.6
16.6	143	22.4
26.7	149	23.2
34.8	141	21.9

3.3.2 Estimation of pore distribution and pore diffusion in Ni/SiO$_2$

It is necessary to estimate the pore diffusion resistance affecting the catalytic activity for $\bar{d}$ = 7.7 nm. Fig. 3.4 shows the pore distribution of the Ni/SiO$_2$ catalysts. The values of $\bar{d}$ for each support was calculated from pore distribution shown in Fig. 3.4, and it is found that the Ni/SiO$_2$ catalyst with $\bar{d}$ = 7.7 nm had many pores smaller than 10 nm in diameter, whereas the others had a defined peak above 10 nm. Note that there peaks at ca. 40 μm for each pore distribution, however these peaks derived from voids of catalysts particle and didn't use to evaluate mean pore diameters. As shown in Fig. 3.4 and Table 3.1, D_{Ni} on Ni/SiO2 catalysts was slightly different from mean pore diameter. Therefore it is speculated that the mean diameter of pores which contributes NH_3 decomposition, in other words where Ni particles were loaded is equal to D_{Ni}.

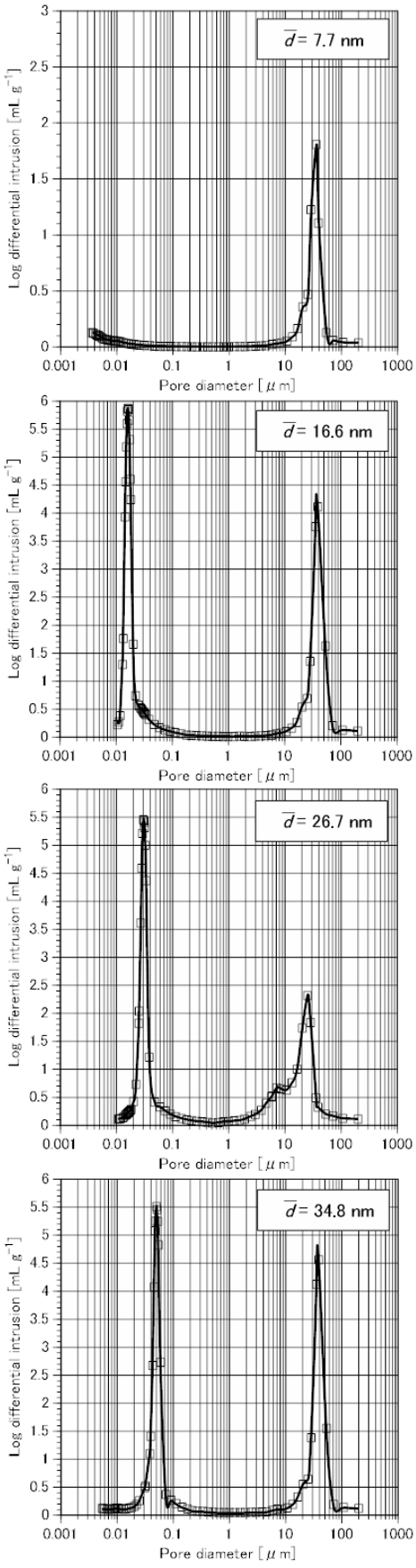

Fig. 3.4 Pore distribution of Ni/SiO_2 catalysts for $\overline{d}$ = 7.7, 16.6, 26.7 and 34.8 nm.

To investigate the gas between mean pore diameter and D_{Ni}, loaded-Ni nanoparticles were observed by a transmission electron microscope (TEM, JEM-1400, JEOL Ltd.). Fig. 3.5 shows the TEM images of Ni/SiO_2 catalysts for $\bar{d}$ = 7.7, 16.6, 26.7 and 34.8 nm. From Fig. 3.5, it is shown that Ni/SiO_2 has Ni nanoparticles whose diameters was almost same to D_{Ni} evaluated by XRD. Thus the pores which contributed to NH_3 decomposition should have the diameter which is equal to D_{Ni}. Note that the Ni/SiO_2 for $\bar{d}$ = 34.8 nm has smaller Ni nanoparticles $\bar{d}$ than D_{Ni}; it is considered that this diameter of pore contributing to the reaction should be equal to $\bar{d}$ evaluated from the pore distribution. In TEM images for $\bar{d}$ = 16.6 and 34.8 nm, oval Ni nanoparticles were observed. It is considered that some pores were filled up with these oval Ni nanoparticles, however these were very minor.

To estimate correlation between the pore diffusion and kinetics, using $\bar{d}$ values and the mean free path of the NH_3 molecule, L_{NH3}, the Knudsen number, Kn for each pore diameter can be calculated, which is a dimensionless number defined as

$$Kn = L/\bar{d} \qquad \text{(Eq. 3-1).}$$

When the mean free path is 10 times greater than the pore diameter ($Kn^{-1} < 0.1$), collisions of the molecule with the pore wall dominate [14]. This diffusion regime is different from molecular diffusion, and is known as Knudsen diffusion [14]. L_{NH3} was calculated from the following equation:

$$L_{NH3} = \frac{k_B T}{\sqrt{2}\pi\rho^2 P} \qquad \text{(Eq. 3-2)}$$

where

k_B is the Boltzmann constant,

T is 973 K,

P is the ambient pressure (0.1 MPa).

For simplification, the diffusion of only NH_3 molecules will be discussed.

Fig. 3.6 shows a plot of the activation energy against the inverse of the Knudsen number for each Ni/SiO_2 catalyst. The activation energy is almost constant above ca. 0.1 of Kn^{-1}, however decreases sharply beneath this value. The activation energy of the surface reaction on each Ni/SiO_2 catalyst should be same and independent of pore structure. However, if $\bar{d}$ is too small to cause strong pore diffusion resistance, the apparent activation energy of the catalyst can be lower than that of others with large pores. Fig. 3.6 suggested that Knudsen diffusion increased the diffusion resistance, and that the apparent activation energy was decreased as a result.

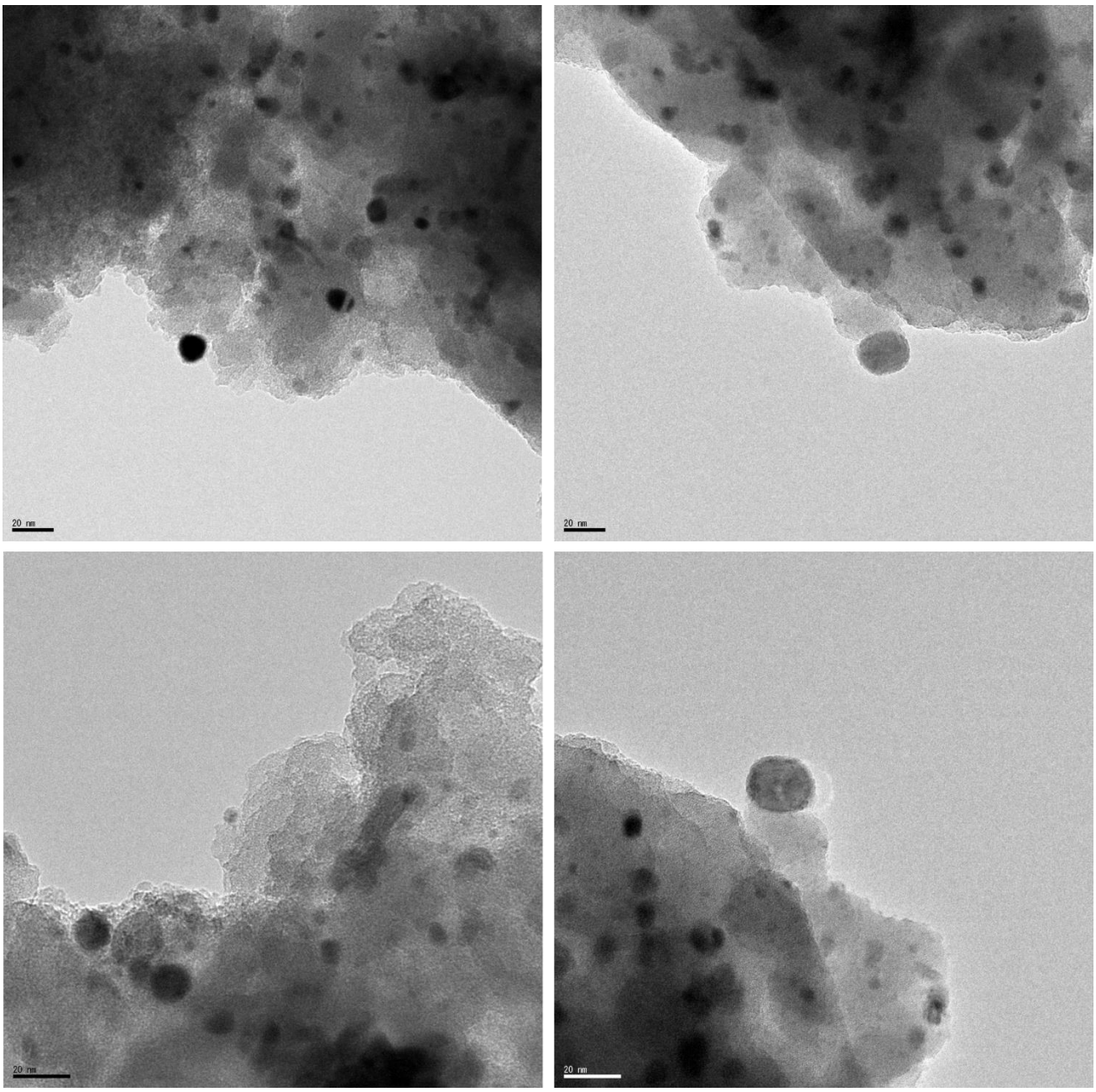

Fig. 3.5 (a) TEM images of Ni/SiO_2 catalyst for $\bar{d}$ = 7.7 nm.

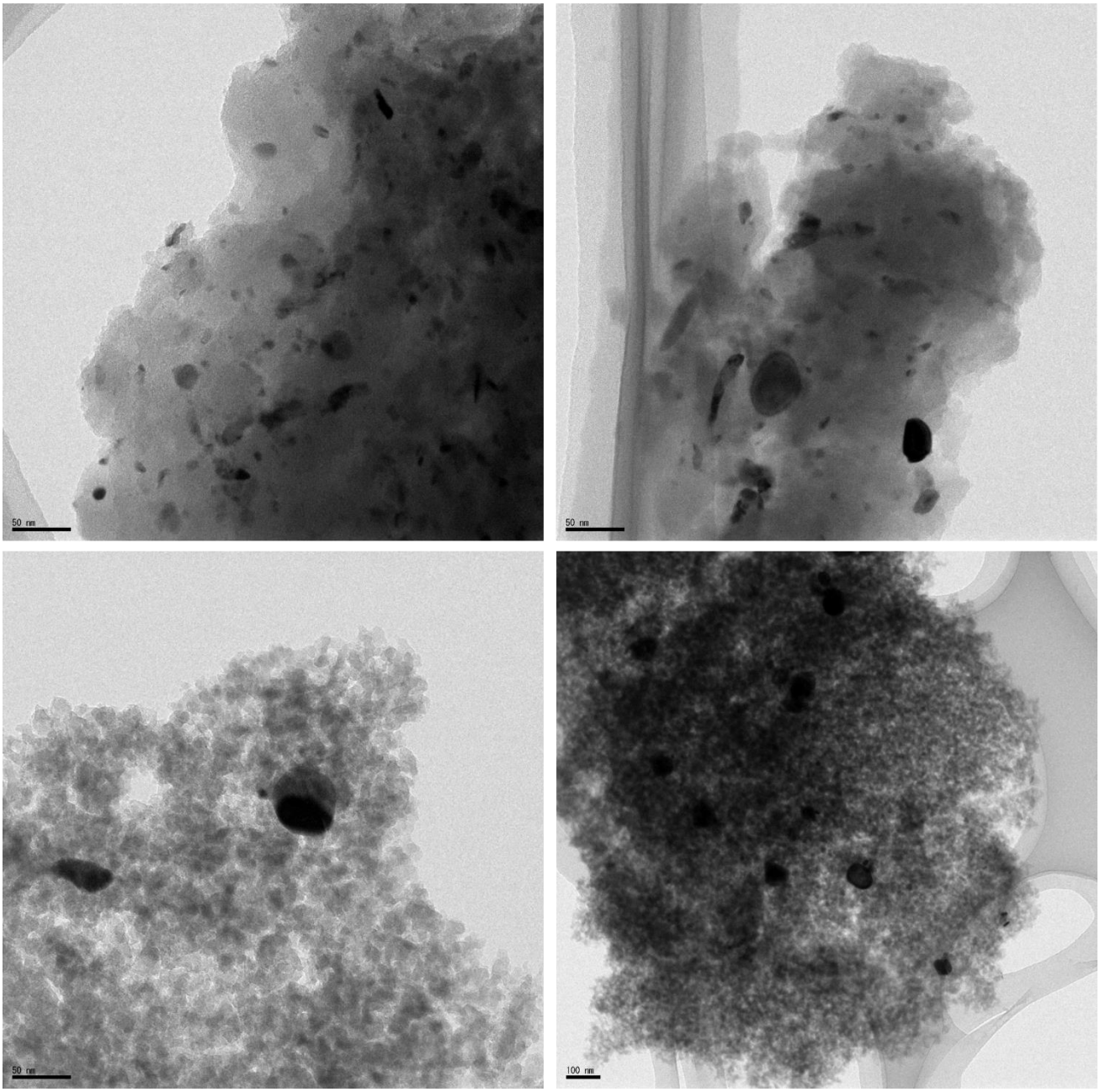

Fig. 3.5 (b) TEM images of Ni/SiO_2 catalyst for $\bar{d}$ = 16.6 nm.

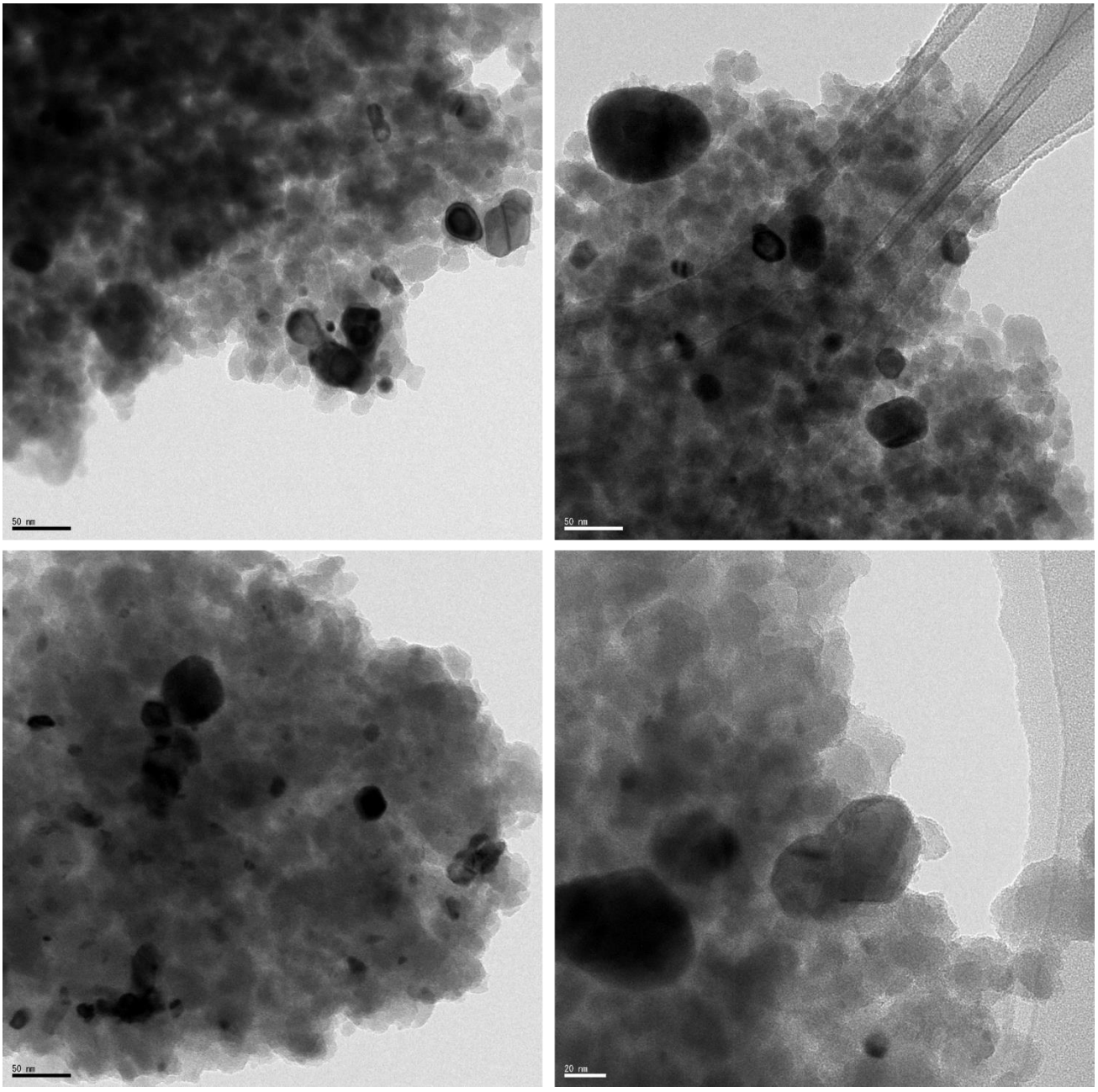

Fig. 3.5 (c) TEM images of Ni/SiO_2 catalyst for $\bar{d}$ = 26.7 nm.

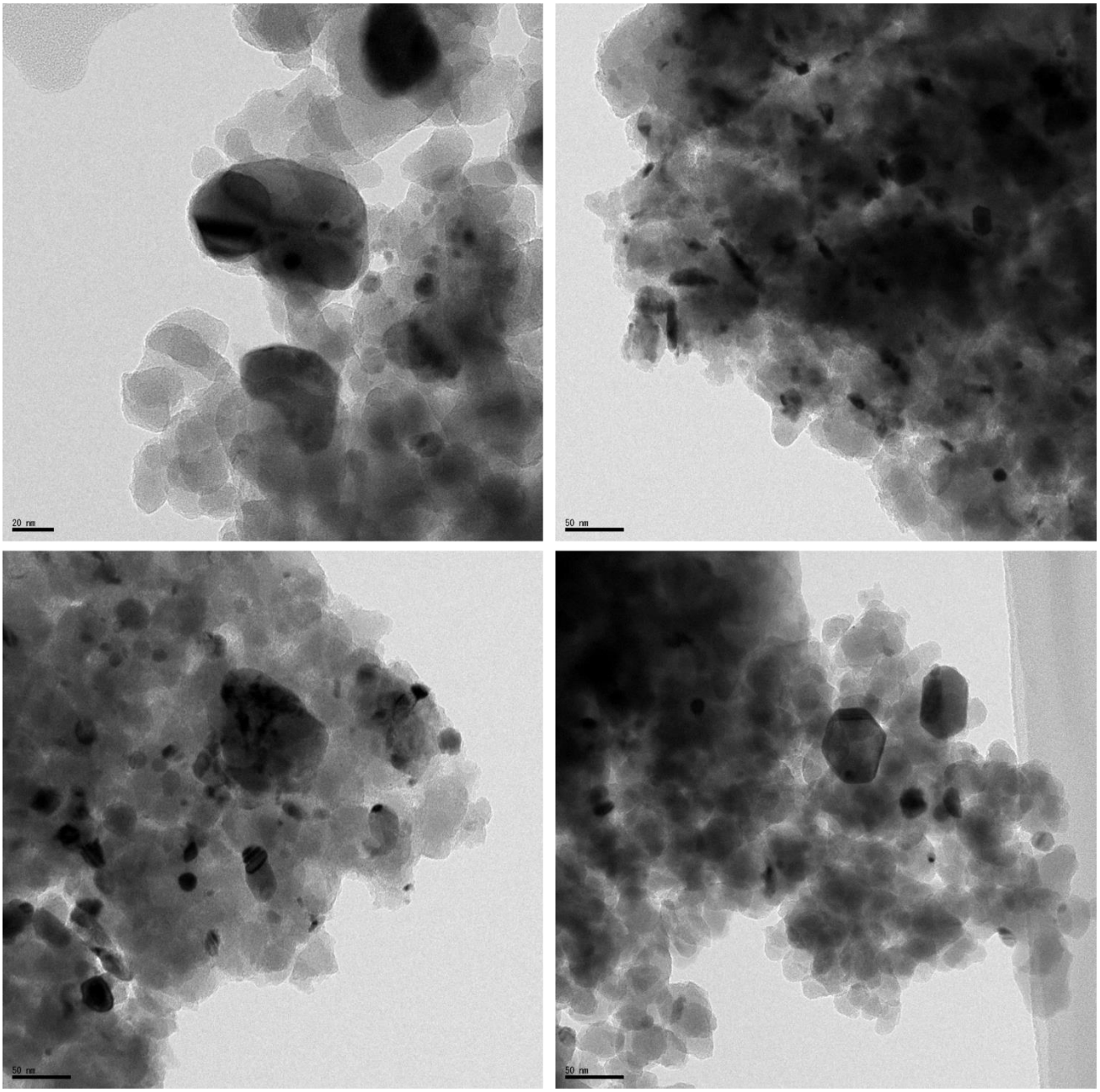

Fig. 3.5 (d) TEM images of Ni/SiO_2 catalyst for $\bar{d}$ = 34.8 nm.

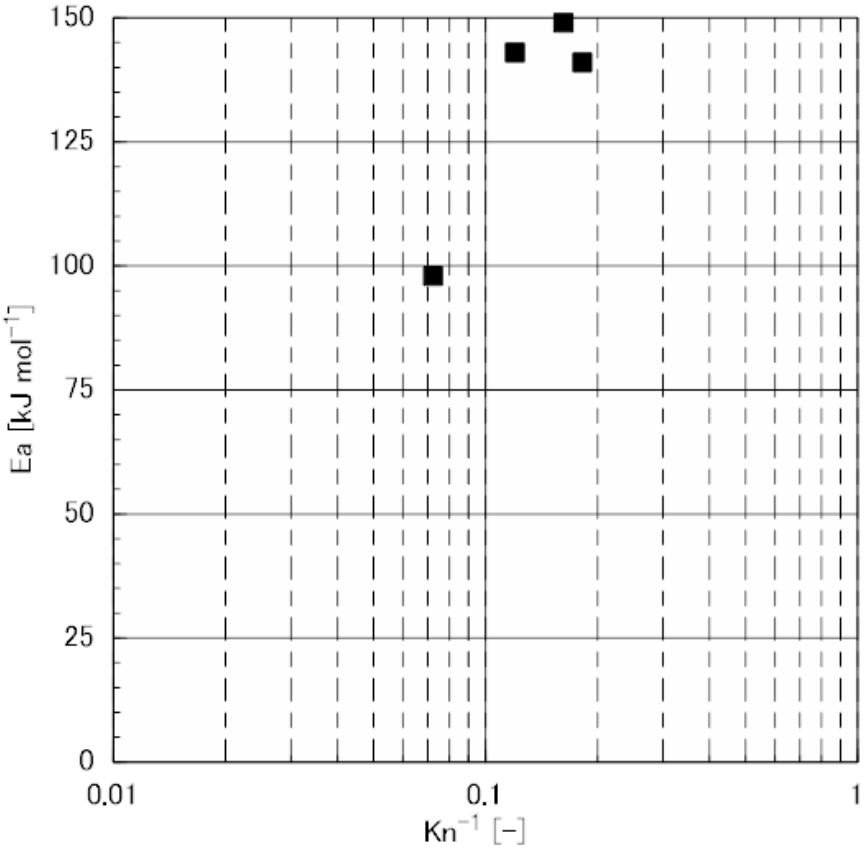

Fig. 3.6 Activation energy plotted against the inverse of the Knudsen number for each catalyst at 973 K.

It is concluded that the Ni/SiO_2 catalysts with $\bar{d}$= 16.6 nm or large had high NH_3 decomposition activity owing to the support's low diffusion resistance. Furthermore, Ni/SiO_2 with $\bar{d}$= 26.7 nm can decompose NH_3 completely at the highest value of GHSV examined, 42,000 h^{-1} at 973 K.

Comparing the activity of the catalysts in this study with the catalysts prepared by Goodman [4], the activation energy of Ni/SiO_2 which was Goodman et. al. prepared is ca. 91 kJ mol^{-1}, and that in this study show slightly higher value, 98 kJ mol^{-1} for $\bar{d}$ = 7.7 nm or ca. 140 or 150 kJ mol^{-1} for other pore diameters. While Goodman et. al. didn't reported the pore structure of SiO_2 support, assuming that they use SiO_2 particle with small pore, the activation energy for $\bar{d}$ = 7.7 nm in this study is nearly equal to that they obtained. In this view point of activation energy, the kinetic constant of Ni/SiO_2 which Goodman et. al. prepared should be compared with the catalyst with $\bar{d}$ = 7.7 nm in this study. For instance, the kinetic constant at 873 K in their study is ca. 4.0 s^{-1} and that in this study is 6.7 s^{-1}. Thus it is considered that the activity of Ni/SiO_2 with $\bar{d}$ = 7.7 nm shows almost same as that of Goodman's Ni/SiO_2. However Ni/SiO_2 $\bar{d}$ = 26.7 nm shows the highest activity at 923 and 973 K (see Fig. 3.1). Thus it is concluded that preparing Ni/SiO_2 catalyst with higher

activity at above 923 K by controlling pore diameter was success in this study.

3.4. Summary

The mass transfer in the support's pore was evaluated using Ni/SiO_2 catalysts with different mean pore diameters ($\bar{d}$). The catalytic activities were almost independent of pore diameter below 873 k, and Ni/SiO_2 with the smallest mean pore diameter ($\bar{d}$ = 7 nm) exhibited the highest activity due to the highest dispersion. However, at 923 K, Ni/SiO_2 with 26.7 nm of $\bar{d}$ showed the highest activity. From the results of kinetics and estimation of diffusion regime using Knudsen number, strong pore diffusion resistance within the Ni/SiO_2 $\bar{d}$ of which is below 7.7 nm decrease the apparent activity of the catalyst.

Reference

[1] R. T. Yang. Gas Separation by Adsorption Processes. *Imperial College Press* (1997)

[2] O. Leavenspiel. Chemical Reaction Engineering (3rd edition). P101. *John Wiley and Sons, Inc.*, New York (1998)

[3] 橋本健治, 反応工学 改訂版, 培風館 (1993)

[4] T. V. Choudhary, C Sivadinarayana, D. W. Goodman. Catalytic ammonia decomposition: COx-free hydrogen production for fuel cell applications. *Catalyst letter*, 72, 197-201 (2001)

Chapter 4 Support Effects on Ammonia Decomposition Activity of Ni-loaded Catalysts

4.1. Introduction

Heat and mass transfer in the Ni/SiO_2 bed was studied in Chapter 2 and 3. It is found that under the condition of high gas velocities NH_3 conversion can be decrease due to decreasing of a reactor-wall temperature. In the Ni/SiO_2 catalysts, the apparent activity can be estimated lower than the true activity above 15 cm s^{-1}. Furthermore, NH_3 conversion also can be decreased by the strong diffusion resistance derived from Knudsen diffusion in pore at 973 K. it was concluded that elimination of the effects of heat and mass transfer in the bed and catalyst particle was required to evaluate the true activity of the Ni surface.

As mentioned in Chapter 2, Muroyama et. al. systematically evaluated the support effects of Ni-loaded catalysts NH_3 conversion [1], however they have not discussed the effects of heat and mass transfer. Moreover in the view point of the kinetics study, experimental data which they reported are limited: they carried out the decomposition test only under 100 ml g_{cat}^{-1} min^{-1} of the specific (per catalyst weight) flow rate. In this chapter, NH_3 conversion against GHSV was observed using Ni-loaded catalysts with various supports to carry out the kinetic study under high GHSV conditions.

4.2. Experimental

Ni-loaded catalysts with various supports were prepared by a wet impregnation method as described below (see Chapter 2). Nominal loading amount of Ni for each catalysts was 10 wt%. Following ceramic particles were selected as support materials: SiO_2 (75-150 μm, Q-30, Fuji Slisia, Ltd.), γ-Al_2O_3 (basic activated alumina, 45-150 μm, Wako Pure Chemical Industries, Ltd.), MgO (about 75 μm, 99 % purity, KMAO-H, Tateho Chemical Industries Co., Ltd.), ZrO_2 (Wako Pure Chemical Industries, Ltd.), anatase form TiO_2 (Wako Pure Chemical Industries, Ltd.), rutile form TiO_2 (Wako Pure Chemical Industries, Ltd.), La_2O_3 (Wako Pure Chemical Industries, Ltd.), zeolite (mordenite, HSZ-600HOA, TOSOH Corporation). The amount of loaded-Ni for the prepared catalysts (M_{Ni}) were analyzed by an XRF. Loaded-Ni nanoparticles were analyzed by an XRD to evaluate mean diameter of Ni (D_{Ni}). The specific surface area (S_{BET}) for each Ni-loaded catalyst measured by means of BET method. Surface structure of catalysts were observed by a TEM. Characteristics of the prepared catalysts were summarized in Table 4.1.

These catalysts was tested in the fixed-bed reactor (see Chapter 2). Note that 0.1 g of the Ni catalysts were loaded in the reactor to carry out NH_3 decomposition test below 15 cm s^{-1} of gas velocity to eliminate the effects of the lack of heat transfer.

Table 4.1 Specific surface area (S_{BET}) of Ni-loaded catalysts.

Catalysts	M_{Ni} [wt%]	D_{Ni} [nm]	S_{BET} [m^2 g^{-1}]
Ni/SiO_2	9.2	30.9	100
$Ni/\gamma\text{-}Al_2O_3$	9.7	8.1	106
Ni/ MgO	9.4	21.5	5
Ni/ ZrO_2	8.8	16.7	3
Ni/TiO_2 (Anatase form)	8.0	32.1	11
Ni/TiO_2 (Rutile form)	8.9	18.2	7
Ni/La_2O_3	10.0	21.6	9
Ni/Zeolite	9.1	21.0	522

4.3. Results and discussion

4.3.1. Supports effects on kinetics of Ni catalysts for ammonia decomposition

Fig. 4.1 shows the NH_3 conversion against GHSV at 773-973 K for Ni catalyst. From this figure, it is found that NH_3 conversion increased as temperature increased because NH_3 decomposition reaction is an endothermic reaction (Eq. 2-1). In the view point of perfect decomposition, at 973 K, $Ni/\gamma\text{-}Al_2O_3$, Ni/MgO and Ni/ZrO_2 has the highest activity: these catalysts can decompose above 100,000 h^{-1} of GHSV; especially 140,000 h^{-1} of NH_3 was decomposed perfectly over $Ni/\gamma\text{-}Al_2O_3$ catalyst. Below 923 k, despite $Ni/\gamma\text{-}Al_2O_3$, prepared catalysts can't decompose NH_3 perfectly in the whole GHSV tested. From Fig. 4.1 it is shown that support effects for NH_3 decomposition were ranked in the order of $\gamma\text{-}Al_2O_3$ > MgO = La_2O_3 = ZrO_2 > TiO_2 (rutile form) > SiO_2 > TiO_2 (anatase form) > Mordenite with the temperatures ranged from 773 to 973 K.

Kinetic study was carried out from Fig. 4.1. Assuming a first-order reaction (see Chapter 2), kinetic constant, k for each catalysts at 773-973 K was evaluated using Eq. 2-9. Fig. 4.2 shows the k values against inverse of temperature. From this figure, it is found that $Ni/\gamma\text{-}Al_2O_3$ exhibited the highest activity, whereas Ni/Zeolite had the lowest activity. Activation energies, E_a and frequency factor, k_0 were summarized in Table 4.2. From this table, it is shown that Ni/SiO_2, TiO_2 (anatase form) and zeolite has the relatively lower value than that of others. Activation energy means independency of temperatures, thus it is considered that theses catalysts showed lower activity at higher temperature.

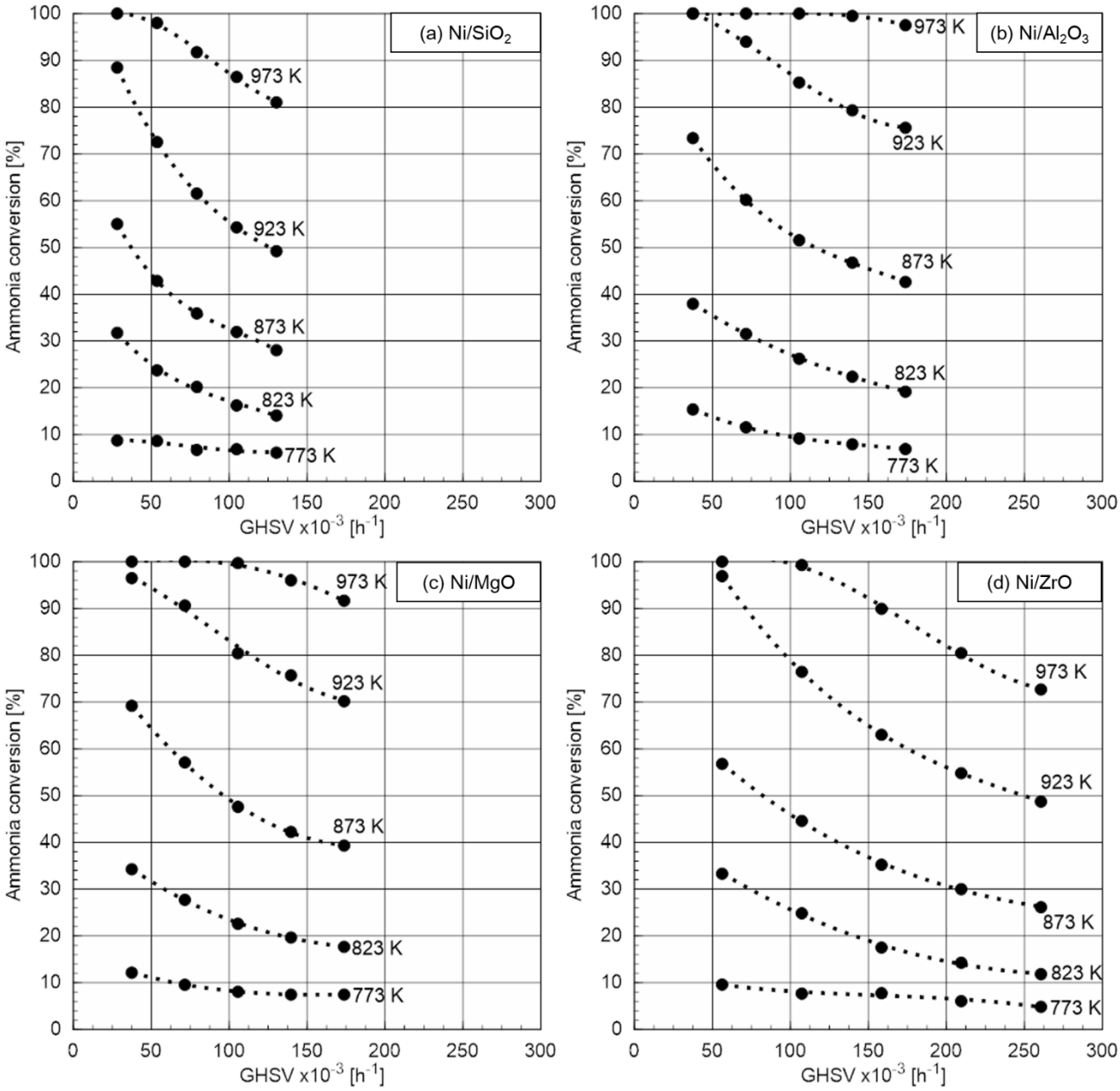

Fig. 4.1 (continued on next page) Ammonia conversion against GHSV via Ni/SiO_2, γ-Al_2O_3, MgO, ZrO_2, TiO_2 (Anatase or Rutile form), La_2O_3, Zeolite (Mordenite) at 773-973 K.

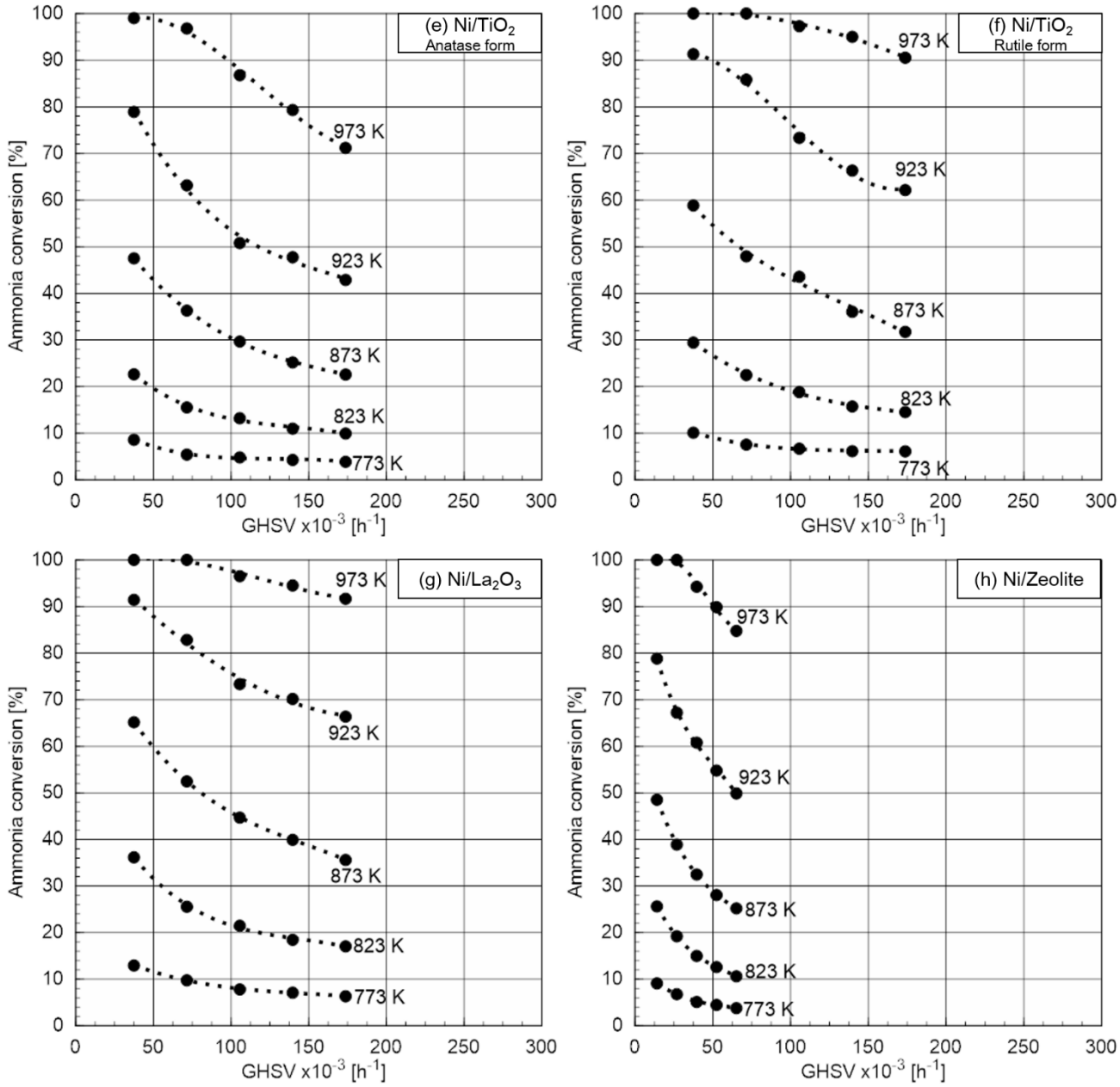

Fig. 4.1 (continued from previous page) Ammonia conversion against GHSV via Ni/SiO_2, γ-Al_2O_3, MgO, ZrO_2, TiO_2 (Anatase or Rutile form), La_2O_3, Zeolite (Mordenite) at 773-973 K.

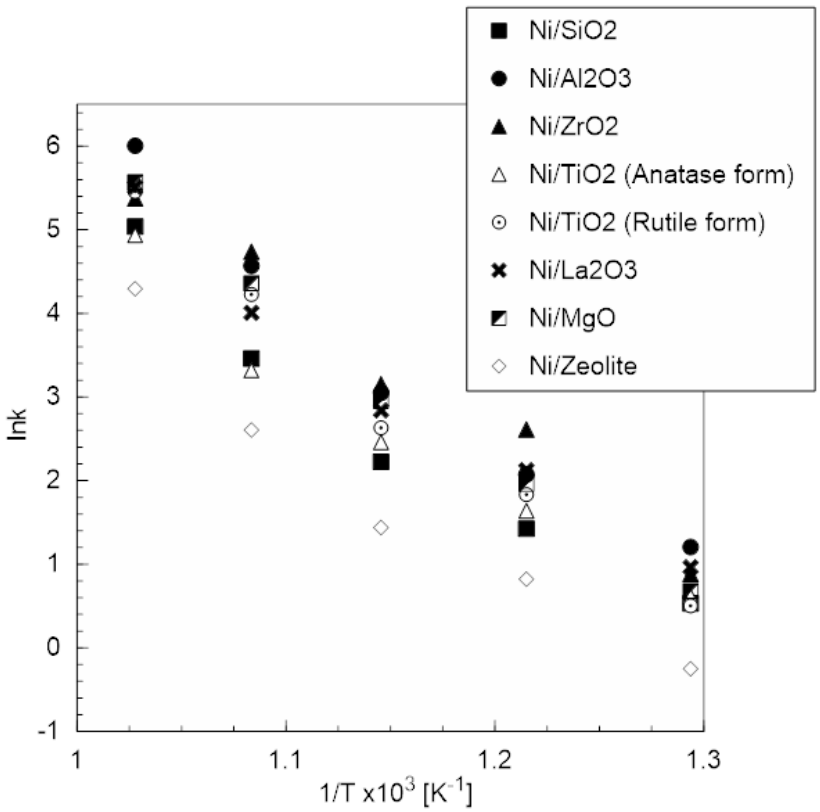

Fig. 4.2 Arrhenius plot of the Ni/SiO_2, γ-Al_2O_3, MgO, ZrO_2, TiO_2 (Anatase or Rutile form), La_2O_3, Zeolite (Mordenite) at 773-973 K.

Table 4.2 Activation energies and frequency factors of Ni-loaded catalysts.

Catalysts	Activation energy, E_a [kJ/mol]	Frequency factor, k_0 [s^{-1}]
Ni/SiO_2	149	22.4
Ni/γ-Al_2O_3	152	24.1
Ni/ MgO	154	23.9
Ni/ ZrO_2	146	23.4
Ni/TiO_2 (Anatase form)	131	20.9
Ni/TiO_2 (Rutile form)	152	23.1
Ni/La_2O_3	143	23.8
Ni/Zeolite	129	19.8

4.3.2. Mechanisms of support effects

As reviewed and discussed by Au et. al., there is the correlation between turnover frequency (TOF) of hydrogen on catalyst and catalytic activity [2]. In other word, the catalytic activity for NH_3 decomposition over Ni and Ru decreases with the declining of the basicity evaluated by TOF_{H2}. Though the detailed mechanisms are not figured out, it is speculated that basicity of the support can enhance the rate of N_2 desorption from catalyst's surface [2]. From Fig. 4.1, it is found that γ-Al_2O_3, MgO, La_2O_3 and ZrO_2 which well known as solid base materials [3,4] show the higher support effect than others. Thus it is concluded that the basicity of the support strongly affected the activity of Ni catalysts. To understand detailed mechanisms between basicity and catalytic activity, the evaluation of the basicity of the catalysts which were used in this study should be investigated as the future work.

TEM observation was carried out to discuss correlations between the morphology of loaded-Ni and its kinetics. Fig. 4.3 shows the TEM images of prepared catalysts. Note that Ni/MgO could not be observed by TEM, because the shadow of MgO was too deep to observe the loaded-Ni nanoparticles. Fig. 4.3 (b) shows the TEM images of Ni/Al_2O_3, and it is found that relatively small Ni-nanoparticles were loaded. This high dispersion of loaded-Ni also facilitate its catalytic activities due to high surface area of the support. Although SiO_2 also has a higher surface area comparable to Al_2O_3, the dispersion of Ni/SiO_2 were lower (see Table 4.1). It is considered that SiO_2 surface is inert to facilitate the sintering of loaded-Ni nanoparticles. As described in Table 4.1, the loaded-Ni nanoparticles of Ni/ZrO_2 and Ni/La_2O_3 were ca .20 nm. Form TEM images, relatively small particles were observed on Ni/ZrO_2, however, as shown in Fig. 4.2. (g) Ni-nanoparticles could not be clearly observed. Muroyama et. al. have pointed out that loaded-Ni potentially form $LaNiO_3$ with La_2O_3 support [1]. Therefore it is speculated that $LaNiO_3$ formation made the border between Ni-nanoparticles and L_2O_3 support ill-defined.

Rutile and anatase form of TiO_2 showed the different activity in this study. As described in Table 4.1, loaded-Ni amount of the anatase-catalyst was lower than that of the rutile-catalysts. Furthermore, Ni-nanoparticle on the anatase-catalyst is larger than that on the rutile-catalysts. TEM images in Fig. 4.3 (e) and (f) also illustrated that the dispersion of Ni on rutile-catalysts were higher. Crystallite structure of rutile or anatase TiO_2 can affect the NH3 decomposition rate, however it cannot be discussed from the data in this study.

As shown in Fig. 4.3 (h), the dispersion of loaded-Ni of the zeolite catalysts seems to be relatively higher. Though it is minor, some Ni/Zeolite has the > 10 nm small Ni-nanoparticles within its support: it is considered that these Ni-particles were formed in pores formed by zeolite's crystallite. Nonetheless Ni/Zeolite has the smaller Ni-nanoparticles, as shown Fig. 4.2 this catalyst has the lowest support effects and there is relatively low temperature-dependency. It is considered that the strong acidity of the mordenite decreased the activity of loaded Ni. Thus it is speculated that, for instance, high-silica zeolite with weak acidity and basic zeolite decorated by alkaline metal

(a) Ni/SiO2

See Fig. 3.5 (c).

(b) Ni/Al_2O_3

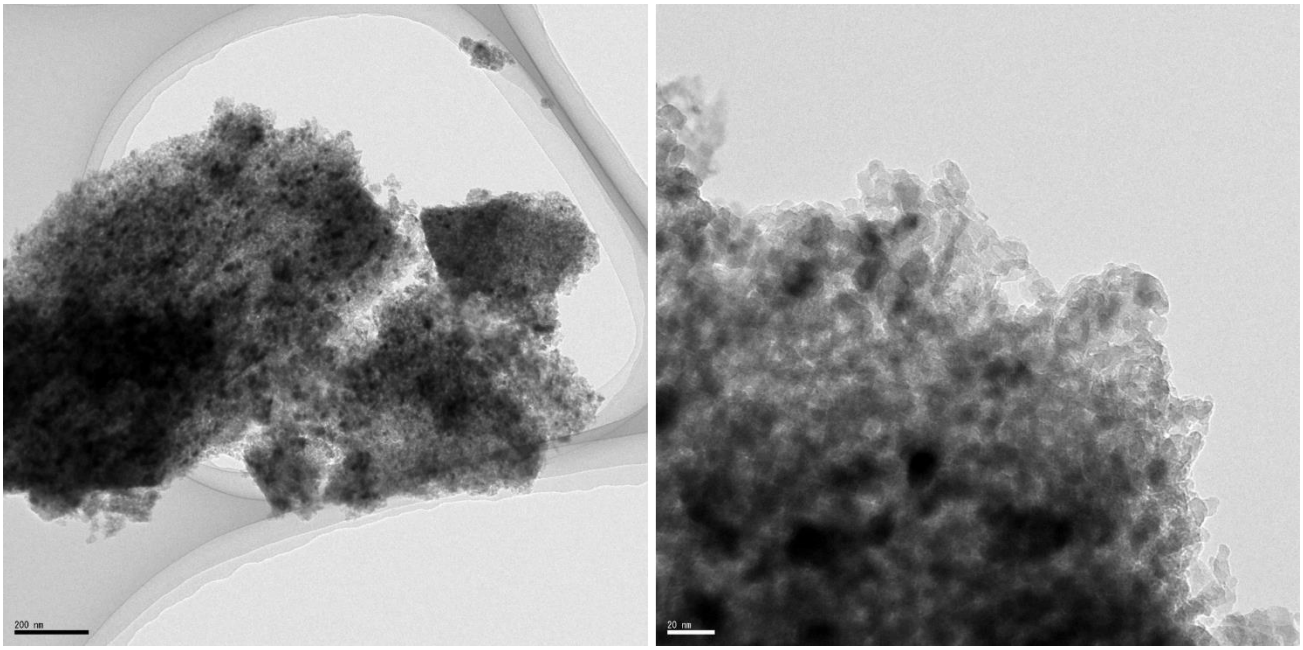

(c) Ni/MgO

No images, because the shadow of MgO was too deep to observe the loaded-Ni nanoparticles

(d) Ni/ZrO_2

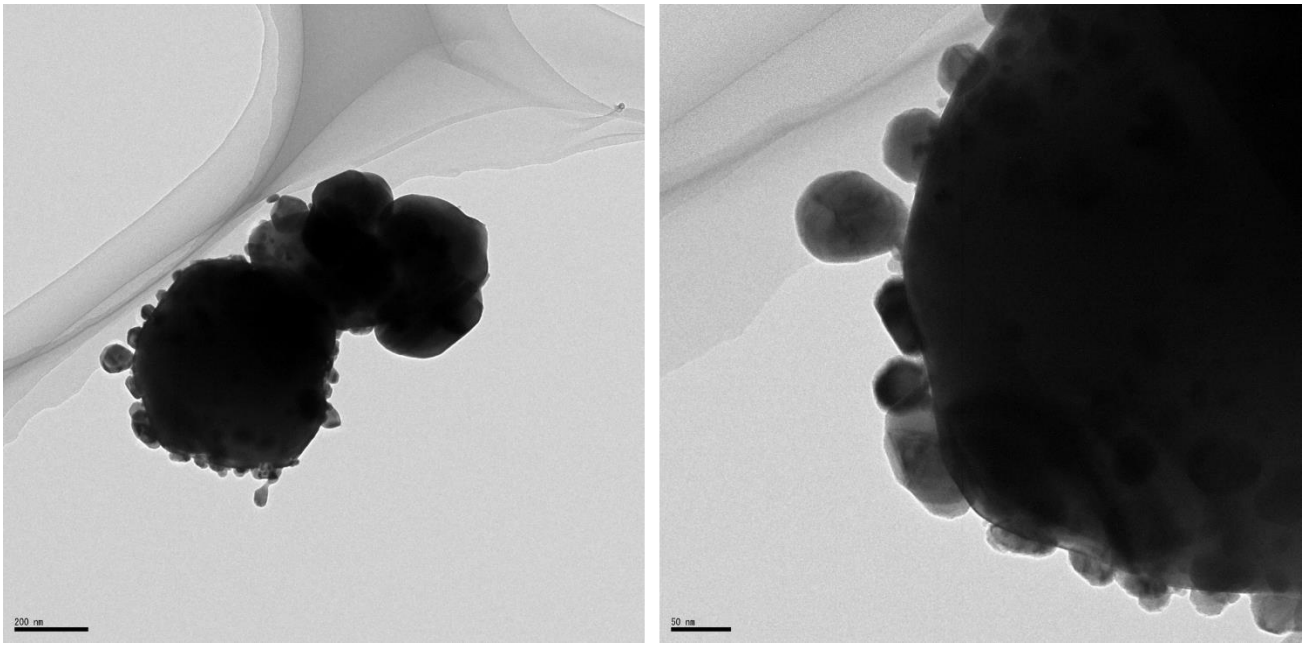

Fig. 4.3. (continued on next page) TEM images of Ni-loaded catalysts.

(e) Ni/TiO_2 (Anatase)

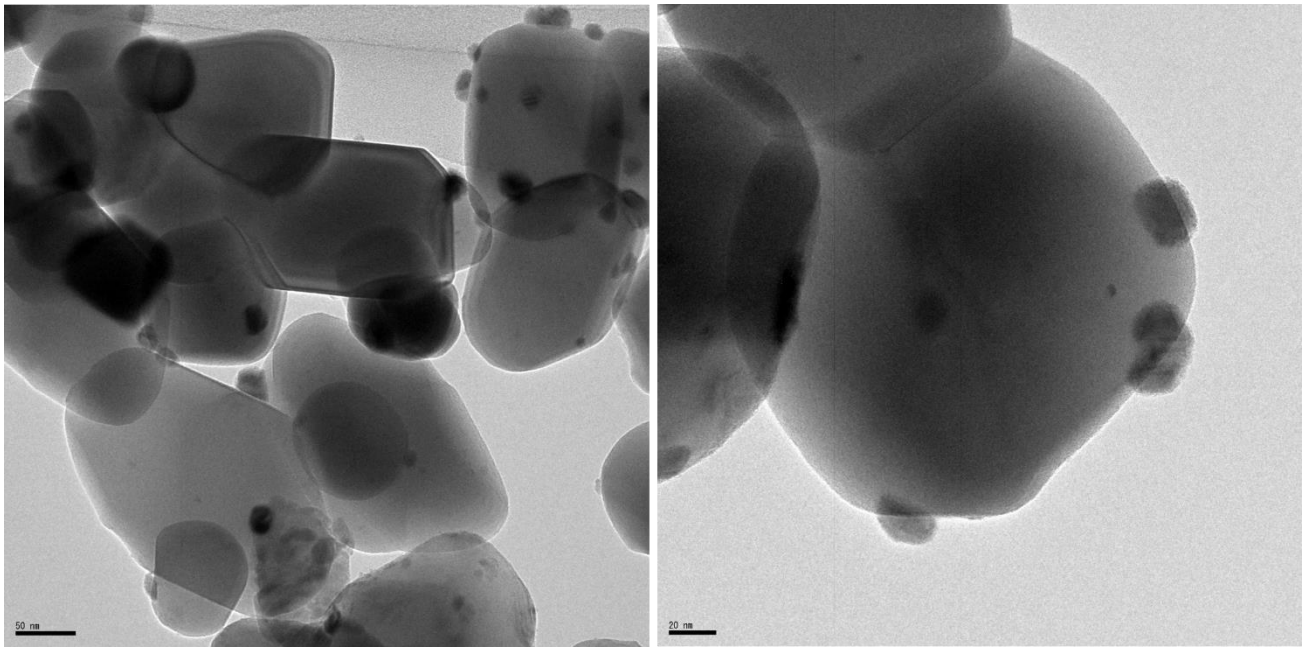

(f) Ni/TiO_2 (Rutile)

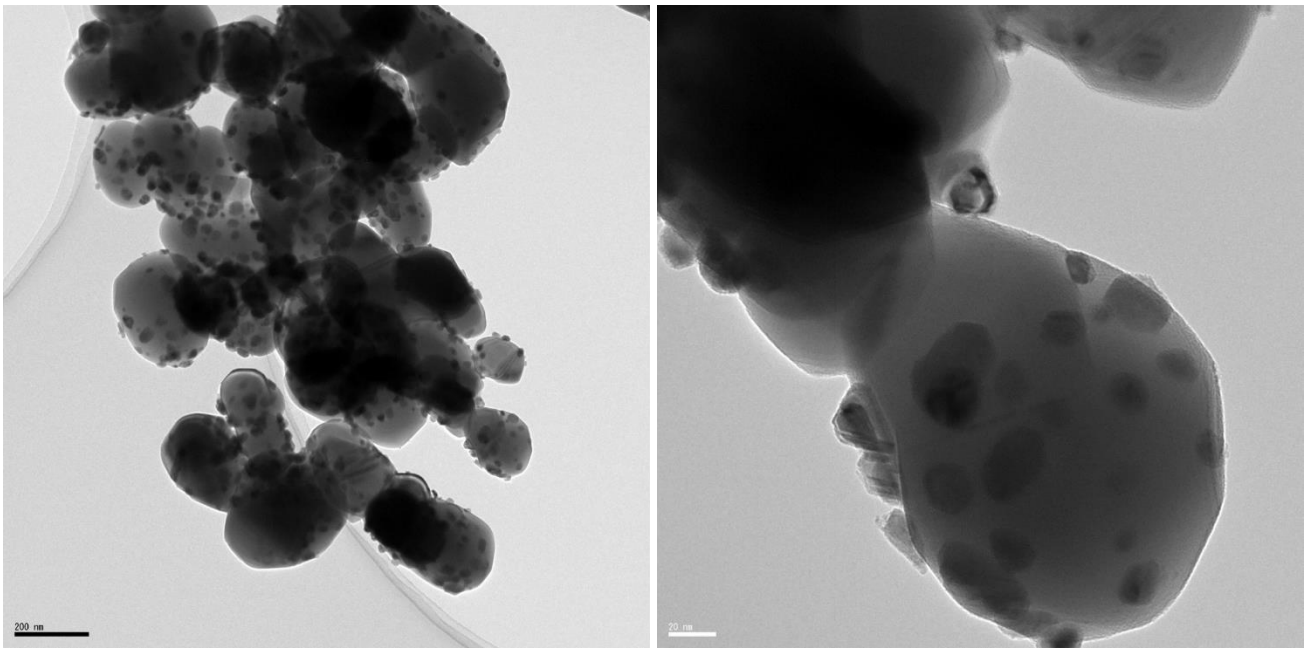

Fig. 4.3. (continued from previous page) TEM images of Ni-loaded catalysts.

(g) Ni/La2O3

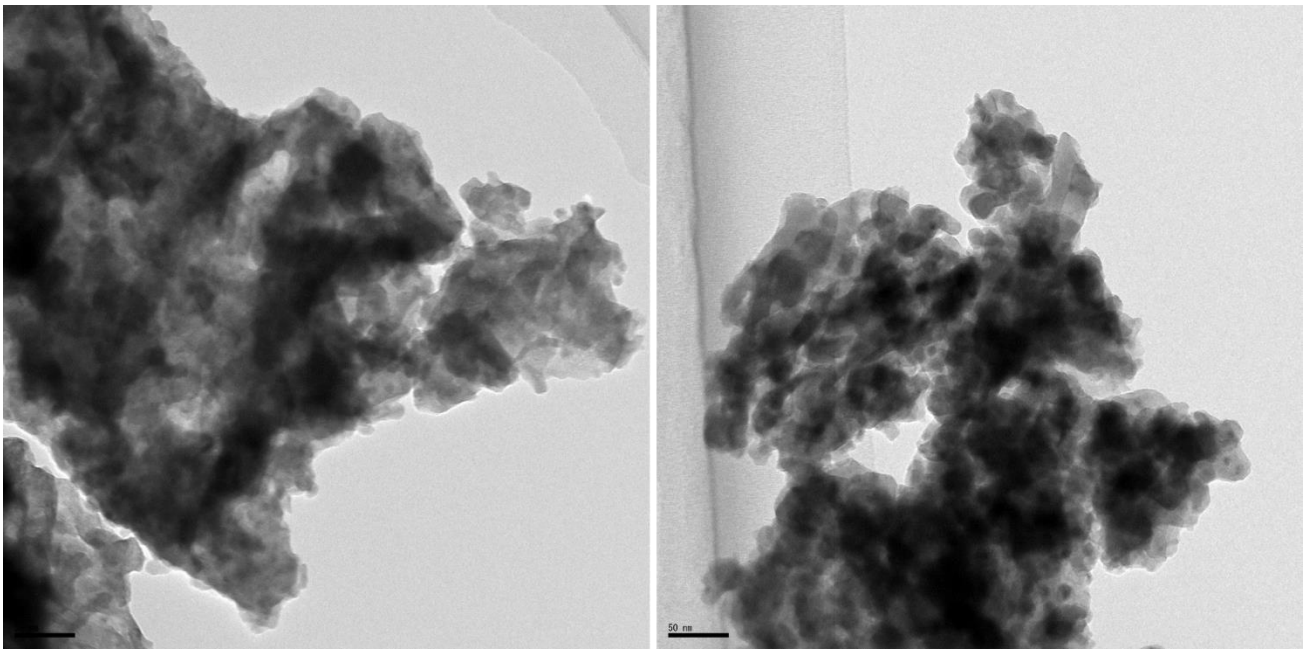

(h) Ni/Zeolite (Mordenite)

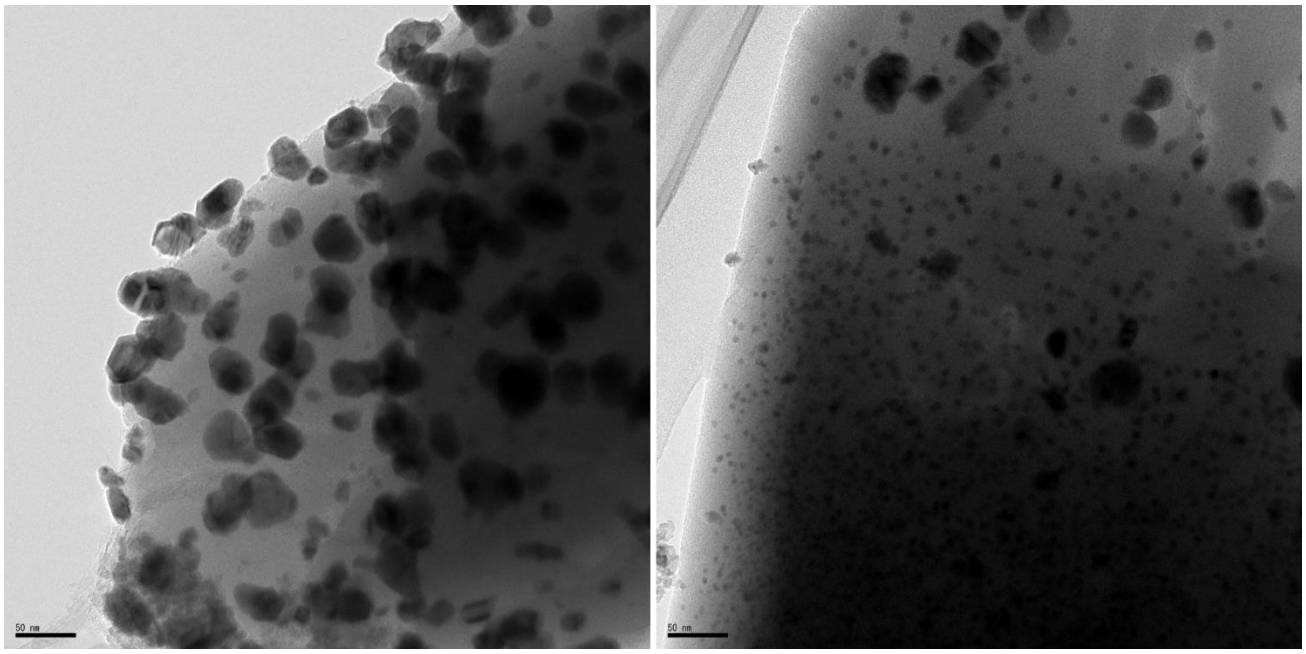

Fig. 4.3. (continued from previous page) TEM images of Ni-loaded catalysts.

potentially exhibit the high support effects.

4.4. Summary

NH_3 decomposition via various support materials on which 10 wt% of Ni loaded was carried out using a fixed-bed reactor to clarify the kinetics of support effects. Support effects were ranked in the order of γ-Al_2O_3 > MgO = La_2O_3 = ZrO_2 > TiO_2 (rutile form) > SiO_2 > TiO_2 (anatase form) > Mordenite from 773 to 973 K. Ni/γ-Al_2O_3 showed the highest activity in the whole temperatures examined due to supports high basicity. Other solid base materials, e.g. MgO, La_2O_3, and ZrO_2 showed relatively high activity. Rutile or anatase formed TiO_2 exhibited the difference activity. It was considered that this is because of the dispersion and loaded-amount Ni-nanoparticles. Mordenite had relatively small Ni-nanoparticles, however exhibited the lowest activity in the whole catalysts examined. It was considered that the strong acidity of mordenite can decrease the activity of loaded-Ni.

Reference

[1] H. Muroyama, C. Saburi, T. Matsui, K. Eguchi. Ammonia decomposition over Ni/La_2O_3 catalyst for on-site generation of hydrogen. *Applied Catalysis A : General*, 443-444, 119-124 (2012)

[2] S. F. Yin, Q. H. Zhang, B. Q. Xu, X. P. Zhou, W. X. Zhu, C. F. Ng, C. T. Au. Investigation on the catalysis of CO_x-free hydrogen generation from ammonia. *Journal of Catalysis*, 224, 384-396 (2004)

[3] R. Jothiramalingam, M. K. Wang. Review of Recent developments in Solid Acid, Base, and Enzyme Catalysts (Heterogeneous) for Biodiesel Production via Trans-esterification. *Industrial Engineering and Chemistry Research*, 48, 6162-6172 (2009)

[4] H. Hattori. Solid Base Catalysts: Fundamentals and Applications, 20^{th} Annual Saudi-Japan Symposium, Catalysts in Petroleum Refining & Peterochemicals (2010)

Chapter 5 Effects of Steam on Catalytic Activity on Ni/γ-Al_2O_3 for NH_3 Decomposition.

5.1. Introduction

In Chapter 4, the kinetics of Ni catalysts supported by various ceramic particles were evaluated. From these results, it was found that basic γ-Al_2O_3 has the highest support effect due to its high basicity and high surface area, whereas Ni-loaded mordenite, which is well-known as a solid-acid ceramic, exhibited the lowest activity. In this study, highly active Ni/γ-Al_2O_3 was used in the first trial test to decompose NH_3 with steam to demonstrate thermochemical processing of NH_4^+-containing wastewater.

Coexisting-steam potentially deactivates the Ni catalysts. From the study of the steam reforming of hydrocarbons, it is suggested that loaded-Ni can be deactivated by (i) sintering, (ii) formation of nickel oxide (NiO), (iii) poisoning by hydroxyl group (OH^-) derived from adsorbed H_2O molecules and (iv) formation of complex oxides with support material like $NiAl_2O_4$ [1,2]. However, there have been few efforts to figure out the mechanisms of the deactivation of Ni catalysts by coexisting steam. To substantialize the thermochemical wastewater-treatment process for denitrification, it is important to observe the deactivation behavior of Ni catalysts and develop catalysts which can conduct stable decomposition of NH_3 even with high steam partial pressure.

In this chapter, NH_3 conversion of NH_3/steam mixture (wet-NH_3) via Ni/γ-Al_2O_3 was evaluated to discuss the deactivation mechanisms by steam. Steam partial pressure was varied from 10 to 80 kPa, and reaction temperature was adjusted 873, 923 or 973 K.

5.2. Experimental

Catalyst test was conducted using a gas-flow fixed-bed reactor. Fig. 5.1 shows the schematic illustration of the experimental setup. This equipment consists of float meters, syringe pump, an impinge bottle for NH_3 trapping, a soap-film meter and two stainless steel (SUS 316) tubes. These two tubes were used as a main reactor and a vaporizer. Ion-exchanged water was injected into this vaporizer using syringe pump to provide steam to the reactor. Partial pressure was determined by the controlling the flow rate on syringe pump. In the vaporizer tube, alumina particle with 1 mm of outer diameter was loaded in the middle of a vaporizer

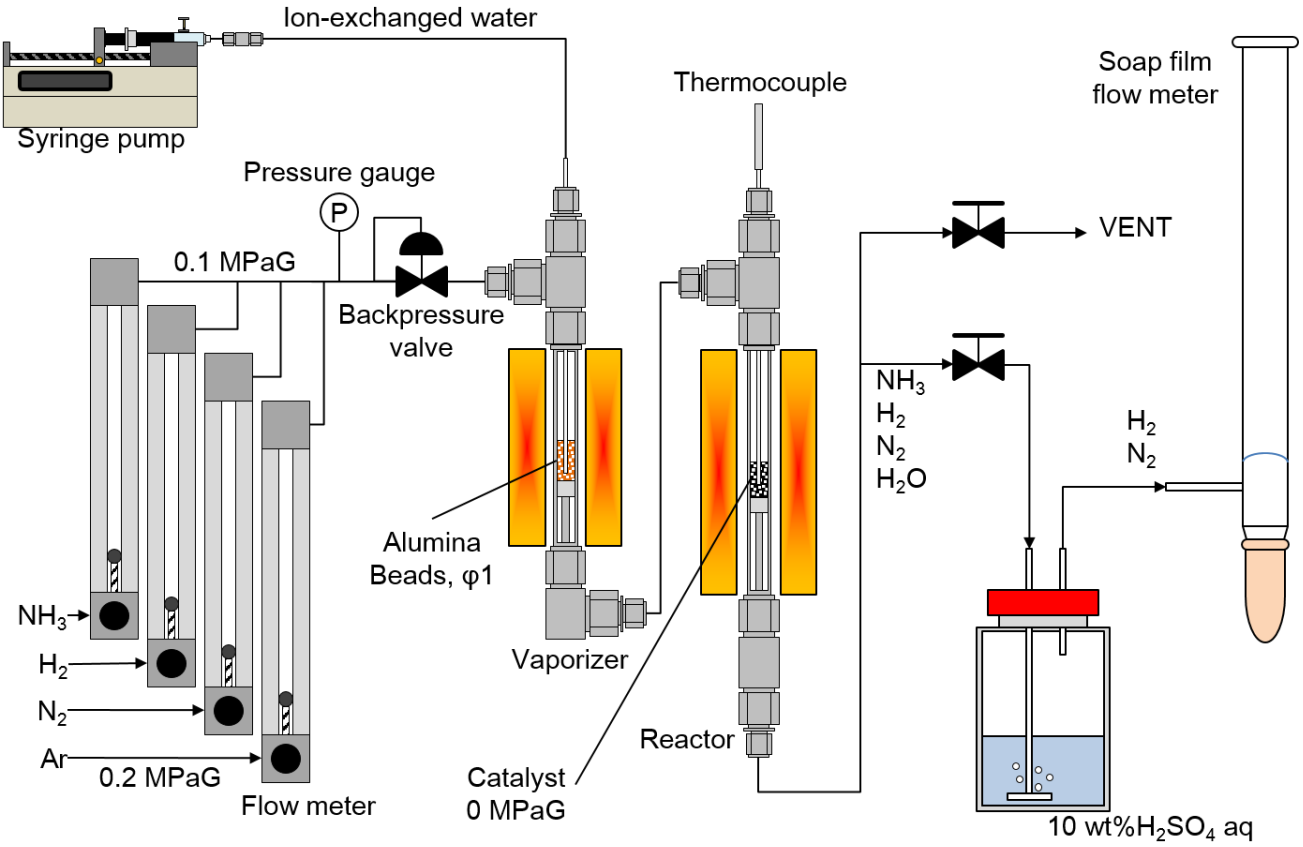

Fig. 5.1 Experimental setup for wet-NH_3 decomposition test.

tube to enhance the vaporization of water: this alumna bed indicated the stable supply of vapor without pulsatile gas flow. Vaporizer tube was heated by electric furnace at 413 k. Wet-NH_3 was fed to the main reactor to decompose NH_3. Unreacted NH_3 and steam in outlet gases were trapped using 10 wt% H_2SO_4 solution. NH_3 conversion was determined by measuring flow rate of H_2/N_2 mixture.

5.3. Results and Discussion

5.3.1. Effects of steam partial pressure on the catalytic activity of Ni/Al_2O_3

Fig. 5.2 shows the plot of the NH_3 conversion over the Ni/γ-Al_2O_3 catalyst at 873 K against the steam partial pressure (10-50 kPa) tested with flow rate of 750 mL min^{-1} g_{cat}^{-1} for both dry- and wet-NH_3. Ni/γ-Al_2O_3 under flowing dry-NH_3 was found to maintain NH_3 conversion ca. 65 % for 1h. When the provided gas was switched from dry-NH_3 to wet-NH_3, the conversions at each stem partial pressure decreased for the first ca. 20 min. however the catalytic activities were not completely lost.

The conversions under flowing wet-NH_3 ($X_{NH3/Steam}$) were normalized by the initial conversion value (X_{NH3}) to obtain the fractional conversion ($X_{NH3/Steam}$ / X_{NH3}). Fig. 5.3 shows the fractional conversion versus

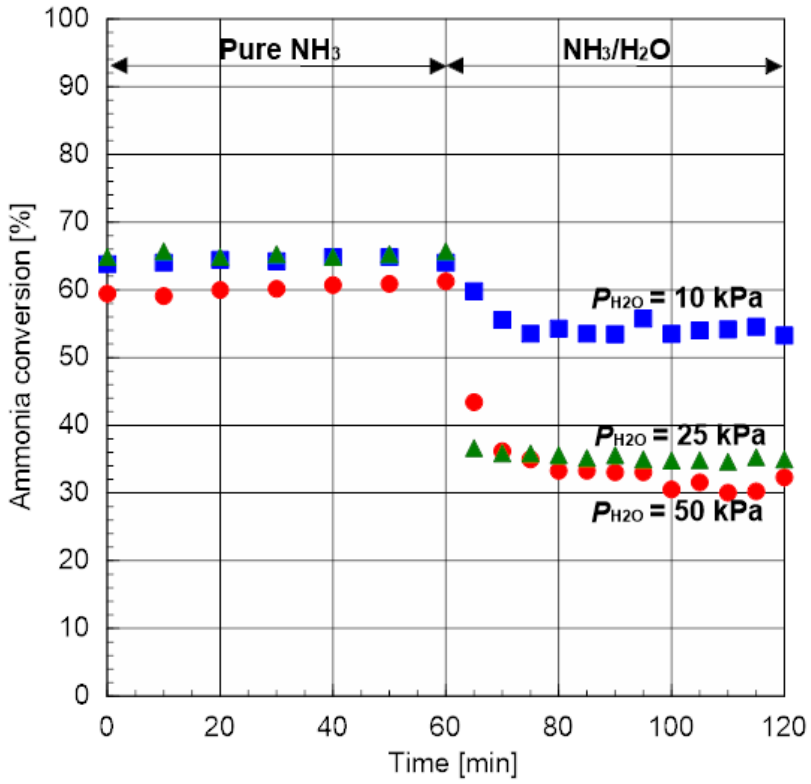

Fig. 5.2 Change in NH_3 conversion with time for dry- or wet-NH_3 decomposition via Ni/γ-Al_2O_3.

The temperature was 873 k and the partial pressure of steam was varied over a range of 10-50 kPa.

NH_3 flow rate was adjusted to 750 mL min^{-1} g_{cat}^{-1} for each steam partial pressure.

steam partial pressure (P_{H2O}) at 873 K. The activation behavior for the conversion of NH_3 above 25 kPa steam were found to be almost same with the catalytic activity for wet NH_3: which were decreased to ca. one-half of the initial conversions value. It had been speculated that the fractional conversions decreased monotonically against steam partial pressure, however the actual deactivation behavior were clearly different from that speculation.

As described above, the catalyst deactivation can occur due to the sintering of Ni nanoparticles, which decreases the active surface area. Therefore the size of Ni crystallite (D_{Ni}) was evaluated by XRD, and then D_{Ni} was calculated by the Scherrer equation (see Eq. 2-2). From results of a XRD analysis, D_{Ni} for as-prepared catalyst was 16.7 nm, while D_{Ni} for the catalyst after decomposition of wet-NH_3 (873 K, P_{H2O} = 80 kPa, 1 h) was 17.9 nm. Thus it was concluded that the sintering of Ni particles didn't occur in this study, and deactivation behavior observed in Fig. 5.2 was not derived from sintering of Ni nanoparticles.

To obtain further understanding of the deactivation mechanisms, thermodynamics equilibrium of

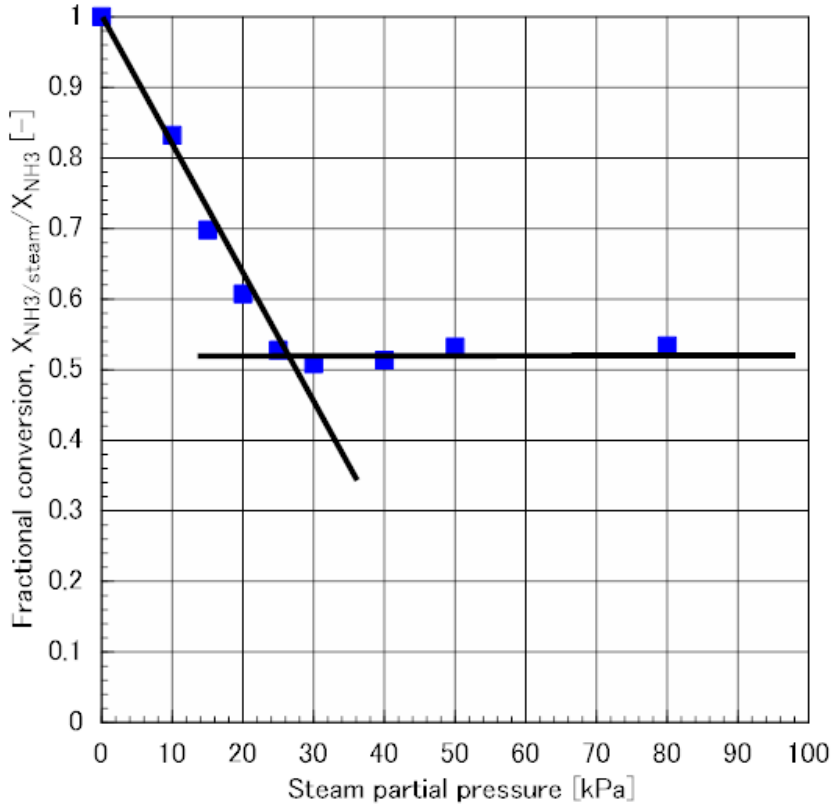

Fig. 5.3 Fractional conversion of NH_3 against the steam partial pressure at 873 K.

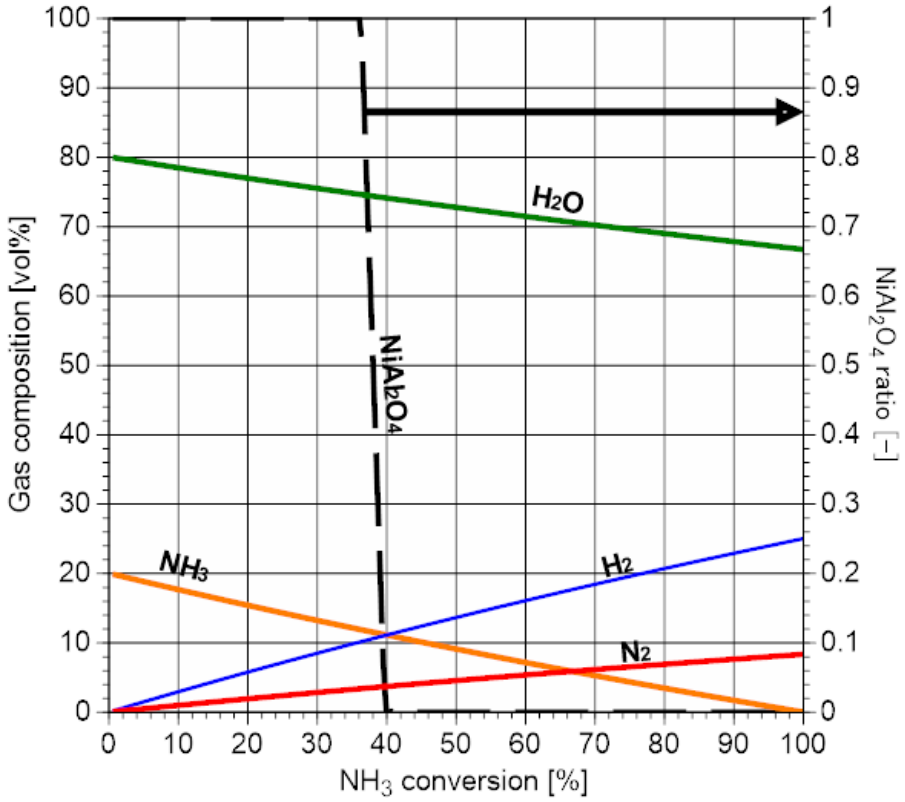

Fig. 5.4 Gas composition and $NiAl_2O_4$ ratio against NH_3 conversion for wet-NH_3 at 873 k.

Steam partial pressure of initial condition is 80 kPa in this calculation.

nickel on γ-Al_2O_3 under a NH_3 and gaseous H_2O atmosphere was calculated. This calculation was conducted by the software for thermodynamics equilibrium calculation, FactSage (Ver. 5.2). Fig. 5.4 shows the gas composition and $NiAl_2O_4$ ratio against NH_3 conversion for wet-NH_3 with a steam partial pressure of 80 kPa at 873 K. Note that the steam with partial pressure for 80 kPa doesn't cause the decrease in the equilibrium conversion of NH_3: NH_3 can be decomposed at equilibrium at 873 K even if the steam atmosphere. $NiAl_2O_4$ ratio means the mole fraction ratio of $NiAl_2O_4$ against Ni, i.e. $[NiAl_2O_4]/([Ni]+[NiAl_2O_4])$. As shown in Fig 5.4, thermodynamics calculation indicated that $NiAl_2O_4$ could form below ca 40 % of NH_3 conversion. One possible deactivation mechanism is the oxidation of the nickel surface by steam, because NiO is probably inactive for NH_3 decomposition [1]. Another possible mechanism is the formation of $NiAl_2O_4$; however, with the present data, it is currently not possible to determine the exact deactivation mechanism.

This calculation indicated that NiO was not generated by steam oxidation, however $NiAl_2O_4$ could potentially be formed as described in the following equation

$$Ni(s) + H_2O(g) + \gamma\text{-}Al_2O_3(s) \rightarrow NiAl_2O_4(s) + H_2(g) \qquad \text{(Eq. 5-1).}$$

In the case of the $NiAl_2O_4$ formation on the Al_2O_3 support surface, loaded-Ni atoms on the surface should diffuse into the Al_2O_3 with O atoms derived from adsorbed H_2O. Although the thermodynamic equilibrium calculation predicted the formation of not NiO but $NiAl_2O_4$, XRD patterns (not shown) for tested catalysts were as almost same as that before deactivation, and didn't show the formation of NiO and $NiAl_2O_4$. In the view point of thermodynamics, it is not surprised that NiO was not formed by steam, however $NiAl_2O_4$ could be generated under steam atmosphere. It is considered that adsorption of hydroxyl group on the Ni surface was a main-factor of deactivation, or the amount of $NiAl_2O_4$ was too small to detect by XRD. Thus it is important to undertake detailed analysis of the catalyst surface to figure out the mechanisms of observed deactivation. However obtained results of characterization for the deactivated catalysts and thermodynamic calculation can deny that the formation of NiO by steam and sintering of Ni nanoparticles occurred the deactivation as shown in Fig. 5.2 and 5.3.

5.3.2. Deactivation behavior of 40 wt% Ni-loaded Al_2O_3 catalysts by steam

In the previous section, the formation of $NiAl_2O_4$ was not detected by XRD. To clearly observe the change of crystallite structure, 40 wt% Ni-loaded Al_2O_3 catalyst was prepared and tested at 873 K, 80 kPa of steam partial pressure and 750 mL min^{-1} g_{cat}^{-1} of NH_3 flow rate for 1 h. Fig. 5.5 shows the change of catalytic activity with time for dry- or wet-NH_3 decomposition. Even loading amount of Ni was increased to 40 wt%, catalytic activity was almost same. It is considered that the diameter increased as loading amount of Ni increased. This result is coincide with the results which Murayama et. al. reported. Although the reason why the conversion

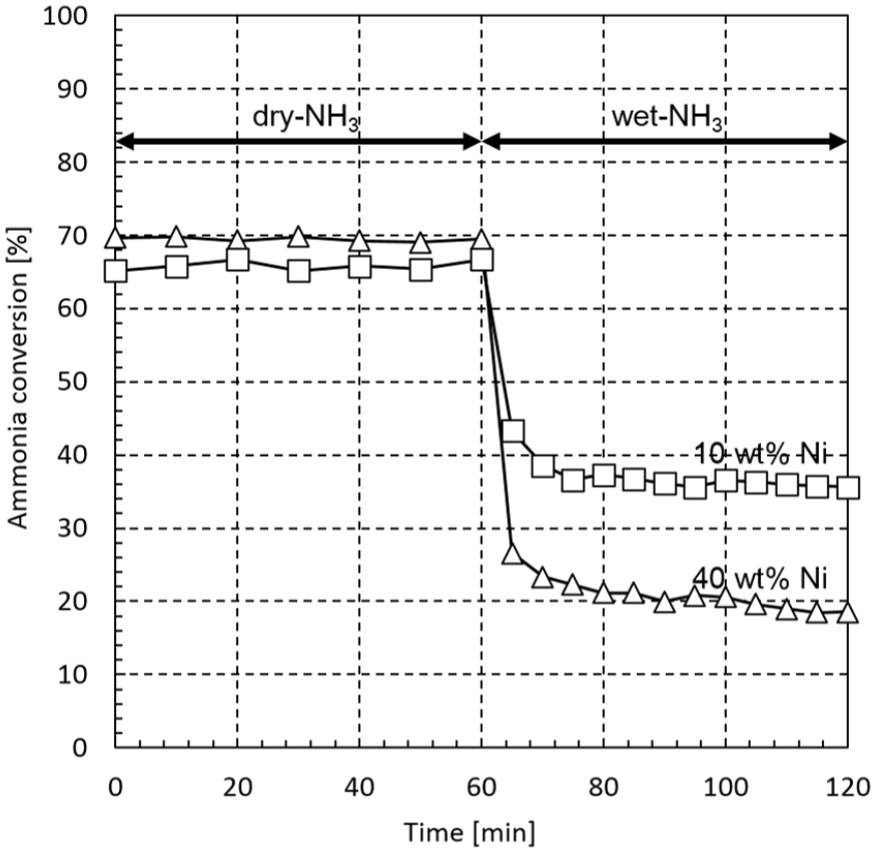

Fig. 5.5 Change in NH_3 conversion with time for dry- or wet-NH_3 decomposition via 10 or 40 wt% Ni/γ-Al_2O_3 catalyst.

The temperature was 873 k and the partial pressure of steam was 80 kPa.

NH_3 flow rate was adjusted to 750 mL min^{-1} g_{cat}^{-1} for each steam partial pressure.

of 40 wt% Ni/γ-Al_2O_3 was less than that of 10 wt% is unclear, deactivation behavior of these catalysts was similar.

As-prepared and deactivated 40 wt% Ni/γ-Al_2O_3 catalysts were analyzed by XRD. Fig. 5.6 shows the XRD patterns of these two catalysts. It is shown that the pattern of as-prepared catalysts indicated peaks derived from γ-Al_2O_3 or $NiAl_2O_4$ at $2\theta = 37.0^o$ and 66.7^o. The as-prepared catalysts was reduced by hydrogen at 973 K, thus $NiAl_2O_4$ was hardly formed on the surface of the as-prepared catalysts. Therefore, it is considered that these two peaks means existing of γ-Al_2O_3. On the other hand, in the XRD patterns of the deactivated catalyst which was tested at 873 K and 80 kPa of steam partial pressure, peaks derived from only γ-Al_2O_3 disappeared (see $2\theta = 43.4^o$ and 62.8^o). This result suggested that the formation of $NiAl_2O_4$ in the 40 wt% of Ni/γ-Al_2O_3 due to steam atmosphere. As shown in Eq. 5-1, the formation $NiAl_2O_4$ of can cause a loss of active sites on the Ni surface. Thus it was concidered that Ni/γ-Al_2O_3 catalyst for wet-NH_3 decomposition can be deactivated due to the

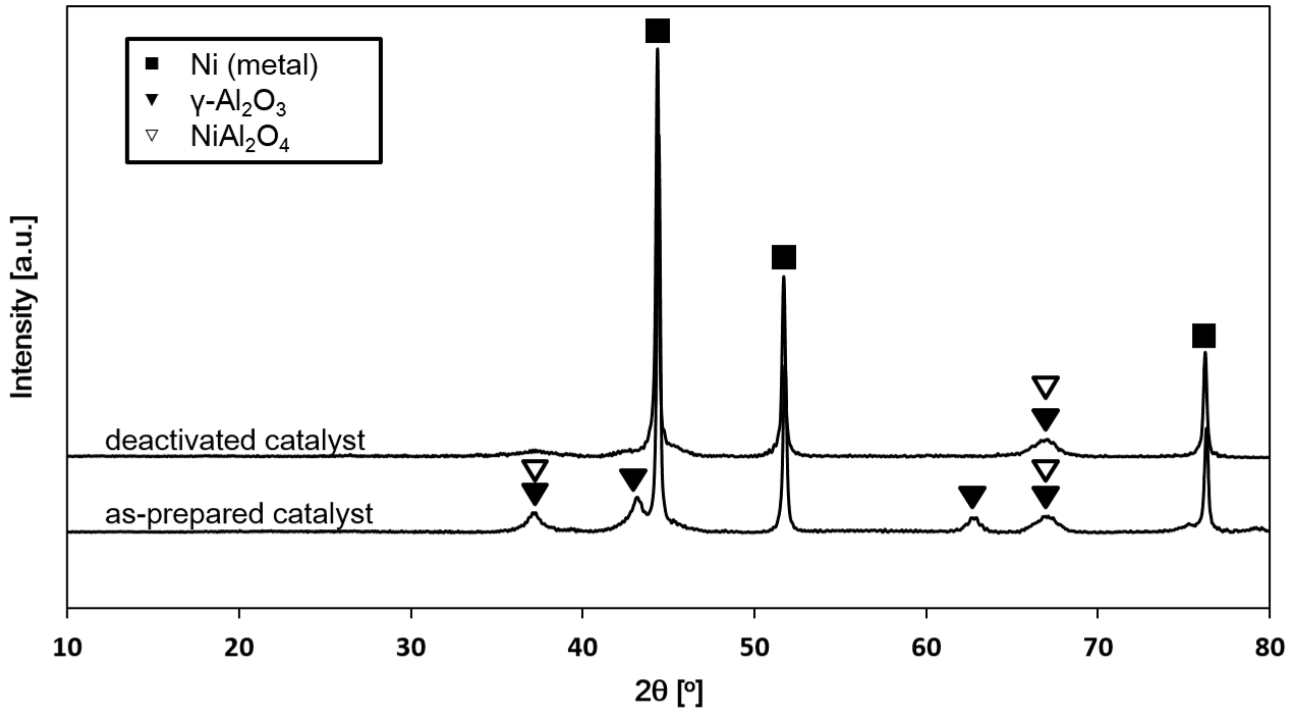

Fig. 5.6 XRD patterns of the as-prepared or deactivated 40 wt% Ni/Al_2O_3.

formation $NiAl_2O_4$ of by steam.

When the formation of $NiAl_2O_4$ decreased the conversion of the Ni catalyst for wet-NH_3, deactivation behavior as observed in Fig. 5.3 can be explained by the mechanisms of the diffusion of Ni and O atoms into alumina. Fig. 5.6 shows the mechanisms of the formation of $NiAl_2O_4$ in γ-Al_2O_3 phase. In the contact of Ni and gaseous H_2O, dissociation of H_2O causes to generate adsorbed OH and H [3] as following equation

$$2(s) + H2O \rightarrow (s)\text{-}OH + (s)\text{-}H \qquad \text{(Eq. 5-2)}$$

where (s) means the adsorption site on Ni surface. Adsorbed OH was also dissociated to generate (s)-O, and atoms of Ni and O are solved in γ-Al_2O_3 phase to generate $NiAl_2O_4$ as shown in Fig. 5.7 [4]. Thus it is considered that diffusion constant, k_{diff} is one of the key factor of the deactivation observed in this study.

Mecartny et. al. investigated behavior of $NiAl_2O_4$ formation from alumina in the N_2/O_2 or $N_2/O_2/H_2O$ atmosphere (dry- or wet-air) at 1573 K [4]. They reported that:

(i). Diffusion rate of Ni atoms is significantly faster than O atoms in the both atmosphere.

(ii). Water-vapor enhances the diffusion of O atoms in the γ-Al_2O_3 phase. Diffusion constant, k_{diff} is 7.93 $x10^{-14}$ or 1.46 $x10^{-13}$ m^2 s^{-1} for dry- or wet-air (with 20 vol% of steam) at 1573 K, respectively.

(iii). k_{diff} increased as steam volume fraction increased below 20 vol% of steam, however above 20 vol% k_{diff} maintained constant value. For instance k_{diff} at 80 vol% of steam was 1.42 $x10^{-13}$ m^2 s^{-1}.

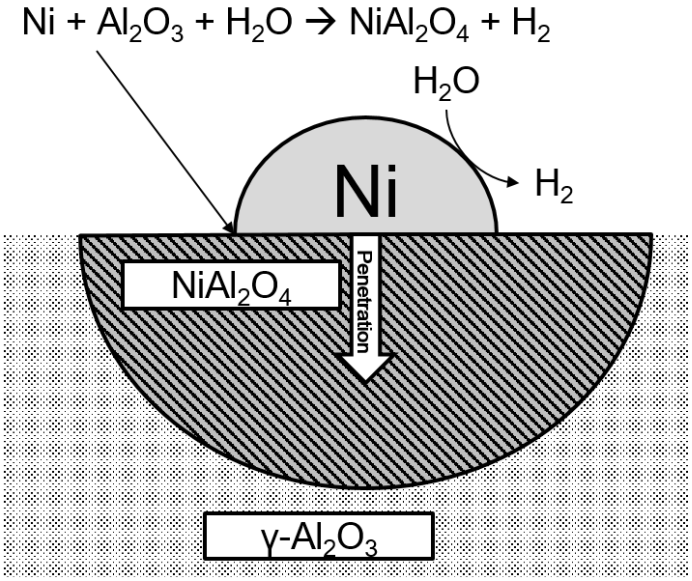

Fig. 5.7 Deactivation mechanism of the Ni/γ-Al_2O_3 by the formation of $NiAl_2O_4$ in humidity environment.

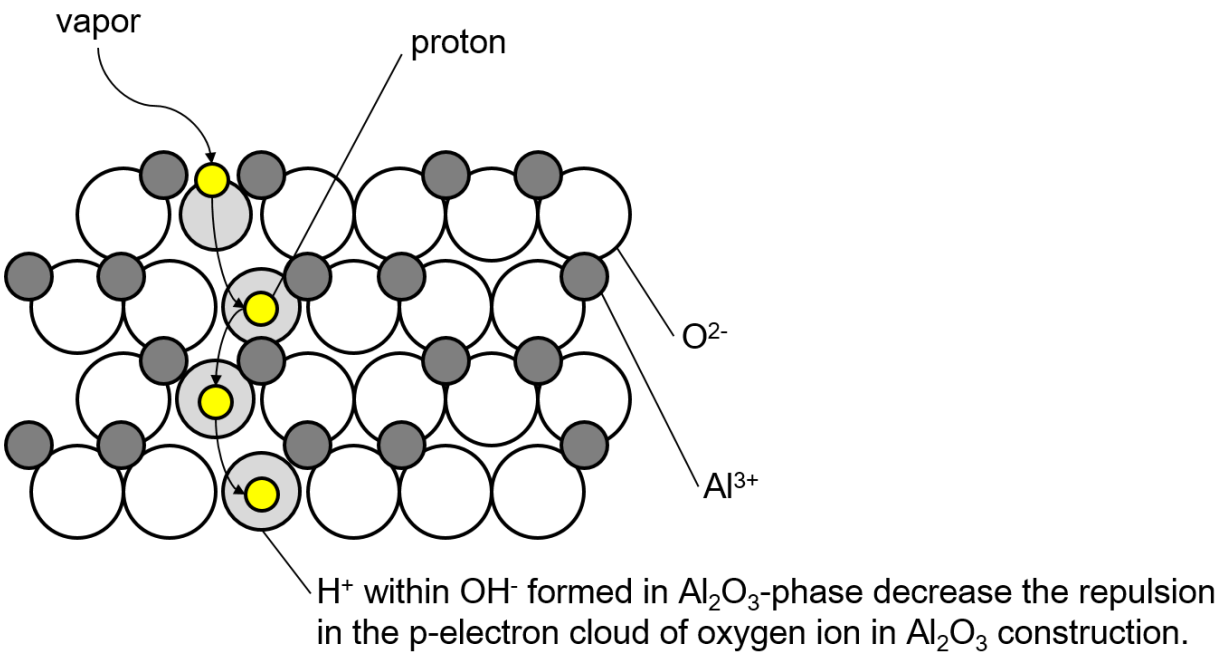

Fig. 5.8 Diffusion mechanism of proton derived from adsorbed hydroxyl group.

Existence of a saturation point of increasing behavior of diffusion constant often has been observed in humidity environment [5]. In steam atmosphere, O^- and H^+ ions derived from adsorbed OH diffuse into γ-Al_2O_3 phase. Diffusing protons can be bonded with O^{2-} ions within the Al_2O_3 as shown in Fig .5.8. Protons derived from the

adsorbed OH are bonded within oxygen anion, O^{2-} in Al_2O_3 phase [6]. Bonded proton within the alumina phase decrease the repulsions in the p-electron cloud of the oxygen anion, as a result, the diameter of oxygen anion in alumina was decreased to enhance the mobility of O derived from adsorbed OH [7,8].

Thus it is considered that below 20 kPa of steam partial pressure deactivation effect by the formation of $NiAl_2O_4$ increased as k_{diff} of O atom in the Al_2O_3 phase increased, while above 20 kPa of steam decreasing ratio of catalytic activity was constant because k_{diff} attained to a saturation point.

5.3.3. Deactivation by adsorbed hydroxyl group on the Ni surface.

In the previous section, the results from XRD analysis suggested that the formation of $NiAl_2O_4$ along with deactivation of 40 wt% Ni/γ-Al_2O_3 of catalyst caused the deactivation, and the deactivation behavior can be explained by the mechanisms of diffusion of Ni ant O atoms into the γ-Al_2O_3 phase. However it is considered that a surface diffusion of hydroxyl group (OH^-) derived from steam is also one of the major factors for deactivation of catalysts. Surface diffusion of hydroxyl ions is known to be significantly faster than oxygen ion diffusion for alumina [3]. Thus it is necessary to investigate the effects of adsorbed OH.

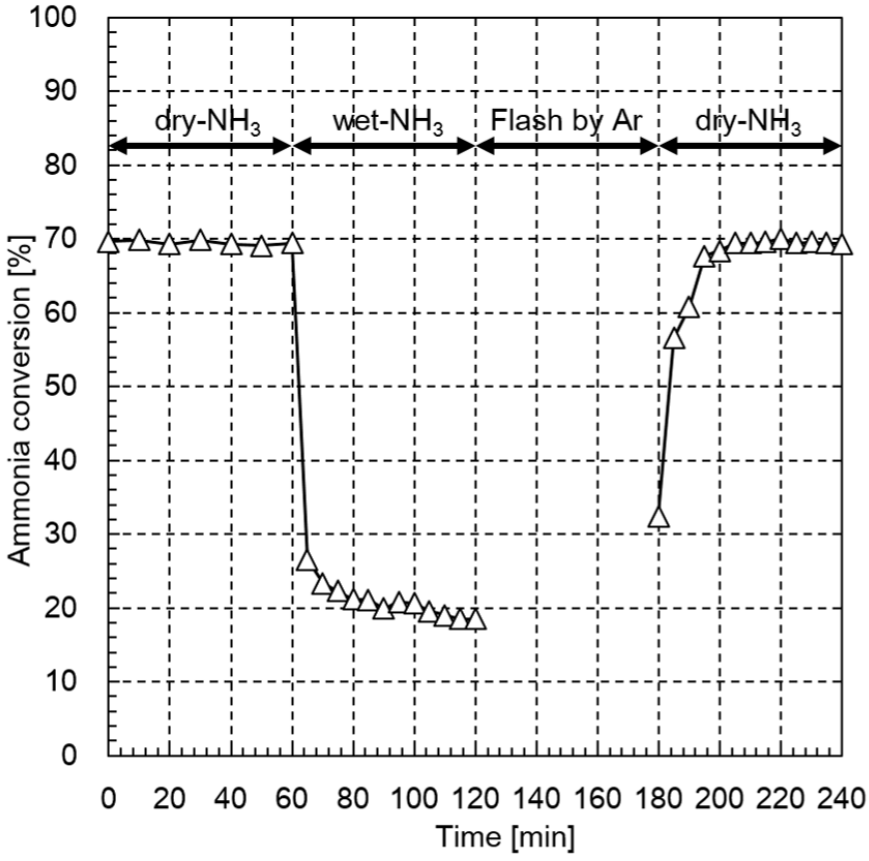

Fig. 5.9 Catalyst regeneration by the Ar flash or dry-NH_3 decomposition via 40 wt% Ni/γ-Al_2O_3 at 873 K and 750 mL min^{-1} g_{cat}^{-1}.

To evaluate the deactivation by OH wet-NH_3 decomposition test as shown in Fig. 5.8 was conducted using 40 wt% Ni/γ-Al_2O_3. In the first 1h, dry-NH_3 decomposition was conducted. Similar to Fig. 5.5, there was no deactivation of catalyst under flowing of dry-NH_3, however the catalyst was deactivated by steam for next 1 h: NH_3 conversion via deactivated catalyst fell out to ca 20 %. Then the catalyst was flashed by flowing of Ar gas for 1h. In Ar atmosphere, the generated $NiAl_2O_4$ probably should be stable: it is unlikely that a thermal decomposition of $NiAl_2O_4$ expressed as following equation progressed.

$2NiAl_2O_4 \rightarrow 2Ni + O_2(g) + Al_2O_3$ (Eq. 5-3)

However adsorbed OH can be desorbed in this 1 h following the reverse reaction of Eq. 5-2.

After Ar flash, dry-NH_3 decomposition was conducted for 1 h. In this sequence, the catalyst regenerated and exhibited as the almost same activity as the initial activity. It is considered that generated hydrogen along with the decomposition of NH_3 reduced $NiAl_2O_4$. Although the conversion was slightly regenerated under flowing dry-NH_3, it seems that NH_3 conversion was increased by Ar flash. It is considered that adsorbed OH was removed in this operation. From Fig. 5.9, adsorption of OH and a formation of $NiAl_2O_4$ could deactivated the catalysts, and the latter had a high impact on catalyst deactivation then the former.

5.3.4. Effects of flow rate and temperature on wet-NH_3 decomposition.

NH_3 decomposition reaction (see Eq. 2-1) is an endothermic reaction. Therefore higher temperatures facilitate the NH_3 decomposition. In practice, NH_3 conversion increased as temperature increased (see Fig. 4.1). Furthermore, the residence time (or flow rate) is a key factor in a fixed-bed reactor. Thus it is important to clarify the effects of these reactor operating conditions on the NH_3 conversion.

Fig. 5.10 shows the NH_3 conversion against dry- or wet-NH_3 flow rate (0 or 80 kPa of steam partial pressure, respectively) at 873, 923 and 973 K. the value of this partial pressure corresponds to the vaporization of 20 wt% of NH_3 solution that is well-concentrated by e.g. membrane separation or NH_3 stripping technique. The solid and dashed lines in this figure show the change in the conversion of NH_3 with the NH_3 flow rate for fry- or wet- NH_3, respectively, at each temperature. The results indicate that NH_3 conversion under dry-NH_3 increased with an increase in the temperature, and decreased as the flow rate increase, whereas expect in the case of 873 K, the conversions under wet-NH_3 didn't decrease monotonically as the flow rates increased. Although the mechanism of this behavior have been unclear, it is possible that deactivation kinetics of catalysts against each flow rate were varied at 923 and 973 K. If the diffusion rate of Ni into $NiAl_2O_4$ was clear, the reason why we-NH_3 conversion at 923 and 973 K was constant may be understood.

The activities of the Ni/γ-Al_2O_3 didn't change under flowing wet-NH_3 with temperature or flow rate, whereas the fractional conversions at high temperature should be lower than that 873 K. Fig. 4.11 shows the

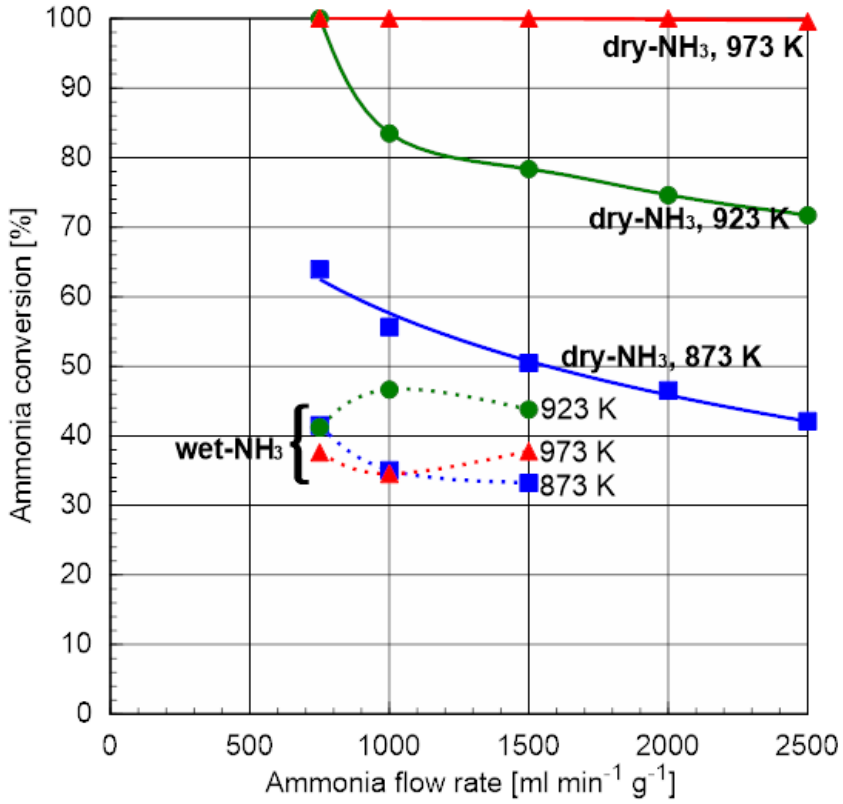

Fig. 4.10 Dry- or wet-NH_3 (80 kPa of steam partial pressure) conversion against flow rate at 873, 923 and 973 K.

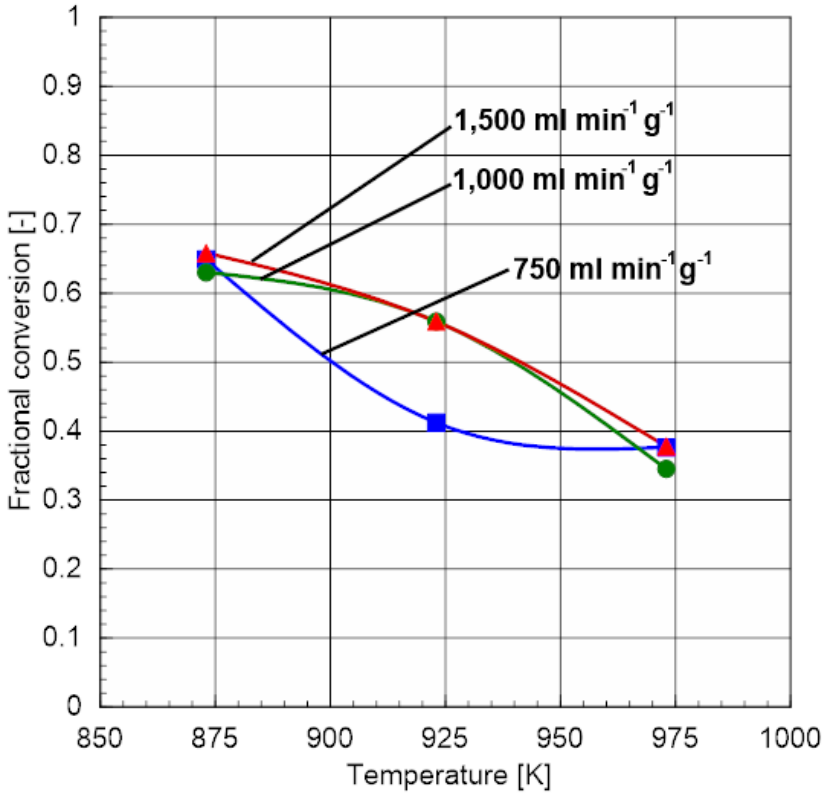

Fig. 4.11 Fractional conversion of wet-NH_3 against temperature (873-973 K) for ammonia flow rates of 750, 1000 and 1500 mL min^{-1} g_{cat}^{-1}.

fractional conversion of wet-NH_3 against temperature for flow rates of 750, 1000 and 1500 mL min^{-1} g_{cat}^{-1}. The fractional conversion is shown to decrease with temperature at each flow rate. It is considered that diffusion coefficient of O atoms increased as the temperature increased. As a result, fractional conversion for each flow rate declined.

5.4. Summary

In this chapter wet-NH_3 decomposition over Ni/γ-Al_2O_3 was conducted by providing NH_3 and steam into the fixed-bed at 873, 923 and 973 K, and verifying the partial but stable decomposition of wet-NH_3 decomposition was succeeded. Although Ni/γ-Al_2O_3 was initially deactivated by steam for ca. 20 min, the catalyst subsequently showed the constant activity. At 873 K the catalytic activity was decreased to half of the initial conversion in the presence of steam with a partial pressure 10–80 kPa. From thermodynamics equilibrium calculation, XRD analysis and the decomposition behavior of wet-NH_3 decomposition, it was considered that the formation of $NiAl_2O_4$ on catalyst surface and adsorption of hydroxyl group (-OH) caused the observed deactivation of the catalyst.

Fractional conversions for wet-NH_3 at 873 K decreased as steam partial pressure increased below 25 kPa of steam, whereas fractional conversions above 25 kPa of steam maintain ca. 0.5. It is considered that this is because increment of diffusion coefficient of O atoms derived from adsorbed -OH with an increase of steam partial pressure attained to the saturation point. Temperature dependency of wet-NH_3 decomposition was also observed with various flow rates. The results showed that fractional conversion decreased as temperature increased. The diffusion of O and Ni in the γ-Al_2O_3 phase can be enhanced due to increase of temperature.

Reference

[1] Y. Matsumura, T. Nakamori. Steam reforming of methane over nickel catalysts at low temperature. *Applied Catalysos A: General*, 258, 107-114 (2004)

[2] J. R. H. Ross, M. C. F. Steel. Mechanisms of the steam reforming of methane over a coprecipitated nickel-alumina catalyst. *Journal of the Chemical Society, Faraday Transactions 1: Physical Chemistry in Condensed Phase*. 69, 10-21 (1973)

[3] M. Pijolat, M. Dauzat, M. Soustelle, Influence of water-vapor and additives on the surface area stability of γ-Al_2O_3, *Solid State Ionics*, 50, 9-31 (1992)

[4] J. P. Angle, P. E. D. Morgan, M. L. Mecartney. Water vapor-enhanced diffusion in alumina. *Journal of the American Ceramic Society*, 96, 3372-3374 (2013)

[5] J. A. Haynes, K. A. Unocic, B. A. Pint. Effects of water vapor on the 1100ºC oxidation behavior of plasma-sprayed TBCs with HVOR NiCoCrAlX bond coating. *Surface and Coating Technology*, 215, 39-45 (2013)

[6] A. K. Kronenberg, J. Castaing, T. E. Mitchell, S. H. Kirby. Hydrogen Defects in α-Al_2O_3 additive water wreaking of sapphire and alumina ceramics between 600 and 1000ºC. Acta Materialia, 48, 1481-1494 (2000)

[7] T. Norby. Proton conduction in oxides. *Solid State Ionics*, 40-1, 857-62 (1990)

[8] R. D. Shanon, R. X. Fischer, Empirical Electronic Polarizabilities in oxide, hydroxidesm oxyfluorides and oxychlorides, *Physical Review B*, 73, 235111 (2006)

Chapter 6 Support Effects on Steam Deactivation in Ni-loaded Catalysts for Ammonia Decomposition

6.1. Introduction

In Chapter 5, the demonstration of thermochemical wet-NH_3 decomposition was succeeded using Ni/γ-Al_2O_3 catalyst at 879-973 K. However wet-NH_3 couldn't be decomposed perfectly due to the deactivation of loaded-Ni catalysts. From XRD analysis and thermodynamic equilibrium calculations, these results indicated that loaded Ni formed composite oxides with γ-Al_2O_3, $NiAl_2O_4$ as Ni/γ-Al_2O_3 was deactivated by steam. Furthermore, deactivation and regeneration behavior of Ni/γ-Al_2O_3 implied that adsorption of hydroxyl group (-OH) on Ni surface can deactivate the catalysts. Thus it was considered that, if the suitable support was selected, deactivation due to the compound-oxides formation between Ni and supports can be inhibited.

From the results in Chapter 4, support effects for various ceramics material for dry-NH_3 were made clear. However reactivity between Ni and supports under steam atmosphere should be important for perfect decomposition of wet-NH_3. In this chapter prepared various Ni-loaded catalysts were tested to evaluate the wet-NH_3 conversion. Support material which can reduce the deactivation of the Ni catalysts was explored, and kinetic study was carried out to compare the kinetics between dry- and wet-NH_3 decomposition.

6.2. Experimental

Ni-loaded catalysts were prepared by the wet-impregnation method (see Chapter 2 and 4). Ni/SiO_2, γ-Al_2O_3, ZrO_2, La_2O_3, TiO_2 and Mordenite were tested. Note that MgO can't be used in a steam atmosphere, because MgO potentially reacts with H_2O as following equation:

$$MgO + H_2O \rightarrow Mg(OH)_2 \qquad \text{(Eq. 6-1)}$$

Thus wet-NH_3 decomposition via Ni/MgO wasn't conducted. Other catalysts were tested using gas-flow fixed-bed reactor as shown in Fig. 4.1 to observed NH_3 decomposition behavior.

6.3. Results and Discussion

6.3.1. Wet-NH_3 decomposition via various Ni-loaded catalysts at 873 K.

Fig. 6.1 shows dry- and wet-NH_3 conversion against time via various Ni-loaded catalysts at 873 K.

(a) Dry- or wet-NH_3 conversion change against time.

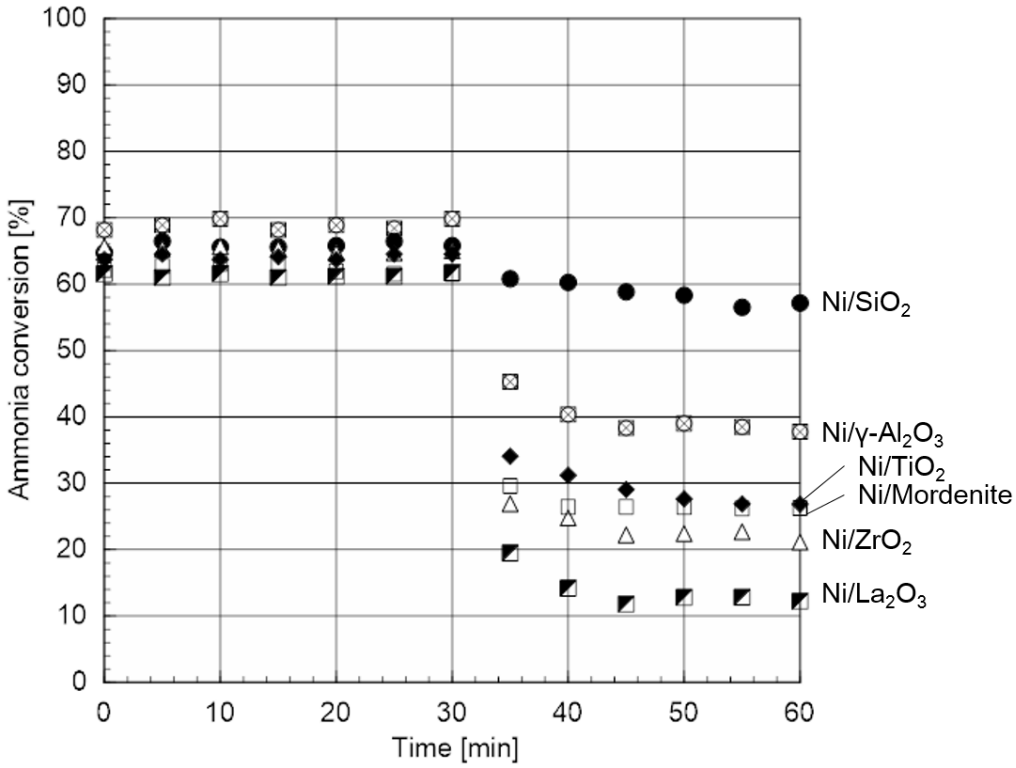

(b) Fractional conversion change for wet-NH_3 decomposition against time.

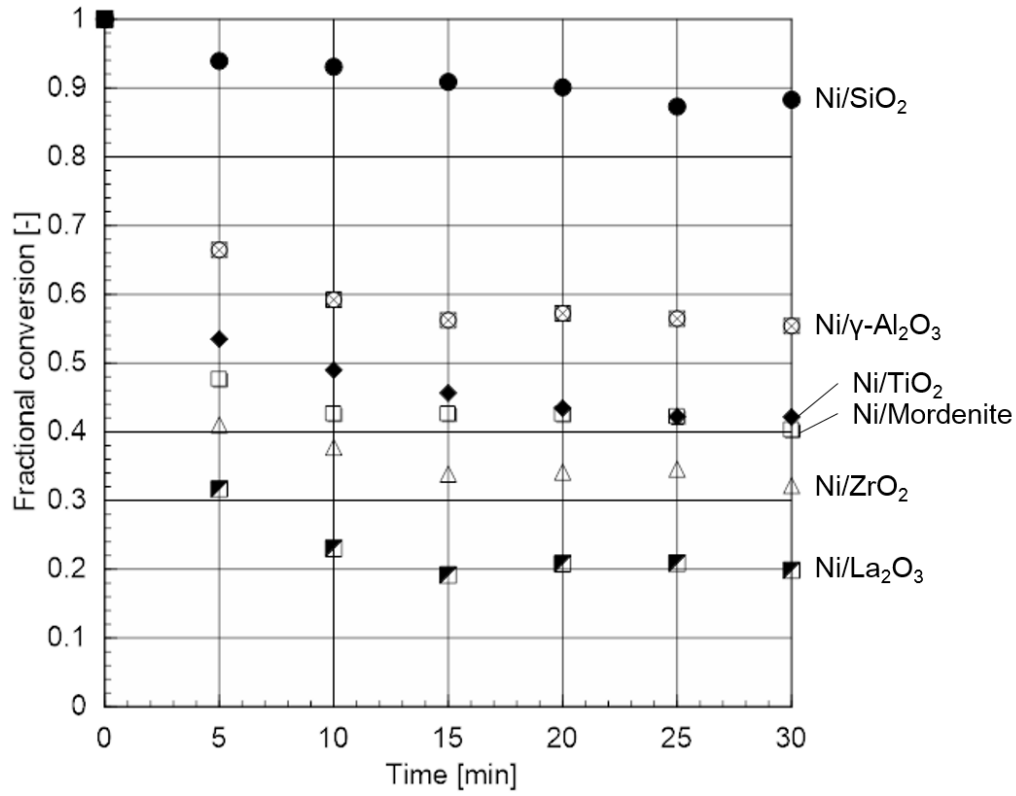

Fig. 6.1 Change in dry- and wet-NH_3 conversion with time via various Ni-loaded catalysts at 873 K.

Flow rate of NH_3 and steam partial pressure were 750 mL min^{-1} g_{cat}^{-1} and 80 kPa, respectively.

NH_3 flow rate for both dry- and wet-NH_3 was adjusted to 750 mL min^{-1} g_{cat}^{-1}. Steam was provided in the wet-NH_3 decomposition as steam partial pressure was 80 kPa. In first 30 min dry-NH_3 decomposition was carried out, and then provided gases was switched to wet-NH_3. Deactivation behavior was observed for 30 min. Dry-NH_3 decomposition for each catalyst kept constant value ranged from 60 to 70 % for 30 min. In the next 30 min, all catalyst decreased in ca. 15 to 20 min, however they lost the catalytic activities perfectly.

As shown Fig. 6.1, the activity of Ni/SiO_2 for wet-NH_3 slightly decreased comparing to other catalysts. The conversion of Ni/SiO_2 for dry-NH_3 was ca. 65 %, and that for wet-NH_3 decreased to ca. 57 %. Though not shown, both of rutile and anatase form of TiO_2 for dry- and wet-NH_3 conversion exhibited same activities in this condition. The coexisting steam on Ni/La_2O_3 and ZrO_2 were relatively high influential than other catalysts. Especially, as shown in Fig. 6.1-(b), 80 % of Ni/La_2O_3's activity was lost along with steam deactivation. Deactivation behavior for each catalyst was similar, thus it was considered that the deactivation mechanisms was same to that of Ni/γ-Al_2O_3: formation of Ni composite oxides and adsorption of –OH decreased NH_3 conversions.

From Fig. 6.1-(b), 90 % of NH_3 decomposition activity remained even with coexisting steam (80 kPa). It was concluded that SiO_2 support can inhibit the deactivation by steam. Because of lack of the thermodynamic data for the composite oxide between Ni and SiO_2 and researches for diffusion of Ni and O atoms into SiO_2 phase, detailed discussion can't be conducted. However the formation of Ni_2SiO_4 was reported [1-3]. To figure out the mechanisms of the tolerability for steam deactivation, it is necessary to evaluate the diffusion coefficients of Ni and O atoms in various ceramic phase.

6.3.2. XRD analysis for deactivated Ni/La_2O_3 catalyst

To investigate the deactivation mechanisms except for that of Ni/γ-Al_2O_3, deactivated Ni/La_2O_3 was analyzed by XRD. In the Chapter 5, it is found that, using 40 wt% Ni-loaded catalyst, the change of XRD pattern could be clearly observe. Thus 40 wt% Ni/La_2O_3 was prepared, and the conversion for wet-NH_3 was evaluated. Fig. 6.2 shows the dry- and wet-NH_3 conversion change via 10 or 40 wt% Ni/La_2O_3 against time. Both of conversions were almost same.

XRD patterns for as-prepared or deactivated 40 wt% Ni/La_2O_3 are shown in Fig. 6.3. The XRD pattern of the as-prepared catalyst indicates the peaks derived from metal Ni and La_2O_3, whereas for the deactivated catalyst most of La_2O_3's peak were disappeared, and peaks derived from $NiLa_2O_4$ were observed.

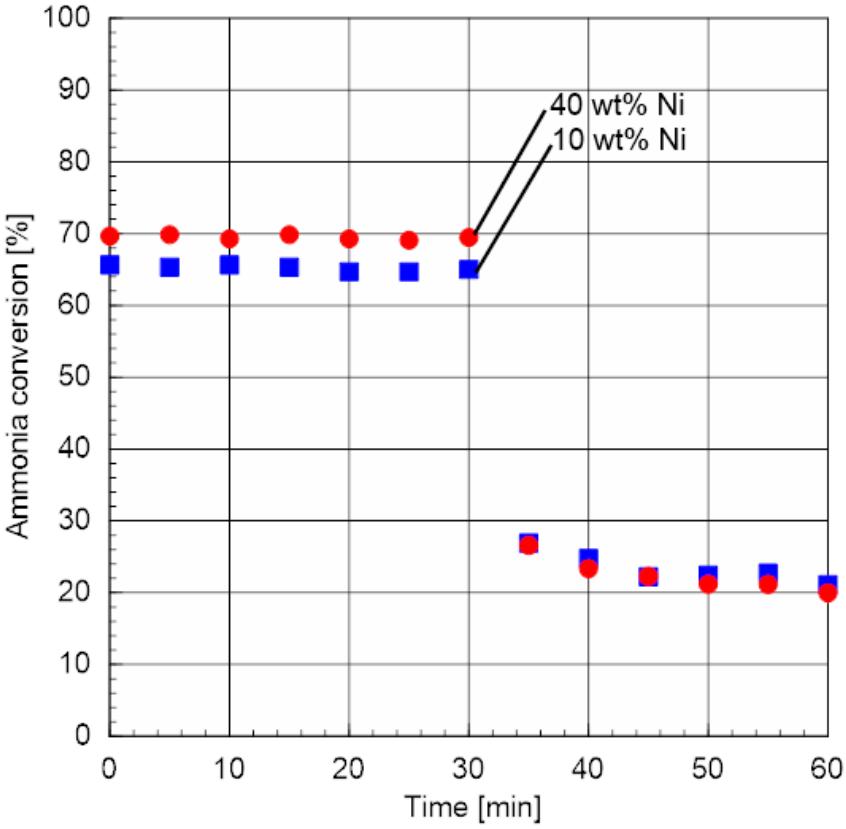

Fig. 6.2 Dry- or wet-NH_3 conversion against time via 10 or 40 wt% Ni/La_2O_3 at 873 K.

Flow rate of NH_3 and steam partial pressure were 750 mL min^{-1} g_{cat}^{-1} and 80 kPa, respectively.

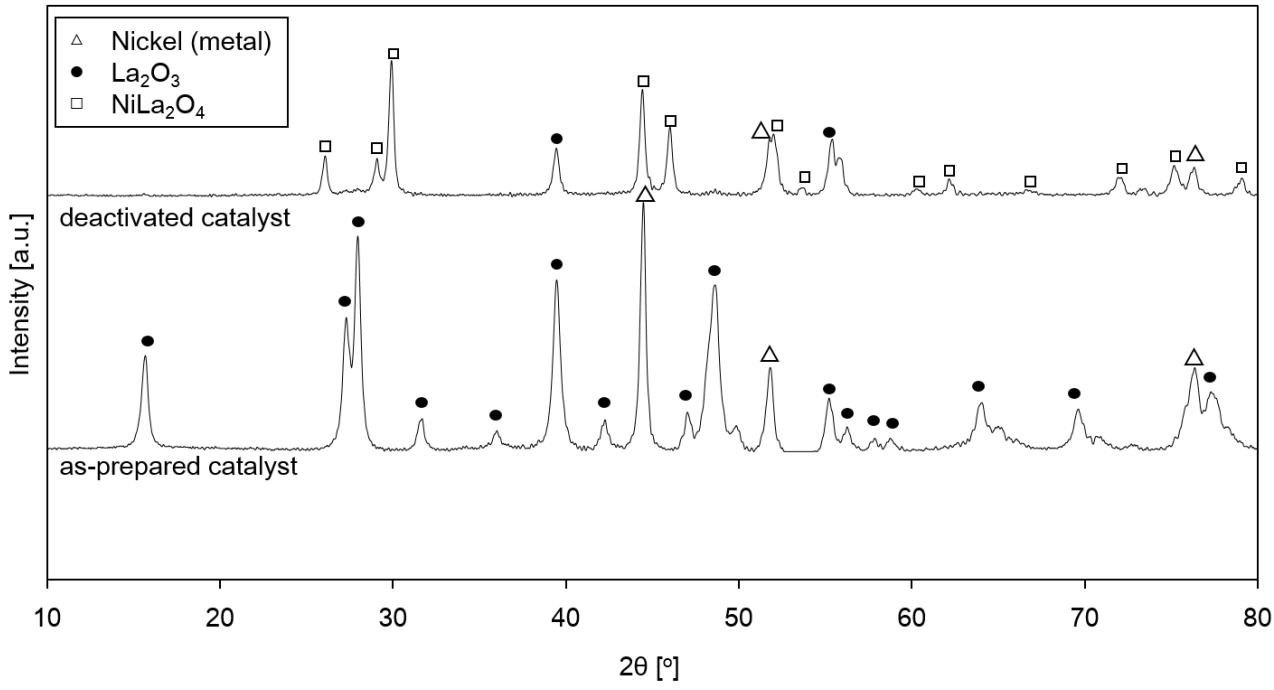

Fig. 6.3 XRD patterns of as-prepared or steam-deactivated 40 wt% Ni/La_2O_3.

Note that the unknown peaks were not observed in the both of XRD patterns. Moreover an intensity ratio of support/Ni was clearly different between as-prepared and deactivated catalysts. An intensity ratio ($I_{support}/I_{Ni}$) between the major peak of support (La_2O_3, $2\theta = 28.0^o$) and metal nickel ($2\theta = 44.5^o$) was 0.87 [-] for the as-prepared catalyst. This means that intensity derived from Ni crystallite was stronger than that from support's crystallite. On the other hand, an intensity ratio between the major peak of support ($NiLa_2O_4$, $2\theta = 29.9^o$) and metal nickel was 1.29 [-] for the deactivated catalyst. It is considered that this intensity ratio indicated the decrease of the diameter of Ni crystallite along with diffusion of Ni atoms into La_2O_3 phase. The result from Fig. 6.3 suggested that Ni and O atoms diffused into La_2O_3 phase to occur catalytic deactivation as well as the mechanism of deactivation of Ni/γ-Al_2O_3.

6.3.3. Observation of wet-NH_3 conversion via Ni/SiO_2

From the results shown in Fig. 6.1, it was concluded that Ni/SiO_2 catalyst can show high activity for wet-NH_3 decomposition comparing to other catalysts. Thus temperature of flow rate dependency of wet-NH_3 conversion via Ni/SiO_2 was observed to explore conditions for perfect decomposition of wet-NH_3.

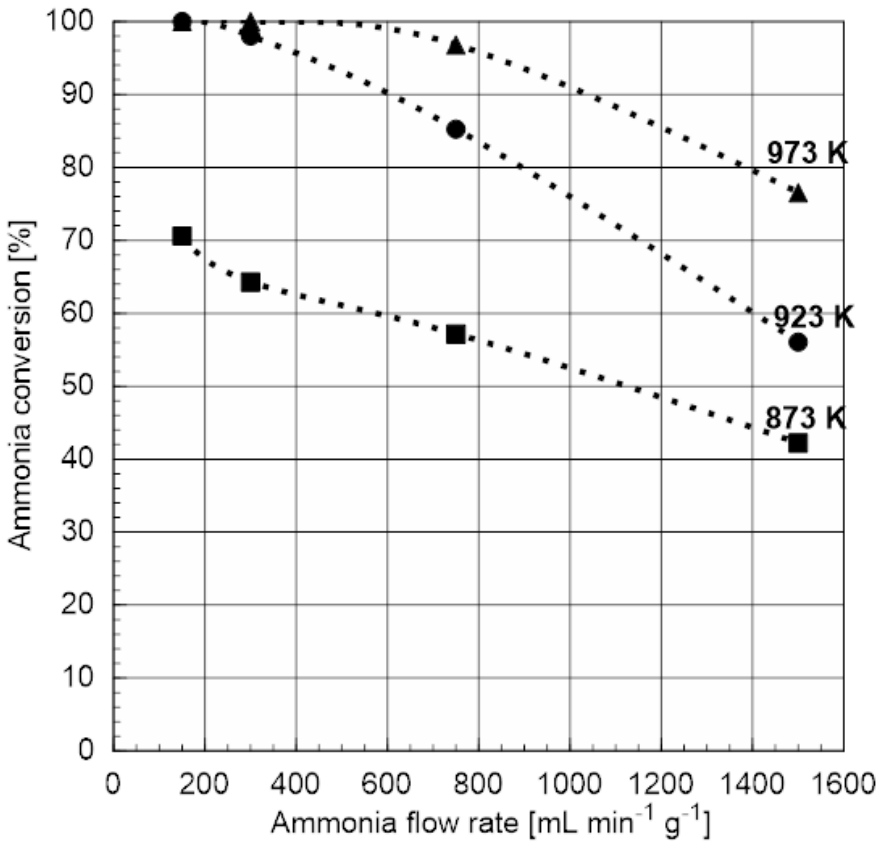

Fig. 6.4 Wet-NH_3 conversion against NH_3 flow rate via Ni/SiO_2 catalyst at 873-973 K.

Steam partial pressure was adjusted to 80 kPa for each decomposition.

Steam partial pressure for each case was adjusted to 80 kPa. NH_3 flow rate in wet-NH_3 was varied from 150 to 1,500 mL min^{-1} g_{cat}^{-1} (GHSV = 3,200-32,000 h^{-1}). At 873 K Ni/SiO_2 catalyst couldn't decompose wet-NH_3 perfectly. However, contrary to Ni/γ-Al_2O_3 (see Fig. 4.10), the conversion increased with a decrease of flow rate. Increasing the temperature to 923 K, the conversions in whole flow rate examined increased, and the catalysts decomposed wet-NH_3 perfectly at 150 mL min^{-1} g_{cat}^{-1} of NH_3 flow rate (GHSV = 3,200 h^{-1}). At 973 K, 300 mL min^{-1} g_{cat}^{-1} of NH_3 in wet-NH_3 could be converted into hydrogen and nitrogen. Thus it was concluded that Ni/SiO_2 has the highest activities for wet-NH_3, and it can decompose wet-NH_3 perfectly above 923 K even if steam partial pressure is 80 kPa.

It is speculated that very few Ni and O atoms can diffuse into SiO_2 phase, or Ni and SiO_2 hardly react to generate some composite oxides, as a result there is a little decrease of wet-NH_3 conversion. Although there are the composite oxides formation such as $NiSiO_3$ and Ni_2SiO_4 at high temperature, unfortunately there is a lock of their detailed thermodynamic date. Moreover, few studies have been carried out to investigate the diffusion of Ni and O atoms into SiO_2 phase. For more detailed consideration of the mechanisms that Ni/SiO_2 inhibits the steam deactivation of catalyst, detailed data of thermodynamics and diffusion behavior in SiO_2 solid were necessary.

6.3.4. Kinetics of wet-NH_3 decomposition via Ni/SiO_2 catalysts.

In the previous section, perfect decomposition of wet-NH_3 via Ni/SiO_2 catalyst was demonstrated. The kinetic study of wet-NH_3 decomposition was carried out to compare kinetics under dry- and wet-atmosphere. Kinetics of the catalytic activities for the wet-NH_3 decomposition was studied based on the design equation of the plug-flow-reactor (see Eq. 2-9).

A temperature dependency of kinetic constants of Ni/SiO_2 catalyst for dry- and wet-NH_3 decomposition was shown in Fig. 6.5: this figure indicates the Arrhenius plot for dry- and wet-NH_3 decomposition. It is found that the reaction rates of wet-NH_3 decomposition were slower than that of dry-NH_3 due to steam deactivation of the catalyst. As shown in Table 4.2, the activation energy (E_a) and frequency factor (k_0) for dry-NH_3 decomposition are 149 kJ mol^{-1} and 22.4 s^{-1}, respectively, whereas E_a and k_0 for wet-NH_3 decomposition which are evaluated from Fig. 6.5 are 120 kJ mol^{-1} and 18.3 s^{-1}, respectively. The frequency factor for wet-NH_3 was lower than that of dry-NH_3, thus it was considered that active sites on Ni surface was decreased by the adsorption of hydroxyl group. The activation energy for wet-NH_3 decomposition also decreased. As shown in Fig. 5.6, loaded Ni nanoparticles on out surface which don't exist in support's pore were preferentially deactivated by adsorption of –OH. When outer Ni particles were poisoned, only Ni particles in inmost pore were used as active sites for NH_3 decomposition. In this situation, pore diffusion

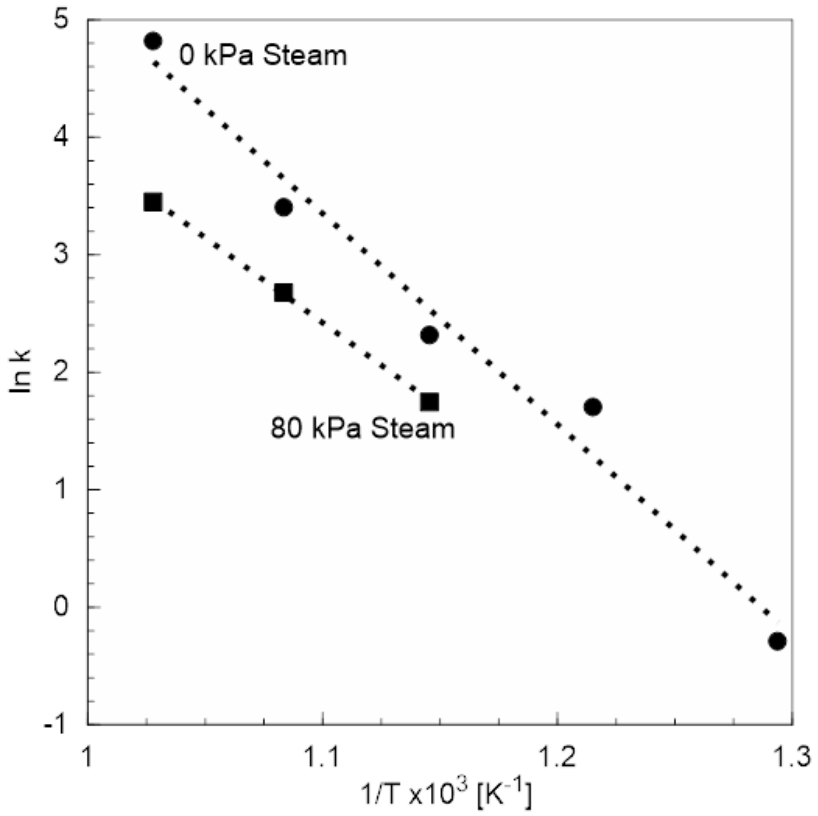

Fig. 6.5 Arrhenius plot of dry- or wet-NH_3 decomposition via Ni/SiO_2 catalysts.

Steam partial pressure in wet-NH_3 decomposition was 80 kPa.

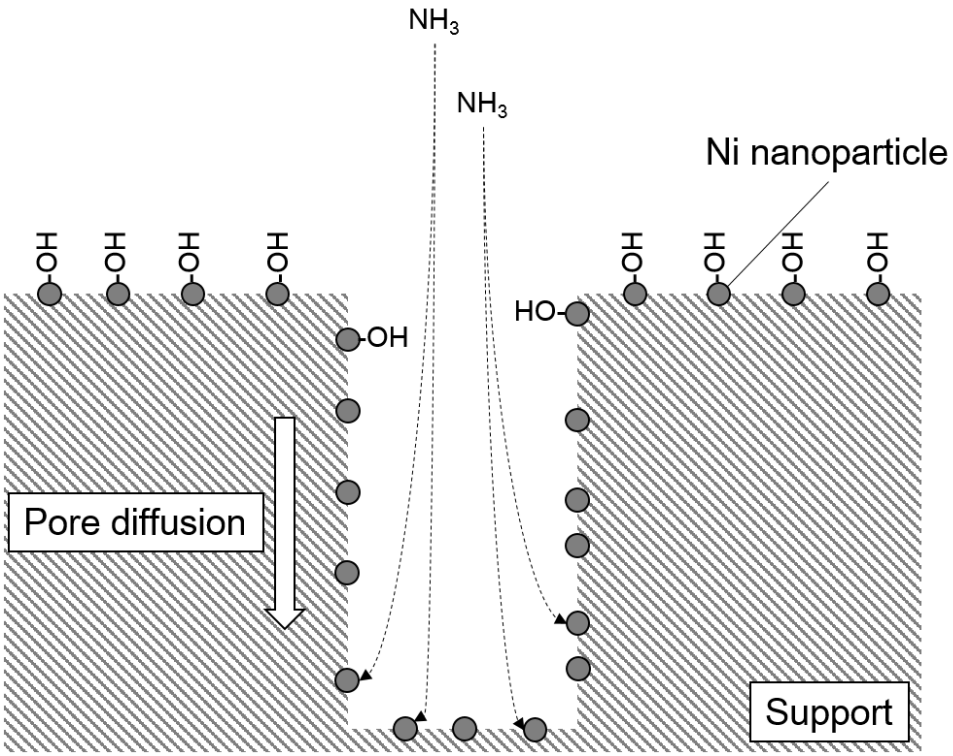

Fig. 6.6 Schematic illustration of steam deactivation mechanisms of Ni-loaded catalyst and pore diffusion of NH_3 in support material.

resistance should affect the overall conversion of wet-NH_3 decomposition [4,5]. As figured out in Chapter 3, the apparent activation energy decreased as diffusion resistance increase. Thus, it was considered that the activation energy for wet-NH_3 was lower than that for dry-NH_3 due diffusion resistance of pore.

6.4 Summary

Ni-loaded various ceramic particles were used for wet-NH_3 decomposition. It is found that Ni/SiO_2 can exhibited the steam activation, whereas the effect of steam was the most serious in whole catalyst examined. Fractional conversion of Ni/SiO_2 at 873 k was ca. 0.9 [-]. To investigate the deactivation mechanism of Ni/La_2O_3, XRD patterns of as-prepared and deactivated catalyst were compared. The XRD patter of the steam-deactivated catalyst indicated the formation of $NiLa_2O_4$, and most of peaks derived from La_2O_3 were disappeared. It is considered that the composite oxide formation derived from Ni and La_2O_3 deactivated the catalysts as well as Ni/γ-Al_2O_3.

To demonstrate the perfect decomposition of wet-NH_3, Ni/SiO_2 was tested at 873, 923 and 973 K in the NH_3 flow rates ranged from 150 to 1,500 mL min^{-1} g_{cat}^{-1}. The wet-NH_3 conversion increased as temperatures increased or NH_3 flow rates decreased. At 923 K, wet-NH_3 via Ni/SiO_2 was decomposed perfectly below 150 mL min^{-1} g_{cat}^{-1}. It is considered that Ni and SiO_2 hardly react to form some composite oxides, as a result wet-decomposition could be achieved.

The kinetic study for dry- and wet-NH_3 via Ni/SiO_2 decomposition indicated that the activation energy and the frequency factor decreased affected by steam. Decrease of frequency factor can be explained the adsorption of hydroxyl group (-OH) on Ni surface. This adsorption was occurred preferentially on the outer surface, and it is considered that contribution of Ni nanoparticles in inmost pore for NH_3 decomposition should increase. The diffusion resistance in pore decreased the apparent activation energy along with adsorption of –OH.

Reference

[1] H. S. C. O'Neill. Free energies of formation of NiO, CoO, Ni_2SiO_4 and Co_2SiO_4. *American Mineralogist*, 280-291 (1987)

[2] 塩見純雄, 佐野信雄, 松下幸雄. $FeSiO_4$, $CoSiO_4$ および Ni_2SiO_4 の標準生成自由エネルギーの電気化学的測定, 鉄と鋼, 2, 177-181 (1986)

[3] K. T. Jacob, A. K. Shukla. Kinetic decomposition of Ni2SiO4 in oxygen potential gradients, 2, 338-344 (1987)

[4] O. Leavenspiel. Chemical Reaction Engineering (3rd edition). P485. *John Wiley and Sons, Inc.*, New York (1998)

[5] 久保田宏, 関沢恒男. 反応工学概論, P89, 日刊工業新聞社 第 2 版 (1986)

[6] 井本立也, 反応工学, P282, 日刊工業新聞社 (1977)

Chapter 7 Conclusion

In Chapter 1, two application of Ni-loaded catalysts for NH_3 decomposition were proposed: application for (i) NH_3 energy process to convert NH_3 to H_2 and (ii) for thermochemical denitrification of ammonia nitrogen (NH_4^+) in wastewater treatment. The thermochemical denitrification process targeted in this study decompose NH_3 gas from in wastewater over Ni-loaded catalysts.

In Chapter 2, 3 and 4, heat and mass transfer phenomena in the catalysts bed was analyzed to estimate support effects of various ceramic materials under conditions where the influences of cold-spot formation and pore diffusion resistance can be ignored to explore the active Ni catalysts. In Chapter 5 and 6, to demonstrate the denitrification of and hydrogen production from wet-NH_3, kinetic study of various Ni-loaded catalysts was carried out, and subsequently wet-NH_3 decomposition over Ni catalysts was conducted. Statements of each chapter of this thesis described below.

In Chapter 1, the progress of the development of Ni-loaded catalysts were reviewed, and described that after 1990s NH_3 decomposition catalysts over cheap but active transition metals have been investigated to established hydrogen energy system via NH_3 energy carrier. Various Ni-loaded catalyst have been widely investigate, however few works discussed the heat and mass transfer in the catalyst beds. To certainly evaluate and explore effective support, it is important to analyze temperature distribution along which NH_3 decomposition and pore diffusion regime. Furthermore, this thesis proposed the novel thermochemical denitrification process via NH_3/steam mixture decomposition for wastewater treatment. Present bioreactor have been relatively larger, in other words its reaction rate was too slow. Therefore, the development of the compact and stable wastewater treatment processes have been desired. In this chapter the process of the thermochemical ammonia decomposition for denitrification and hydrogen production. However to conducted catalytic decomposition of NH_3 co-existing steam.

In Chapter 2 and 3 the heat and mass transfer in the catalyst bed and kinetics were figured out.

In Chapter 2, dry-NH_3 decomposition via Ni/SiO_2 catalysts was conducted with various gas velocity to investigate the effects of temperature distribution in the bed. Although kinetics constants, k for > 80,000 h^{-1}

was almost constant, those for < 80,000 h^{-1} decreased as gas velocity decreased. From the numerical calculations it is concluded that the cold spot formation with lower gas velocity decreases the total conversion of catalysts bed. At more than 80,000 h^{-1} of the gas velocity, the variation of the temperature distribution for T_r = 973 K was less than ±10 K, and those below 923 K was less than ±5 K: in these conditions the influences can be eliminated to evaluate certain kinetic constants.

In Chapter 3, diffusion regime in Ni/SiO_2 with different mean pore diameter were evaluated. The mean pore diameter was varied from 7.7 to 34.8 nm. From the evaluation of Knudsen number for pore diffusion and kinetics for Ni/SiO_2 catalysts, it is found that, above 923 K, the catalytic activities Ni/SiO_2 with 7.7 nm of mean pore diameter increased due to strong diffusion resistance derived from Knudsen diffusion.

In Chapter 4, the support effects of various ceramic particles were investigated in the view point of kinetics of dry-NH_3 decomposition. From the results of NH_3 conversion change against NH_3 gas hourly space velocity (GHSV), support effects for NH_3 decomposition were ranked in the order of γ-Al_2O_3 > MgO = La_2O_3 = ZrO_2 > TiO_2 (rutile form) > SiO_2 > TiO_2 (anatase form) > Mordenite with the temperatures ranged from 773 to 973 K. It is considered that γ-Al_2O_3 has the most effective support due to its high basicity. On the other hand, moredenite decreased activity of Ni because it was a solid base.

Previous chapter showed that Ni/γ-Al_2O_3 is the most active catalysts for dry-NH_3 decomposition. Thus, in Chapter 5, decomposition of wet-NH_3 with 0.8 kPa of steam partial pressure via this catalyst was conducted. Although steam deactivation was observed, the results showed verifying the partial but stable decomposition of wet-NH_3 decomposition was succeeded. From the XRD analysis and thermochemical equilibrium calculations, it is considered that diffusion of Ni and O atoms into γ-Al_2O_3 phase and $NiAl_2O_4$ formation decreased the conversion over Ni/γ-Al_2O_3 catalyst.

In Chapter 6, to achieve the perfect decomposition of wet-NH_3, the most effective catalyst for wet-NH_3 decomposition was explored. It was found that SiO_2 support could inhibit the steam deactivation. Ni/SiO_2 catalyst can decompose wet-NH_3 perfectly at 923 K and 150 mL min^{-1} g_{cat}^{-1} of NH_3 flow rate. The kinetic study for dry- and wet-NH_3 via Ni/SiO_2 decomposition was carried out. The frequency factor of wet-NH_3 decomposition was lower than that of dry-NH_3. This is because of the adsorption of hydroxyl group. The activation energy of wet-NH_3 decomposition was also lower than that of dry-NH_3. Adsorption of hydroxyl group was occurred preferentially on the outer surface, and it is considered that contribution of Ni nanoparticles in inmost pore for NH_3 decomposition should increase. The diffusion resistance in pore decreased the apparent activation energy along with adsorption of –OH.

This thesis evaluated the kinetics of Ni-loaded catalysts under the conditions where uniform temperature distribution can be assumed, and estimated the influences of pore diffusion regime on kinetics of Ni catalysts. The obtained insights in this thesis should be useful to design the NH_3 decomposition reactor and its catalysts. Furthermore, to demonstrate the hydrogen production and denitrification from ammonium-nitrogen in wastewater, NH_3 decomposition behavior with co-existing steam was observed. The experimental results show that –OH adsorption and the formation of complex oxides of Ni with support material may decrease the NH_3 decomposition rate. Exploring the most active catalysts, it is found that SiO_2 has the highest support effects, and wet-NH_3 via Ni/SiO_2 was decomposed perfectly below 150 mL min^{-1} g_{cat}^{-1} at 923 K.

研究業績一覧表

【査読付原著論文】

- R. Atsumi, R. Noda, H. Takagi, L. Vecchione, A. Di Carlo, Z. Del Prete, K. Kuramoto, Ammonia decomposition activity over Ni/SiO_2 catalysts with different pore diameters. *International Journal of Hydrogen Energy*, 39, 13954-13961 (2014)
- R. Atsumi, R. Noda, H. Takagi, L. Vecchione, A. Di Carlo, Z. Del Prete, K. Kuramoto, Effects of steam on Ni/Al_2O_3 catalysts for ammonia decomposition. *Industrial & Engineering Chemistry Research*, 53, 17894-17853 (2014)

【特許】

- 熱海良輔、倉本浩司、野田玲治、“アンモニア態窒素含有廃棄物からのアンモニア分解水素製造方法”、特願 2014-150927、出願中

【賞罰】

- International Symposium on Ecotopia Science 2013, Outstanding Presentation Award (2013)

【学会活動歴】

1. 熱海良輔、高木英行、野田玲治、倉本浩司、「アンモニア分解を目的とした Ni 担持 SiO_2 触媒の経時的な活性低下挙動の観察」、化学工学会第 78 年会、P115（2013）
2. 熱海良輔、高木英行、野田玲治、倉本浩司、「NH3 分解水素製造を目的とした Ni 担持触媒の開発：担体構造が NH3 分解活性に与える影響」、第 20 回 E&E フォーラム（2013）
3. R. Atsumi, H. Takagi, R. Noda, K. Kuramoto. “NH_3 as a fuel for fuel cells:

Effects of support on Ni loaded catalysts for NH3 decomposition", JSPS-NRFK International Seminar between Japan and Korea in 2013, Korea (2013)

4. R. Atsumi, H. Takagi, R. Noda, K. Kuramoto. "NH_3 as a fuel for fuel cells: Effects of support on Ni loaded catalysts for NH3 decomposition", International Symposium on Ecotopia Science '13, P-3-18, Aichi (2013)
5. **熱海良輔**、高木英行、野田玲治、倉本浩司、「アンモニア分解を目的とした Ni 担持触媒における細孔構造が触媒活性に与える影響」、化学工学会岩手大会、B113（2013）
6. **熱海良輔**、高木英行、野田玲治、倉本浩司、「アンモニア分解反応活性に対する触媒担体の細孔構造の影響の評価」、第 22 回日本エネルギー学会大会、4-3-3（2013）
7. **熱海良輔**、高木英行、野田玲治、倉本浩司、「アンモニア分解を目的とした Ni 担持触媒における担体効果」、化学工学会第 45 秋季大会、H320（2013）
8. **熱海良輔**、野田玲治、高木英行、倉本浩司、「金属担持触媒を用いた NH_3 分解水素製造における共存水蒸気の影響」、化学工学会第 79 年会、E217（2014）
9. **熱海良輔**、高木英行、野田玲治、倉本浩司、「水素製造を目的とした NH_3 分解流動層技術の開発」、第 23 回日本エネルギー学会、4-4-3（2014）

以上

謝辞

本論文は平成二十一年度から、産業技術総合研究所 エネルギー技術研究部門と群馬大学大学院 野田研究室との共同研究で得られた成果の一部をまとめたものである。アンモニアをエネルギーキャリアとして利用する水素社会を現実のものとするために、様々な技術開発に取り組んできたが、現在では地球上の窒素循環という大きな流れの中でアンモニアを捉え直し、脱窒・水素製造を行うという大きな枠組みで研究を行っている。

こうした壮大な研究テーマへと成長するに至った過程で、様々な方にお世話になったし、指導教員の野田玲治 先生は勿論のこと、特に群馬大学 中川伸好 先生、石飛宏和 先生、金沢大学 辻口拓也 先生、産業技術総合研究所 松岡浩一 様には実に様々な薫陶を賜った。共同研究者である産業技術総合研究所 倉本浩司 様、高木英行 様には研究や論文発表の課程で貴重な助言を数多く頂いた。野田先生とお二人の指導が無ければ博士論文の完成は困難であったと思う。

本博士論文の主査である宝田恭之 先生、副査である渡邉智秀 先生には予備審査から公聴会まで数多くの貴重なご助言を頂き、より一層、博士論文の内容がブラッシュアップすることができた。

指導教官の野田先生には、アンモニアからの脱窒・水素製造プロセスを考える際に、有益なご助言を数多くいただいた。先生の指導により、物質循環・化学プロセスの設計に関する理解が深まったと思う。また機械工作の技術に関しても先生はかなり深い知識を持っており、実験装置をつくる段階で親身な指導をして頂いた。

産業技術総合研究所の倉本様には、「アンモニア」という壮大なテーマを頂いた。ある意味、倉本様から投げかけられたこのテーマから、私の研究活動が本格的にスタートした。倉本様は固体酸化物型燃料電池の技術開発に取り組んでおられ、その燃料電池評価試験装置の完成度の高さは、世界的に見ても高いレベルにあると思う。こうした実験装置を作れる御方が身近にいて下さったおかげで、研究所で研究活動を行っていた時期は毎日強い刺激を受けることができたと思う。論文執筆や研究発表をはじめ、基本的な仕事のやり方や実験技術などはほとんど全て倉本様から吸収したものである。これまで用いた実験装置や本論文の内容に未熟な点があれば、それは全て私の不勉強の致すところである。

最後に、博士後期課程を卒業するまで私を支えてくれた家族、友人に感謝申し上げる。特に中川研究室の友人である上野裕二 君とは大学入学当初からお互いに刺激し合う仲であった。また、研究室配属後は、曲澤一史 君や滝野大樹 君という優秀で気さくな友人に恵まれたことを嬉しく思う。

平成二十七年 二月十三日
研究室居室にて 熱海 良輔